Theoretical Modeling in Very Long Baseline Interferometry

Ojars J. Severs, John L. Fanselow, Christopher S. Jacobs

Jet Propulsion Laboratory, California Institute of Technology,

Pasadena, California 91109

(November 20, 1995)

Abstract

Interferometry at radio frequencies between Earth-based receivers separated by intercontinental distances has made significant contributions to astrometry and geophysics during the past three decades. Analyses of such very long baseline interferometric (VLBI) experiments now permit measurements of relative positions of points on the Earth's surface, and angles between celestial objects, at the levels of 1 crn and 1 nanoradian, respectively. The relative angular positions of extragalactic radio sources inferred from this technique presently form the best realization of an inertial reference frame. This review summarizes the current theoretical models that are needed to extract results from the VLBI observables at such levels of accuracy. An unusually broad cross-section of physics contributes to the required modeling. Both special and general relativity need to be considered in properly formulating the geometric part of the propagation delay. While high-altitude atmospheric charged particle (ionospheric) effects are easily calibrated if measurements arc performed employing at least two well separated frequencies, the contribution of the neutral atmosphere at lower altitudes is more difficult to remove. Mismodeling of the troposphere in fact remains the currently dominant error source. Numerous small periodic and quasi-periodic tidal effects also make important contributions

to space geodetic observables at the centimeter level, and some of these are just beginning to be characterized. Another area of current rapid advances is the specification of the orientation of the Earth's spin axis in inertial space (nutation and precession). The order-of-magnitude improvement of accuracy that was achieved during the last decade provides essential input to geophysical models of the Earth's internal structure. Most aspects of VLBI modeling are also directly applicable to interpretation of other space geodetic measurements, such as active and passive ranging to Earth-orbiting satellites, interplanetary spacecraft, and the Moon.

95.75Kk, 95.70Dk, 95.10Jk

CONTENTS

1. IN'J1K)DIJC'I'1ON 10
11. GEOMETRIC DELAY 16
A. Time interval for the arrival ofa wavefront at two stations 20
1. Plane wave front 21
2. Curved wave front 22
3. Gravitational delay 24
B. Time information 29
C. Station locations 31
1. Tectonic plate motion 32
2. Tidal station motion 33
a, Solid Earth tides 34
b. Pole tide 39
c. Ocean loading 40
3. Non-tidal station motion 41
a. Atmosphere loading 42
b. Post-glacial rebound 44
1). Source structure 44
E. Transformation from terrestrial to celestial coordinate systems 48
1. UT1 and polar motion 50
a. Tidal UTPM variations 53
b. Solid Earth tide UTPM variations 54
c. Ocean tide UTPM variations 54
2. Nutation 56
a. Corrections to the 1980 IAU model 58
3. Precession 62
4. Perturbation rotation 63
F. Earth orbital motion 65
G. Antenna geometry 71
1. Axis offset 72
2. Refraction 73
3. Unique antennas 75
4, Site vectors 75
5. Feed rotation 76
6. Thermal expansion 77
7. Antenna subreflector focusing 78
111. CLOCKMODEL 79
IV. ATMOSPHERIC DELAY 80
A. ionosphere 81
1. Dual-frequency calibration 83
2. Total electron content 85
B. Troposphere 87
1. Mapping functions 90
2. Antenna axis offset altitude correction 92
V. PHASE DELAY RATE (FRINGE FREQUENCY) 93
VI. PHYSICAL CONSTANTS 95
VII. FUTURE MODEL IMPROVEMENTS 96
A. Relativity 96
B. Effects of the Galaxy 97
C. Earth tidal models 97
1), Source structure 98
E. Earth orientation models 98
F. Antenna deformation 98
G. Antenna alignment 99
II. Ionosphere 99
]. Troposphere 99
J. Thermal effects 100
K. Phase delay rate 100
ACKNOWLEDGMENTS 100
References 101

A_{ij}	nut ation amplitudes in longitude
B	baseline vector
B_{ij}	nutation amplitudes in obliquity
BIH	Bureau International de l'Heure
BIPM	Bureau International des Poids et Mesures
BWS	bandwidth synthesis
CDP	Crustal Dynamics Project
CEI	Connected Element Interferometry
CIO	Conventional International Origin
$C_{\psi j}$	planetary nutation amplitudes in longitude [Eq. (2.1 36)]
$C_{\varepsilon j}$	planetary nutation amplitudes in obliquity [Eq. (2.137)]
c	speed of light
D	obliquity of Moon from Sun
DSN	Deep Space Network
1)ss	Deep Space Station
E	elevation angle
1"	latitude argument of Moon
f	Earth flattening factor
G	universal gravitational constant
GPS	Global Positioning System
GSFC	Goddard Space Flight Center
g	Earth surface gravitational acceleration
g	angle for barycentric dynamic time [Eq. (2.34)]
$g^{\mathrm{I}}_{1,2,3}$	local tidal displacements (i = 2,3: quadrupole, octupole)
H	hour angle
h_γ	hour angle of mean equinox of date

h_i	vertical Love number (i = 2,3: quadrupole, octupole)
$h_{1,2}$	ionosphere or troposphere height limits
IAU	International Astronomical Union
IERS	International Earth Rotation Service
IRIS	International Radio Interferometric Surveying
IUGG	International Union of Geodesy and Geophysics
JD	Julian elate
JPL	Jet Propulsion laboratory
k	unit vector in signal propagation direction from source
l	mean anomaly of MoorI
l'	mean anomaly of Sun
l_E	mean anomaly of Earth
l_J	mean anomaly of Jupiter
l_M	mean anomaly of Mars
l_S	mean anomaly of Saturn
l_V	mean anomaly of Venus
l_i	horizontal Love number (i = 2,3: quadrupole, octupole)
MERIT	Monitor Earth Rotation and Intercompare Techniques
MTT	Mapping Temperature Test
m	speed of precession in right ascension
m_p	mass of body p
M_{we},	first moment of wet troposphere refractivity
N	nutation transformation matrix
N'	lunar node argument
NASA	National Aeronautics and Space Administration
NEOS	National Earth Orientation Service
NIST	National institute of Standards and Technology

NMF	Niell(new) mapping function
NNR	No Net Rotation
NOAA	National Oceanic and Atmospheric Administration
NRA()	National Radio Astronomy observatory
Nuvel	new(tectonic) velocity model
n	refractive index
n	speed of precession in declination
P	precession transformation matrix
$\bar{p}$	extended pressure anomaly
p_0	local pressure anomaly
p_a	general precession
p_{LS}	lunisolar precession
p_{PL}	planetary precession
Q	rotation matrix for terrestrial to celestial transformation
R_E	Earth equatorial radius
$\mathbf{R}_c$	SSB Earth center coordinates
$\mathbf{R}_p$	position of perturbing source in terrestrial system
R_{EG}	distance from Earth to gravitating body G
$R_{dry,wet}$	dry, wet troposphere mapping function
$\hat{\mathbf{r}}$	unit vector in radial direction
r_0	classical electron radius
$\mathbf{r}_0$	station position in terrestrial system
$\mathbf{r}_c$	station position in celestial system
$\mathbf{r}_s$	phase shifted station position
$\mathbf{r}_s$	position of gravitating body s
$\mathbf{r}_t$	station position in terrestrial system
$\mathbf{r}_{1,2}$	SSB position of station 1,2

$\mathbf{r}_{date}$	station position of date
r_{sp}	station radius from spin axis
$S(E)$	slant range factor
S/X	S-band + X-band
SGP	Space Geodesy l'reject
SSB	Solar System Barycenter
$S_{\psi j}$	planetary nutation amplitudes in longitude
$S_{\epsilon j}$	planetary nutation amplitudes in obliquity
TDB	temps dynamique barycentrique
TDT	terrestrial dynamic time
TEMPO	Time and Earth Motion Precision Observations
T_g	galactic rotation period
T_u	time in centuries since J2000
t_0	reference time
t_1	time of arrival of wave front at station 1
t_1'	proper time of arrival of wave front at station 1
t_2	time of arrival of wave front at station 2
t_e	time of emission by source
t_{tr}	light transit time
U	UT1 transformation matrix
U	gravitational potential
USNO	U. S. Naval Observatory
UT1	universal time 1
UTC	universal time coordinated
UTPM	universal time and polar motion
u,v	projections of $\mathbf{B}$ on plane of sky
V	transformation matrix from local to 1{kirtll-fixed frame [Eq. (2.66)]

VEN	Vertical, East, North (local coordinates)
VLBA	Very Long Baseline Array
VLBI	Very Long Baseline Interferometry
V_i	astronomical argument of tidal constituent i
W	atmospheric temperature lapse rate
W	transformation matrix from local to Earth-fixed frame [Eq. (2.65)]
WVR	Water Vapor Radiometer
X	polar motion transformation matrix, x component
x_i, y_i, z_i	cartesian coordinates of station i
x_i^0, y_i^0, z_i^0	cartesian coordinates of station i at reference time
$\dot{x}_i, \dot{y}_i, \dot{z}_i$	cartesian velocities of station i
Y	polar motion transformation matrix, y component
Z	auxiliary angle for precession [Eq. (2.149)]
ZMOA	Zhu, Mathews, Oceans, Anelasticity (nutation model)
α	right ascension
α_E	equation of equinoxes
$\boldsymbol{\beta}_{1,2}$	velocity of station 1, 2
γ_{PPN}	general relativity (Parametrized Post-Newtonian) gamma factor
$\boldsymbol{\Delta}$	total tidal shift in terrestrial coordinate system
$\boldsymbol{\Delta}_{atm}$	atmospheric loading station position shift
Δ_{gd}	ionosphere contribution to group delay
$\boldsymbol{\Delta}_{ocn}$	ocean loading station position shift
Δ_{pd}	ionosphere contribution to phase delay
$\boldsymbol{\Delta}_{pol}$	pole tide station position shift
$\boldsymbol{\Delta}_{sol}$	solid tide station position shift
$\Delta_{x,y,z}$	components of perturbation rotation matrix
ΔG_p	gravitational contribution to coordinate time delay, body p

$\Delta G'_p$	gravitational contribution to proper time delay, body p
ΔU	Earth gravitational potential
$\Delta\Theta$	gravitational deflection
$\Delta\Theta_l$	tidal contribution to UTPM
$\Delta\Theta_{l'}$	companion tidal contribution to UTPM
$\Delta\psi$	nutation in (celestial) longitude
$\Delta\psi^0$	out of phase nutation in longitude
$\Delta\psi^f$	free core nutation in longitude
$\Delta\varepsilon$	nutation in obliquity
$\Delta\varepsilon^0$	out of phase nutation in obliquity
$\Delta\varepsilon^f$	free core nutation in obliquity
$\Delta\tau_s$	source structure contribution to delay
$\Delta\dot{\tau}_s$	source structure contribution to delay rate
δ	declination
$\boldsymbol{\delta}$	tidal displacement in local (VEN) coordinates
δ_i^j	phase of component j of tidal constituent i
$\delta\psi$	empirical correction to longitude
$\delta\varepsilon$	empirical correction to obliquity
$\boldsymbol{\epsilon}_{1,2}$	curved wave front expansion quantities [Eqs. (2.7-2.8)]
$\bar{\varepsilon}$	mean obliquity
ζ	auxiliary angle for precession [Eq. (2.148)]
Θ	auxiliary angle for precession [Eq. (2.150)]
$\Theta_{1,2}$	angular coordinates of Earth rotation axis
$\hat{\boldsymbol{\lambda}}$	unit vector in longitude direction
λ_s	station longitude
μ_p	Gm_p
ν_S	S-band VLBI frequency

ν_X	X-band VLBI frequency
ν_g	electron gyrofrequency
ν_p	electron plasma frequency
ξ_i^j	amplitude of component j of tidal constituent i
ρ	density
$\rho z_{d,w}$	dry, wet zenith troposphere delay
Σ	SSB reference frame
Σ'	geocentric reference frame
τ	geometric delay
τ_c	delay due to clock imperfections
τ_{pd}	phase delay
τ_{sr}	delay due to antenna subreflector motion
τ_{trop}	troposphere delay
$\hat{\phi}$	unit vector in latitude direction
ϕ_s	geodetic station latitude
ϕ_s	structure phase
ψ	phase shift of tidal effect
Ω	longitude of ascending lunar node
Ω	perturbation transformation matrix
ω_E	rotational speed of Earth
ω_f	free core nutation frequency
ω^j_{xyz}	angular velocity of tectonic plate j

1. INTRODUCTION

Astrometry and geodesy have undergone a revolution during the past three decades. This revolution was initiated by the development of interferometry at radio frequencies using

antennas separated by thousands of kilometers in the late 1960s. Subsequently, the "Very Long Baseline Interferometry" (VLBI) technique was refined to reach its present capability of point positioning on the Earth's surface at the centimeter level, and angular positioning for extragalactic radio sources at the milliarcsecond (nanoradian) level. These refinements are expected to continue until insurmountable problems are reached, probably in the submillimeter regime. Geodetic measurements on the Earth's surface have been enormously expanded and densified by satellite techniques during the past five years, but VLBI remains the prime technique for astrometry employing natural radio sources. It is unique in its ability to measure the Earth's orientation in an inertial frame of reference.

An outline of the basic VLBI experiment is sketched in Fig. 1. Two antennas, separated by a baseline $\mathbf{B}$, are aimed at the same intragalactic radio source at the same time, and detect the wave front arriving along unit vector $\hat{\mathbf{k}}$. The digitized signals are recorded on high-density magnetic (video) tapes for a period of several minutes, yielding a total of ≈ 10 gigabits of data. In routine observing sessions, this procedure is repeated several hundred times, for numerous sources, over a 24 hour period. Note that the independent station clocks must be well enough synchronized to permit simultaneous integration when sampling the incoming signal. The signal flux is on the order of 1 Jansky (Jy $= 10^{-26}\,\mathrm{W \cdot m^{-2} \cdot Hz}$), necessitating antennas with large collecting areas, as well as highly sensitive and stable detectors and frequency standards. The observing schedule (station network, locations, observation epochs, and local elevation angles of the selected sources) plays a crucial role in determining the types and precision of parameters that can be extracted in subsequent data analyses. Options become severely limited on baselines approaching an Earth diameter in length, when only a small patch of sky is simultaneously visible from both observing sites.

Normally the tapes that were recorded at the observing stations are later brought together at a special-purpose computer called a correlator. The function of the correlator is to determine the difference in arrival times at the two stations by examining the recorded bit streams and time tags. It generates the "observables" - time delay ($\mathbf{B} \cdot \hat{\mathbf{k}}/c$ in the simplest mode]) and its rate of change, together with statistical estimates of their precision. During

this process of correlation and post-correlation processing the amount of data is compressed by a factor of 10:', from terabytes to kilobytes. A variant of the experimental arrangement that can be used if the two antennas are in sufficiently close proximity is called connected element interferometry (CEI). The stations share frequency standards and data acquisition systems, and the correlation is performed in real time. With the recent explosive advances in communications, computing, and data storage technology, sue]] experiments may become more frequent in the future..

The basic VLBI observable is the difference in arrival times of the wave front at antennas separated by intercontinental distances (baselines). To measure such vector baselines with a precision on the order of 1 cm, the time delays must be known to small fractions of a nanosecond (1 cm = 33 picosecond light travel time.) Such accuracy was made possible by advances in technology, such as development of precise timing standards (1 part in 1014), and data recording techniques that permit data acquisition at rates in excess of 100 Incgabits/second. VLBI is a differential technique in the sense that the basic observable is nearly completely disconnected from the orientation and shape of the Earth. Other techniques must supply this connection externally. Such a link minimally consists of the geocentric position of one of the VLBI observing stations at a given epoch. However, tile observed time delay is relatively insensitive to the geocentric coordinates of this reference station.

Analyses of the VLBI observables of necessity involve an uncommonly broad cross-section of the subfields of physics, ranging from considering tile effects of the Earth's internal structure on its dynamics, to the tectonic plate motions and numerous terrestrial tidal effects. through quantification of turbulence in the atmosphere, to description of general relativistic bending of tile paths of radio signals traveling from the distant sources. With the exception of gravimetric and oceanographic experiments, VLBI is perhaps the most demanding technique for various aspects of global Earth models. It therefore provides results that are used in numerous related fields. While extension of experiments to platforms in Earth orbit and elsewhere in the Solar system is in planning stages (Burke, 1991), the present review

is limited to Earth-based VLBI. A large fraction of the necessary modeling is common to VLBI and the newer satellite techniques. For these reasons, it is important to review the complete details of current modeling of the VLBI observables. Following the principle that the accuracy of a theoretical model should exceed the accuracy of the experiments which it interprets by at least an order of magnitude, the VLBI model should be complete at the 1 ps level. This requirement is currently not satisfied for a number of parts of the model. As experimental techniques are refilled, possibly to improve the accuracy by another order of magnitude, numerous aspects of the model will need to be re-examined.

Each of the three basic aspects of a VLBI measurement (source, intervening medium, and receiver) imposes limits to VLBI resolution and accuracy that are of comparable magnitude. Two such limits are presently clue to incomplete modeling of the structures and time-dependent behavior of both the radio sources and receiving antennas. They can both amount to tenths of a milliarcsecond (mas) (1 nrad) or several mm. For day-long Earth-based measurements, the dominant limit is due to the transmission medium: commonly used models of atmospheric propagation can be incomplete at nearly the 1-cm level. in fact, present troposphere modeling is probably less accurate than the VLBI observables. Details of the tidal motions of the Earth's surface have also not been fully characterized at the mm level. For longer periods (on the order of 1 year), aperiodic time-dependent processes come into play. At present, these are also not *apriori* well enough understood at the mm or nrad level. Improved models of the Earth's tidal response and atmosphere, the physical processes in quasars, and the mechanical response of large antenna structures, will be required to realize the full potential accuracy of the VLBI technique. It is hoped that this review will provide a good foundation for such model extensions.

The first step in analysis of a VLBI experiment is the correlation of the random noise bit streams recorded by the receiving antennas looking at the same radio source, in order to form the two observables for each baseline. As indicated in Fig. 1, this is performed by bringing together the magnetic tapes recorded by the individual stations at a correlator. Several such installations are presently operating in the U.S.A. (Haystack Observatory,

JPL/Caltech, USNO, VLBA), Germany (Bonn), and Japan (Kashima). Post-correlation software then generates the observables and their error estimates from the raw correlator output (Lowe, 1992). Under routine conditions, the uncertainties in the delay observables produced by these correlators are on the order of 10 picoseconds. Numerous aspects of hardware, instrumentation, and software contribute to this limit (Rogers, 1991).

In applications of radio interferometry to geodynamics and astrometry, the values of group delay and phase delay rate obtained from observations of many different radio sources are processed by a multiparameter least-squam estimation algorithm to extract the desired mode.1 parameters. As the accuracy of the observables improves, increasingly complete models for the delays and delay rates are being developed. Modeling is inextricably linked to the software used for data analyses in these experiments. This report describes the current status of these delay models, predominantly based on their implementation in the multiparameter estimation code "Masterfit/Modest". Its foundation was laid by J. G. Williams (1970a), who also developed many of the original algorithms. Software development has continued at the Jet }'repulsion Laboratory (J]'],) since the 1970s (Fanselow, 1983; Sovers and Jacobs, 1994). Independent code of similar scope and ancestry is the "Calc/Solve" package (GSFC, 1981) used in the National Aeronautics and Space Administration (NASA) CrustalDynamics and Space Geodesy Projects (CDP and SIG}'), National Oceanic and Atmospheric Administration (NOAA) International Radio Interferometric Surveying (I ItIS), and National Earth Orientation Service (NEOS) analyses. This is an outgrowth of the original algorithms of Hinteregger *et al.* (1972) and Robertson (1 975), and has been evolving at the Goddard Space Flight Center (GSFC). It has undergone numerous mutations over the years, with the consequence that there now also exist at least three related, but not identical, packages used for VLBI analyses in Germany (Campbell, 1988), Japan (Kunimori *et* al., 1 993), and Spain (Zarraoa *et al., 1 W).* More recently, independent code has been developed in Norway (Andersen, 1995), France (Gontier, 1992), and Ukraine (Yatskiv *et al.*, 1991). There have been limited comparisons between the various software packages (Sovers and Ma, 1985; Gontier, 1992; Rius *et al.*, 1992). Such comparisons have notably resulted in

a fundamental revision of the CALC relativity modeling algorithm (Ryan, 1989).

The history of VLBI can be traced from the first interferometric observations by the NRAO-Arecibo group (Bare *et al.*, 1967) at 0.6 GHz on a 220-km baseline, the MIT-NRAO group (Moran *et al.*, 1967; 1.7 GHz, 845 km), and the Canadian LBI group (Broten *et* al., 1967; 0.4 GHz, 3074 km). Early work in geodesy, astrometry, and clock synchronization) was done in 1969 (Hinteregger *et al.*, 1972), yielding accuracies in distances of 2--5 meters, and in source positions on the order of 1 arc second. A few years later, Shapiro (1 976) reviewed the analysis and information content of geodetic VLBI experiments. Some Ph.D. dissertation of the period arc those of Whitney (1974), Robertson (1975) and Ma (1978). 1,argc-scale international cooperation began in 1979 with the establishment of the Crustal Dynamics Project (CDP) by NASA (Boswor th, Coates, and Fischetti, 1993).

Some references which provide an introduction to the principles of very long baseline interferometry are the book by Thompson, Moran, and Swenson (1 986), the aforementioned review by Shapiro (1976), and two reports by Thomas (1 %S1, 1987). Additional background material is provided by the recent review of geophysical VLBI applications by Robertson (1991), and in more detail and more recently, in the three-volume compilation that summarims accomplishments of N'ASA's Crustal Dynamics Project during the past decade (Smith and Turcotte, 1993). Various periodic reviews, including the quadrennial IUGG geodesy reports (Clark, 1979; Carter, 1 983; Ray, 1 991), IERS annual reports (Paris Observatory, 1995a), and yearly reports on CDP results (Ma, Ryan and Caprette, 1992) are also good sources of detailed information concerning current VLBI techniques and results. The International Earth Rotation Service (IERS) periodically publishes a compilation of standard models recommended for analyses of space geodetic data (IERS, 1992, 1995 b). in large part, the model description in the Present paper is in agreement with the specifications of these "IERS Standards".

The interferometric delay model is the sum of four major model components: geometry, clock, troposphere, and ionosphere. Sections 11 through V of this review present the best current models of these components. The longest section (11) deals with the purely

geometric portion of the delay and considers time definitions, tidal and source structure effects, coordinate frames, Earth orientation (universal time and polar motion), nutation, precession, Earth orbital motion, wave front curvature, gravitational bending, and antenna offsets. Sections III and IV discuss the non-geometrical (clock and atmosphere) components of the model. Section V describes the technique used to obtain the delay rate model from the delay model. Section VI gives the current values of physical constants used in VLBI modeling, while Section VII outlines model improvements that we anticipate to be required by more accurate data in the future.

The most convenient units in geodetic. VLBI are millimeters, picosm.ends, and nanoradians. The first two are connected by the speed of light = 299792458 m/s = 1 mm/3 ps, and will be used interchangeably. Most commonly for the purposes of illustration, a 10,000-km baseline will be considered. A length change of 1 cm on such a baseline is equivalent to an angular change of 1 nrad (1 part per billion, ppb); thus the second common equivalence is 10 mm/nrad.

II. GEOMETRIC DELAY

The geometric delay is the difference in time of arrival of a signal at two geometrically separate points which would be measured by perfect instrumentation, perfectly synchronized, if there were a perfect vacuum between the observed extragalactic or Solar-System source and the Earth-based instrumentation. For Earth-fixed baselines, this delay is limited to the light time of one Earth radius (20 milliseconds) by non-transparency of the Earth. It can change rapidly (by as much as 3 μs per second) as the Earth rotates. While VLBI experiments are occasionally carried out with more than ten participating stations, the correlator generates observable delays aud their time rates of change independently for each baseline connecting every pair of stations. Without loss of generality, the delay model can thus be developed for a single baseline involving only two stations. Such a development will be presented here. In general the geometric component is by far the largest component of the observed delay.

The main complexity of this portion of the model arises from the numerous coordinate transformations that are necessary to relate the reference frame used for locating the radio sources to the Earth-fixed reference frame in which the station locations are represented.

In the following we will use the term "celestial reference frame" to denote a reference frame in which there is no net proper motion of the extragalactic radio objects which are observed by the interferometer. This is only an approximation to some truly "inertial" frame. Currently, this celestial frame implies a Solar-System-barycentric, equatorial frame with the equator and equinox of 2000 January 1.5 (J2000) as defined by the 1976 International Astronomical Union (1 AU) conventions, including the 1980 nutation series (Seidelmann, 1982; Kaplan, 1981). In this equatorial frame, some definition of the origin of right ascension must be made. The right ascension is nearly arbitrary (neglecting higher-order Solar System effects). It differs by a simple rotation from any other definition. The important point is that consistent definitions must be used throughout the model development. The need for this consistency may soon lead to a definition of the origin of right ascension via the planetary ephemerides, with interferometric observations of both natural radio sources and spacecraft, at planetary encounters connecting the planetary and the radio reference frames (Folkner *et al.*, 1994; Newhall *et al.*, 1986).

Unless otherwise stated, we will mean by "terrestrial reference frame" some reference frame tied to the mean surface features of the Earth. The most common such frame is a right-handed version of the Conventional International Origin (CIO) reference system with the pole defined by the 1903.0 pole, which we use here. In practice, the tie is realized by defining the position of one of the interferometric observing stations, and then determining the positions of the other stations under this constraint. For example, in Deep Space Network (DSN) experiments, the reference position is generally Deep Space Station (DSS) 15 at the Goldstone, California tracking complex. This constraint requires that the determinations of Earth orientation agree on the average with the International Earth Rotation Service (IERS) (1995a) [and its predecessor, Bureau International de l'Heure (BIH) (1983)] measurements of the Earth's orientation over some substantial time interval ($\approx$ years). Such a procedure,

or some functional equivalent, is necessary to tie the measurement to the Earth, since the interferometer is sensitive only to the baseline vector. With the exception of minor tidal and tropospheric effects, the VLBI technique does not have any preferred origin relative to the structure of the Earth. The rotation of the Earth does, however, provide a preferred direction in space which can be associated indirectly with its surface features.

In contrast, geodetic techniques which involve the use of artificial satellites or the Moon are sensitive to the center of mass of the Earth as well as its spin axis. 'Thus, such techniques require only a definition of the origin of longitude. Laser ranging to the retroreflectors on the Moon allows a realizable practical definition of a terrestrial frame, accurately positioned relative to a celestial frame which is tied to the planetary ephemerides (Folkner *et al.*, 1994). The required collocation of the laser and VLBI stations is being provided by Global Positioning Satellite (GPS) measurements of baselines between VLBI and laser sites starting in the late 1980s (*e.g.*, Ray *et al.*, 1991). Careful definitions and experiments of this sort are required to realize a coordinate system of centimeter accuracy.

Except for subcentimeter relativistic complications caused by the locally varying Earth potential (as discussed below), construction of the VLBI model for the observed delay can be summarized in 7 steps as:

1. Specify the proper locations of the two stations as measured in an Earth-fixed frame at the time that the wave front intersects station 1. Let this time be the proper time t_1' as measured by a clock in the Earth-fixed frame.

2. Modify the station locations for Earth-fixed effects such as solid Earth tides, tectonic motion, and other local station motion.

3. Transform these proper station locations to a geocentric celestial coordinate system with its origin at the center of the Earth, but moving with the Earth. This is a composite of 12 separate rotations, represented by a rotation matrix $Q(t)$.

4. Perform a Lorentz transformation of these proper station locations from the

geocentric- celestial frame to a frame at rest relative to the center of mass of the Solar System, and rotationally aligned with the celestial geocentric frame.

5. In this Solar-System-barycentric (SSB) frame, compute the proper time delay for the passage of the specified wave front from station 1 to station 2. Correct for source structure. Add the effective change in proper delay caused by the differential gravitational retardation of the signal within the Solar system.

6. Perform a Lorentz transformation of this SSB geometric delay back to the celestial geocentric frame moving with the Earth. This produces the adopted model for the geometric portion of the observed delay.

7. To this geometric delay, acid the contributions clue to clock offsets, to ropospheric delays, and to the effects of the ionosphere on the signal (see Sectic 11s 111 and IV).

As indicated in step 5, the initial calculation of delay is carried out in a frame at rest relative to the center of mass of the Solar System (SSB frame.) First, however, steps 1 through 4 are carried out in order to relate proper locations in the Earth-fixed frame to corresponding proper locations in the SSB frame. Step 4 in this process transforms station locations from the geocentric celestial frame to the SSB frame. This step incorporates sl)ccial-relativistic effects to all orders of the velocity ratio v/c. In the presence of gravity, this transformation can be viewed as a special relativistic transformation between proper coordinate of two local frames (geocentric and SSB) in relative motion. For both frames, the underlying gravitational potential can be taken approximately as the suIn of locally constant potentials caused by all masses in the Solar System. The complications caused by small local variations in the Earth's potential are discussed below. initial proper delay is then computed (step 5) in the SS11 frame on the basis of these SSB station locations and an *a priori* SSB source location. A small ~)ro~xv-delay correction is then applied to account for the differential gravitational retardation introduced along the two ray paths through the

Solar System, including retardation by the Earth's gravity. A final Lorentz transformation including all orders of v/c then transforms the corrected SSB proper delay to a model for the observed delay in the geocentric reference frame.

Since the Earth's gravitational potential varies slightly across the Earth ($\Delta U_E/c^2 \approx$ 3.5 x 10-10 from center to surface), the specification of proper distance is not as straightforward with respect to the Earth's potential as it is with respect to the essentially constant potentials of distant masses. To overcome this difficulty, VLBI-derived station locations are now customarily specified in terms of the "TDT spatial coordinates" that are used in Earth-orbiter models. A proper length that corresponds to a modeled baseline can be obtained through appropriate integration of the local metric (Shahid-Saless *et al.*, 1991), Such proper lengths deviate slightly ($\leq$ 3 mm) from baselines modeled on the basis of the TDT convention in the worst case (a full Earth diameter). In practice, such a conversion is not necessary if baseline measurements obtained by different investigators are reported in terms of TDT spatial coordinates.

The current model has been compared (Thomas, 1991; Treuhaft, 1991) with the "1-picosecond" relativistic model for VLBI delays developed by Shahid-Saless *et al.* (1 991). When reduced to the same form, the model presented here is identical to that model at the picosecond level, term by term, with one exception. Treuhaft and Thomas (1 991) show that a correction is needed to the Shahid-Saless *et al.* SSB system modeling of the atmospheric delay. This correction changes the Shahid-Saless *et al.* result by as much as 1 O picoseconds. The remainder of this section provides the details for the first six steps of the general outline above.

A. Time interval for the arrival of a wave front at two stations

The fundamental part of the geometric model is the calculation (step 5 above) of the time interval for the. passage of a wave front from station 1 to station 2. This calculation is actually performed in a coordinate frame at rest relative to the center of mass of the Solar

System. This part of the model is presented first to provide a context for the subsequent sections, all of which are heavily involved with the details of time definitions and coordinate transformations. We will use the same subscript and superscript notation which is used in Section II.F to refer to the station locations as seen by an observer at rest relative to the center of mass of the Solar System.

First, we calculate the proper time delay that would be observed if the wave front were planar. This calculation is next generalized to a curved wave front, and finally we take into account the incremental effects which result from the wave front propagating through the various gravitation] potential wells in the Solar System.

1. Plane wave front

Consider the case of a plane wave moving in the direction, $\hat{\mathbf{k}}$, with station 2 having a mean velocity, $\boldsymbol{\beta}_2$, as shown in Fig. 2. As mentioned above, distance and time are to be represented as proper coordinates in the SSB frame. The speed of light c is set equal to 1 in the following formulation. The proper time delay is the time it takes the wave front to move the distance 1 at speed c. This distance is the sum of the two solid lines perpendicular to the wave front in Fig. 2:

$$t_2^* - t_1 = \hat{\mathbf{k}} \cdot [\mathbf{r}_2(t_1) - \mathbf{r}_1(t_1)] + \hat{\mathbf{k}} \cdot \boldsymbol{\beta}_2 [t_2^* - t_1] \tag{2.1}$$

where the superscript * serves to emphasize that station 2 has moved since t_1. The second term represents the distance that station 2 moves before receiving the signal at t_2^*. This leads to the following expression for the geometric delay:

$$t_2^* - t_1 = - \frac{\hat{\mathbf{k}} \cdot [\mathbf{r}_2(t_1) - \mathbf{r}_1(t_1)]}{1 - \hat{\mathbf{k}} \cdot \boldsymbol{\beta}_2} \tag{2.2}$$

The baseline vector, $\mathbf{r}_2(t_1) - \mathbf{r}_1(t_1)$, is computed on the basis of proper station locations calculated according to Eq. (2.1 78) in Sec. II.F.

2. Curved wave front

In the case of a signal generated by a radio source within the Solar System it is necessary to include the effect, of the curvature of the wave front. As depicted in Fig. 3, let a source irradiate two Earth-fixed stations whose positions are given by $\mathbf{r}_{1,2}(t)$ relative to the Earth's center. The position of the Earth's center, $\mathbf{R}_c(t_1)$, as a function of signal reception time, t_1, at station 1 is measured relative to the position of the emitter at the time, t_e, of emission of the signal received at time t_1. While this calculation] is actually done in the Solar System barycentric coordinate system, the development that follows is by no means restricted in applicability to that frame.

Suppose that a wave front emitted by the source at time t_e reaches station 1 at time t_1 and arrives at, station 2 at time t_2^*. The geometric delay in this frame will be given by:

$$\tau = t_2^* - t_1 = |\mathbf{R}_2(t_2^*)| - |\mathbf{R}_1(t_1)| \tag{2.3}$$

where all distances are again measured in units of light travel time. If we approximate the velocity of station 2 by

$$\boldsymbol{\beta}_2 = \frac{\mathbf{R}_2(t_2^*) - \mathbf{R}_2(t_1)}{t_2^* - t_1} \tag{2.4}$$

and use the relation (i=1,2)

$$\mathbf{R}_i(t_1) = \mathbf{R}_c(t_1) + \mathbf{r}_i(t_1) \tag{2.5}$$

we obtain:

$$\begin{aligned} \tau &= |\mathbf{R}_c(t_1) + \mathbf{r}_2(t_1) + \boldsymbol{\beta}_2\tau| - |\mathbf{R}_c(t_1) + \mathbf{r}_1(t_1)| \\ &= R_c(t_1)\ [\ |\widehat{\mathbf{R}}_c + \boldsymbol{\varepsilon}_2| - |\widehat{\mathbf{R}}_c + \boldsymbol{\varepsilon}_1|\ ] \end{aligned} \tag{2.6}$$

where

$$\boldsymbol{\varepsilon}_2 = \frac{\mathbf{r}_2(t_1) + \boldsymbol{\beta}_2\tau}{R_c(t_1)} \tag{2.7}$$

and

$$\varepsilon_1 = \frac{\mathbf{r}_1(t_1)}{R_c(t_1)} \tag{2.8}$$

For ε_1 and $\varepsilon_2 \leq 10^{-4}$, only terms of order ε^3 need to be retained in expanding the expression for τ in Eq. ('2,6), if the computer representation employs sixteen significant decimal digits. This gives:

$$\tau = \frac{\widehat{\mathbf{R}}_c \cdot [\mathbf{r}_2(t_1) - \mathbf{r}_1(t_1)]}{[1 - \mathbf{R}_c \cdot \boldsymbol{\beta}_2]} + \frac{R_c \Delta_c(\tau)}{2\,[1 - \widehat{\mathbf{R}}_c \cdot \boldsymbol{\beta}_2]} \tag{2.9}$$

where to order ε^3

$$\Delta_c(\tau) = [\varepsilon_2^2 - \varepsilon_1^2] - [(\widehat{\mathbf{R}}_c \cdot \boldsymbol{\varepsilon}_2)^2 + (\widehat{\mathbf{R}}_c \cdot \boldsymbol{\varepsilon}_1)^2 + (\widehat{\mathbf{R}}_c \cdot \boldsymbol{\varepsilon}_2)^3 - (\widehat{\mathbf{R}}_c \cdot \boldsymbol{\varepsilon}_2)\varepsilon_2^2 - (\widehat{\mathbf{R}}_c \cdot \boldsymbol{\varepsilon}_1)^3 + (\widehat{\mathbf{R}}_c \cdot \boldsymbol{\varepsilon}_1)\varepsilon_1^2] \tag{2.10}$$

The first term in Eq. *(2.9)* is just the plane wave approximation, *i.e.*, as $R_c \rightarrow$ cm, $\widehat{\mathbf{R}}_c \rightarrow \hat{\mathbf{k}}$, with the second term in brackets in Eq. (2.1 O) approaching zero as r^2/R_c. Given that the ratio of the first term to the second term is $\approx r/R$, wave front curvature is not calculable using sixteen-decimal-digit arithmetic if $R > 10]6 \times r$. For Earth-fixed baselines that are as long as an Earth diameter, requiring that the effects of curvature be less than 1 ps $\approx$ 0.3 mm implies that the above formulation [Eq. (2.10)] must be used for $R < 3 \times 10^{14}$ km, or approximately 30 light years. At the same accuracy level, fourth and higher order terms in ε become important for R <2 x 105 km, or approximately inside the Moon's orbit. Fukushima (1994) has presented a formulation which should be applicable for Earth-based VLBI with radio sources as close as the Moon.

The procedure for the solution of Eq. (2.9) is iterative for ε <10--4, using the following:

$$\tau_n = \tau_0 + \frac{R_c \Delta_c(\tau_{n-1})}{2[1 - \mathbf{R} \cdot \boldsymbol{\beta}_2]} \tag{2.11}$$

where

$$\tau_0 = \tau_{plane\ wave} \tag{2.12}$$

For ε > 10-4, directly iterate on the equation (2.6) itself, using the procedure:

$$\tau_n = R_c|\widehat{\mathbf{R}}_c + \boldsymbol{\varepsilon}_2(\tau_{n-1})| - R_c|\widehat{\mathbf{R}}_c + \boldsymbol{\varepsilon}_1| \tag{2.13}$$

where again τ_0 is the plane wave approximation.

3. Gravitational delay

Because a light signal propagating in a gravitational potential is retarded relative to its motion in field-free space, the computed value for the differential time of arrival of the signals at $\mathbf{r}_1(t_1)$ and $\mathbf{r}_2(t_2^*)$ must be corrected for gravitational effects. Gravitational potential effects and curved wave front effects are calculated independently of each other since the former are a small perturbation ($\approx$ 8.5 microradians or $\leq$ 1."75), even for Sun-grazing rays.

The relativistic light travel time was first derived by Tausner (1 966) and Holdridge (1967), and incorporated into the JPL orbit determination software by Moyer (1971). For the (exaggerated) geometry illustrated in Fig. 4, the required correction to *coordinate* time delay due to the pth gravitating body is given by Moyer as:

$$\Delta_{Gp} = \frac{(1 + \gamma_{PPN})\mu_p}{c^3} \left[\ln \left[\frac{r_s + r_2(t_2^*) + r_{s2}}{r_s + r_2(t_2^*) - r_{s1}} \right] - \ln \left[\frac{r_s + r_1(t_1) + r_{s1}}{r_s + r_1(t_1) - r_{s1}} \right] \right] \qquad (2,14)$$

where r_{si} is defined as:

$$r_{si} = |\mathbf{r}_i(t_i) - \mathbf{r}_s(t_e)| \qquad (2.15)$$

Here γ_{PPN} is the γ factor in the parametrized post-Newtonian gravitational theory (e.g., Misner *et al.*, 1 973). For general relativity, $\gamma_{PPN} = 1$, However, γ_{PPN} can be allowed to be an estimated parameter to permit experimental tests of general relativity. Setting $\gamma_{PPN} = -1$ gives the option of "turning off" the effects of general relativity on the estimate of the delay, which proves useful for software development. The gravitational constant, μ_p, is

$$\mu_p = Gm_p \qquad (2.16)$$

where G is the universal gravitational constant, and m_p is the mass 0f body p. A higher-order term ($\propto \mu_p{}^2/c^5$) contributes to Δ_{Gp} only for observations extremely close to the Sun's limb (IERS, 1992).

Depending on the particular source-receiver geometry in a VLBI experiment, a number of approximations are possible for the correction Δ_{Gp} of Eq. (2.14). Dropping the time arguments in Eq. (2.14), we have:

$$\Delta_{Gp} = \frac{(1+\gamma_{PPN})\mu_p}{c^3} \cdot \ln\left[\left[\frac{r_s + r_2 + r_{s2}}{r_s + r_1 + r_{s1}}\right]\left[\frac{r_s + r_1 - r_{s1}}{r_s + r_2 - r_{s2}}\right]\right] \tag{2.17}$$

This formulation is appropriate for tile most genera] geometry, in which $r_s \approx r_i \approx r_{si}$. For the practical case of ltartl-based VLBI with distant sources and closely spaced VLBI receivers, however, $|\mathbf{r}_2 - \mathbf{r}_1|/r_1 \to 0$, $r_i/r_s \to 0$. The gravitational time delay Δ_{Gp} may then be expanded in terms Of $r_i/r_s, r_{si}/r_s$. Making use of the relationsl ip

$$r_{si} = [\mathbf{r}_s^2 - 2\mathbf{r}_s \cdot \mathbf{r}_i + \mathbf{r}_i^2]^{1/2} \approx r_s - \mathbf{r}_i \cdot \hat{\mathbf{r}}_s \tag{2.18}$$

leads to

$$\Delta_{Gp} = \frac{(1+\gamma_{PPN})\mu_p}{c^3} \cdot \ln\left[\frac{r_1 + \mathbf{r}_1 \cdot \hat{\mathbf{r}}_s}{r_2 + \mathbf{r}_2 \cdot \hat{\mathbf{r}}_s}\right] \tag{2.19}$$

for $r_i/r_s \to o$.

If we further require that $|\mathbf{r}_2 - \mathbf{r}_1|/r_1 \to 0$, and make use of

$$\mathbf{r}_2 = \mathbf{r}_1 + \Delta\mathbf{r} \tag{2.20}$$

then:

$$\begin{aligned} r_2 + \mathbf{r}_2 \cdot \hat{\mathbf{r}}_s &= r_1\left[1 + 2\,\hat{\mathbf{r}}_1 \cdot \Delta\mathbf{r}/r_1 + (\Delta\mathbf{r}/r_1)^2\right]^{1/2} + \mathbf{r}_1 \cdot \hat{\mathbf{r}}_s + \Delta\mathbf{r} \cdot \hat{\mathbf{r}}_s \\ &\approx r_1\left(1 + \hat{\mathbf{r}}_1 \cdot \Delta\mathbf{r}/r_1\right) + \mathbf{r}_1 \cdot \hat{\mathbf{r}}_s + \Delta\mathbf{r} \cdot \hat{\mathbf{r}}_s \end{aligned} \tag{2.21}$$

In the limit of $\Delta\mathbf{r}/r_1 \to 0$:

$$r_2(1 + \mathbf{r}_2 \cdot \hat{\mathbf{r}}_s) \to r_1(1 + \mathbf{r}_1 \cdot \hat{\mathbf{r}}_s) + \Delta\mathbf{r} \cdot (\hat{\mathbf{r}}_1 + \hat{\mathbf{r}}_s) \tag{2.22}$$

substituting into Eq. (2.19) and expanding the logarithm, we obtain:

$$\Delta_{Gp} = -\frac{(1+\gamma_{PPN})\mu_p}{c^3} \cdot \frac{(\mathbf{r}_2 - \mathbf{r}_1) \cdot (\hat{\mathbf{r}}_1 + \hat{\mathbf{r}}_s)}{r_1(1 + \hat{\mathbf{r}}_1 \cdot \hat{\mathbf{r}}_s)} \tag{2.23}$$

Using whichever of these three formulations Eqs. (2.17, 2.19 or 2.23) is computationally appropriate, the correction Δ_{Gp} is calculated for each of the major bodies in the Solar System (Sun, planets, Earth, and Moon). For sources observed in the Galactic plane near

the Galactic center, the immense central mass (on tile order of 10^{11} Sun masses) contributes an additional delay. Assuming a mass concentration of 2/3 in the nucleus and the current est imate of our distance from the center, it can be estimated that the gravitational influence of the Galactic center on electromagnetic signals exceeds that of the Sun by a facto: of ≈40. Geometrically, this causes a bending of 4 arc seconds for ray paths within ≈ 10° of the center (for the closest routinely observed radio source). Because of the relatively slow motion of the Solar System on galactic scales, however, its time variation is extremely slow, and it merely produces a quasi-static distortion] of the sky.

Before the correction Δ_{Gp} can be applied to a proper delay computed according to Eq. (2.2), it must be converted from a coordinate-delay correction to a proper-cle]ay correction appropriate to a near-1';artll frame. For such proper delays, the gravitational correction i s given (e.g., Hellings, 1986) to good approximation by

$$\Delta'_{Gp} = \Delta_{Gp} - (1 + \gamma_{PPN})U\tau \tag{2.24}$$

where τ is the proper delay given by Eq. (2.2), and where U is the negative of the gravi - tational potential of the given mass divided by c^2, as observed in the vicinity of the Earth (U is a positive quantity). The $U\tau$ term is a consequence of the relationshi p of coordinate time to proper time, and the $\gamma_{PPN}U\tau$ term is a conseque nce of the relationshi p of coordinate distance to proper distance,

The total gravitational correction used is:

$$\Delta'_G = \sum_{p=1}^{A'} \Delta'_{Gp} \tag{2.25}$$

where the summation over p is over the h' major bodies in the Solar System. For the Earth, the $(1 + \gamma_{PPN})U\tau$ term in Eq. (2.24) is omitted if one wishes to work in the "'1'1)']' spatial coordinates" that are used in reductions of Earth-orbiter data. The scale factor $(1 + \gamma_{PPN})U$ is approximately 1.97 X $1\,0^{-8}$ for the Sun. A number of other conventions are possible. One of these, which dots not omit the $(1 + \gamma_{PPN})U\tau$ term for the Earth, but evaluates it at the Earth's surface, yields an additional scale factor of 0.14 x 10^{-8}. In either case, the model

delay is decreased relative to the proper delay. Consequently, all inferred "measured" lengths increase by the same fraction relative to proper lengths (i. e., by 19.7 parts per billion and 21.1 ppb in the two cases).

Some care must be taken in defining the positions given by $\mathbf{r}_s$, $\mathbf{r}_2(t_2^*)$, and $\mathbf{r}_1(t_1)$. The origin has here been chosen as the position of the gravitational mass at the time of closest approach of the received signal to that object. The position $\mathbf{r}_s$ of the source relative to this origin is the position of that source at the time, t_e, of the emission of the received signal. Likewise, the position $\mathbf{r}_i(t_i)$ of the ith receiver is its position in this coordinate system at the time of reception of the signal. Even with this care in the definition of the relative positions, we are making an approximation and implicitly assuming that such an approximation is no worse than the approximations used by Moyer (1971) to obtain Eq. (2.14).

Some considerations follow, regarding the use of appropriate times to obtain the positions of the emitter, the gravitational object, and the receivers. For a grazing ray emitted by a source at infinity, using the position of the gravitating body G at the time of reception of the signal at station 1 (t_1) rather than at the time of closest approach of the signal to G (t_c) can cause a substantial error on baselines with dimensions of the Earth, as shown by the following calculation. From Fig. 5, the distance of closest approach, R, changes during the light transit time, t_{tr}, of a signal from a gravitational object at a distance R_{EG} by:

$$\Delta R \approx R_{EG} \cdot \dot{\alpha} \cdot t_{tr} = \dot{\alpha} \cdot R_{EG}^2/c \tag{2.26}$$

where $\dot{\alpha}$ is the time rate of change of the angular position of G as observed from Earth. Since the deflection is:

$$\Theta \approx 2\frac{(1+\gamma_{PPN})\mu_p}{c^3}\left[\frac{c}{R}\right] \tag{2.27}$$

it changes by an amount

$$\Delta\Theta = -\Theta\left[\frac{\Delta R}{R}\right] = -\Theta\left[\frac{\dot{\alpha} R_{EG}^2}{cR}\right] \tag{2.28}$$

during the light transit time.

We consider the two bodies of largest mass in the Solar System: the Sun and Jupiter. For rays that just graze the surfaces, their respective deflections $\Delta\Theta$ are 8470 and 79 nanoradians. From Solar system ephemerides, the barycentric angular velocities $\dot{\alpha}$ are estimated to be $\approx$ 0.05 and 17 nrad/s for the Sun and Jupiter. (The Sun's motion in the barycentric frame has approximately the orbital period of Jupiter, $\approx$12 years, with a radius on the order of the Sun's radius). Using approximate radii and distances from Earth to estimate R_{EG} and Θ, Eq. (2.2S) gives 30 nrad for Jupiter; the corresponding value for the Sun is only 0.05 nrad. For a baseline whose length equals the radius of the Earth, $\delta(\Delta\Theta)R_E$ is thus approximately 0.03 and 20 cm for the Sun and Jupiter, respectively. The effect is much smaller for the Sun in spite of its much larger mass, due to its extremely slow motion in the barycentric frame.

In view of the very rapid decrease of gravitational deflection with increasing distance of closest approach, it is extremely improbable that a random VLBI observation will involve rays passing close enough to a gravitating body for this correction to be of importance. Exceptions are experiments that are specifically designed to measure planetary gravitational bending (e.g., Treuhaft and Lowe, 1991). In order to guard against such an unlikely situation in routine work, and to provide analysis capability for special experiments, it is prudent to perform the transit-time correction for all planets for all observations. To obtain the positions of the gravitational objects, we employ an iterative procedure, using the positions and velocities of the objects at signal reception time. If $\mathbf{R}(t_r)$ is the position of the gravitational object at signal reception time, t_r, then that object's position, $\mathbf{R}(t_a)$, at the time, t_a, of closest approach of the ray path to the object, was:

$$\mathbf{R}(t_a) = \mathbf{R}(t_r) - \bar{\mathbf{V}}[t_r - t_a] \tag{2.29}$$

$$t_r - t_a = |\mathbf{R}_c|/c \tag{2.30}$$

This correction is done iteratively, using the velocity, $\mathbf{V}(t_r)$, as an approximation of the mean velocity, $\bar{\mathbf{V}}$. Because v/c $\approx 10^{-4}$, the iterative solution,

$$\mathbf{R}_n(t_a) = \mathbf{R}(t_r) - |\mathbf{R}_{n-1}(t_a)|\,\mathbf{V}(t_r)/c \tag{2.31}$$

rapidly converges to the required accuracy.

B. Time information

Before continuing with the description of the geometric model, some definitions must be introduced concerning time-tag information in the experiments, and the time units which will appear as arguments below. A general reference for time definitions is the *Explanatory Supplement* (Seidelmann *et al.*, 1992). The epoch timing information in the data is taken from the UTC (Universal Coordinated Time) time tags in the data stream at station 1, UTC_1. This time is converted to Terrestrial Dynamic Time (TDT) and is also used as an argument to obtain au *a priori* estimate of Earth orientation. The conversion consists of the following components:

$$TDT = (TDT - TAI) + (TAI - UTC_{IERS}) + (UTC_{IERS} - UTC_{STD}) + (UTC_{STD} - UTC_1) + UTC_1 \quad (2.32)$$

The four offsets in Eq. (2.32) thus serve to convert the station 1 time tags to TDT. In turn, their meaning is the following:

1. $TDT - TAI$ is 32.184 seconds by definition; TAI (Temps Atomique International) is atomic time.

2. TAI --- UTC_{IERS} is the offset between atomic and coordinated time. The International Earth Rotation Service (IERS), its predecessor, Bureau International de l'Heure (BIH), and Bureau International des Poids et Mesures (BIPM) are the coordinating bodies responsible for upkeep and publication of standard time and Earth rotation quantities. $TAI - UTC_{IERS}$ is a published integer second offset (leap seconds) for any epoch after 1 January, 1972. Prior to that time, it is a more complicated function, which will not be discussed here since normally no observations previous to the mid-1970s are modeled.

3. UTC_{IERS} - UTC_{STD} is the offset in UTC between the coordinated time scales maintained by the IERS (1111' 14) and secondary standards maintained by numerous national organizations. For VLBI stations in the U.S. this secondary standard is that of the National Institute of Standards and Technology (NIST) in Boulder, Colorado. These offsets can be obtained from BIPM Circular T (*e.g.*, BIPM, *1990).*

4. UTC_{STD} - UTC_1 is the (unknown) offset between UTC kept by station 1 and the secondary national standard. This normally amounts to several μs, but may not be precisely known for each experiment. It is a source of modeling error: an error Δt in epoch time causes an error of $\approx B\omega_E \Delta t = 7.3 \times 10^{-6}$ cm per km baseline per μs of clock error, where ω_E is the rotation rate of the Earth (Section VI). For the extreme case of a 10,000 km baseline, however, this amounts to only 0.7 mm per μs clock offset; present-day clock synchronization is usually at least an order of magnitude better, at the hundred-nanosecond level.

A priori UT1--UTC and pole positions are normally obtained by interpolation of the IERS Bulletin A smoothed values. However, any other source of UT1--UTC and pole position could be used provided it is expressed in a left-handed coordinate system (see Section II.E.1). Part of the documentation for any particular set of results needs to include a clear statement of what values of UT1 -- UTC and pole position were used in the data reduction process.

For the Earth model based on the IAU conventions, the following definitions are employed throughout (Kaplan, 1981):

1. Julian date at epoch J2000 = 245 545.0.

2. All time arguments denoted by T below are measured in Julian centuries of 36525 days of the appropriate time relative to the epoch J2000, i.e., $T = (JD$ -- 2451545.0)/36525.

3. For the time arguments used to obtain precession, nutation, or to refer to the Solar system ephemeris, Barycentric Dynamic Time (TDB, Temps Dynamique Barycentrique) is used. This is related to Terrestrial Dynamic Time (TDT, Temps Dynamique Terrestre) by the following approximation which is adequate for analyses of VLBI observations:

$$TDB = TDT + 0.^{s}001658 \sin(g + 0.0167 \sin(g)) \tag{2.33}$$

where

$$g = (357.0528 + 3.5999.^{0}050\ T) \times 2\pi/360^{\circ} \tag{2.34}$$

is the mean anomaly of the Earth in its orbit. A more accurate relation between TDB and TDT is given by Moyer (1981). With a total of 15 terms, it accounts for the major gravitational effects of the planets.

In the future, TDT and TDB will be replaced by two new time scales, TCG and TCB, geocentric and barycentric coordinate time (Fukushima *et al.*, 1986). These will eliminate the necessity for the rescaling of spatial coordinates that was discussed in Section II.A.3.

C. Station locations

Coordinates of the observing stations are expressed in the Conventional International Origin (CIO) 1903.0 reference system, with the reference point for each antenna defined as in Section II.G. The present accuracy level of space geodesy makes it imperative to account for various types of crustal motions. Among these deformations are solid Earth tides, tectonic motions, and alterations of the Earth's surface due to local geological, hydrological, and atmospheric processes. Mismodeled effects will manifest themselves as temporal changes of the Earth-fixed baseline. It is therefore important to model all crustal motions as completely as possible. The current level of mismodeling of these motions is probably one of the leading sources of systematic error (along with the troposphere) in analyses of VLBI data.

Evaluation of the time dependence of station locations is most simply done by estimating a new set of coordinates in the least-squares process for each VLBI observing session. Post-processing software then makes linear fits to these results to infer the time rate of change of the station location. For rigorous interpretation of the statistical significance of the results, care must be taken that the correlations of coordinates estimated at different epochs are accounted for properly. The advantage of this approach is that the contribution of each session to the overall time rate may be independently evaluated, since it is clearly isolated. Also, no model information is imposed on the solution. An alternative second approach is to model long-period tectonic motion directly, and to introduce time rates of change of the station coordinates as parameters. The model is linear, with the Cartesian coordinates of station i at time t expressed as

$$x_i = x_i^0 + \dot{x}_i(t - t_0) \tag{2.35}$$

$$y_i = y_i^0 + \dot{y}_i(t - t_0) \tag{2.36}$$

$$z_i = z_i^0 + \dot{z}_i(t - t_0) \tag{2.37}$$

Here t_0 is a reference epoch, at which the station coordinates are (x_i^0, y_i^0, z_i^0).

1. Tectonic plate motion

As alternatives to estimating linear time dependence of the station coordinates from VLBI experiments, several standard models of tectonic plate motion are available. They all describe the motion as a rotation of a given rigid plate (spherical cap) about its rotation pole on the surface of a spherical Earth. Time dependence of the Cartesian station coordinates of station i which resides on plate j is expressed as

$$x_i = x_i^0 + (\omega_y^j\, z_i^0 - \omega_z^j\, y_i^0)(t - t_0) \tag{2.38}$$

$$y_i = y_i^0 + (\omega_z^j\, x_i^0 - \omega_x^j\, z_i^0)(t - t_0) \tag{2.39}$$

$$z_i = z_i^0 + (\omega_x^j\, y_i^0 - \omega_y^j\, x_i^0)(t - t_0) \tag{2.40}$$

WI](TC $\omega^j_{x,y,z}$ are the angular velocities.

Although these models are based on paleomagnetic data spanning millions of years, they have been found to provide a good quantitative characterization of present-day plate motions, thus attesting to the smooth character of the latter. The first global tectonic motion model is clue'to Minster and Jordan (1978), and was also the first to be used in VLBI analyses. It is denoted AM0-2 in the original paper. More recent models, denoted Nuvel1 and NNR-Nuvel1, are due to DeMets *et al.* (1990) and Argus and Gordon (1991), respectively. In Nuvel1, the Pacific plate is stationary, while NNR-Nuvel1 is based on the imposition of a no-net-rotation (NNR) condition. Inadequate knowledge of the internal mechanics of the Earth makes uncertain any absolute determination of plate rotation relative to the deep interior. Hence the NNR condition is customarily imposed: v x r integrated over the Earth's surface is constrained to be zero (v is the velocity at point r on one of the rigidly rotating tectonic. plates). With some notable exceptions, the Nuvel1 models give rates that arc very close to those of the AM O-2 model. The A M0-2 India plate has been split into two: Australia and India, and there are four additional plates: Juan de Fuca, Philippine, Rivera and Scotia. A recent revision of the paleomagnetic time scale has led to a rescaling of the Nuvel1 rates. These "Nuvel1 A" and "NNR-Nuvel1 A" model rates arc equal to the Nuvel1 and NNR-Nuvel1 rates, respectively, multiplied by a factor of 0.9562 (DeMets *et al.*, 1994). '1'able I shows the angular velocities of the 16 tectonic plates in the NNR-Nuvel1 A model.

2. Tidal station motion

Crustal motions with periodicities ranging from hours to years are known as tidal effects. Many of them produce station displacements that are far larger than those caused by tectonic motions, and need to be included in modeling VLBI observables. The tidal displacements can be classified into several categories, based on the origin of the tide generating forces. In contemporary VLBI models, four such categories arc normally included. in the standard terrestrial coordinate system, these tidal effects modify the station location r. by an amount

$$A = A_{sol} + \Delta_{pol} + \Delta_{ocn} + \Delta_{atm} \qquad (2.41)$$

where the four terms are due to solid Earth tides, pole tide, ocean loading, and atmosphere loading, respectively. Other l';artll-fixed effects (e.g., glacial loading) can be incorporated by extending the definition of A to include additional terms. All four tidal effects are most easily calculated in some variant of a VEN (Vertical, East, North) local geocentric coordinate system. To transform them to the };artll-fixed coordinate frame, the transformation VW, given in the next section, is applied.

a. *Solid Earth tides*

Calculating the shifts of the positions of the observing stations caused by solid Earth tides is rather complicated due to the solid tides' coupling with the ocean tides, and the effects of local geology. Some of these complications are addressed below (e.g., ocean loading.) The isolated simple model of Earth tides is the multipole response model developed by Williams (1970b), who used Melchior (1966) as a reference. Let $\mathbf{R}_p$ be the position of a tide-producing source in the geocentric reference system, and $\mathbf{r}_0$ the station position in the same coordinate system. '1'0 allow for a phase shift (ψ) of the tidal effects from its nominal value of O, the phase-shifted station vector r_s is calculated from r. by applying a matrix L, describing a right-handed rotation through an angle ψ about the Z axis of date, $\mathbf{r}_s = L\mathbf{r}_0$. This lag matrix, L, is:

$$L = \begin{vmatrix} \cos\psi & \sin\psi & 0 \\ -\sin\psi & \cos\psi & 0 \\ 0 & 0 & 1 \end{vmatrix} \qquad (2.42)$$

A positive value of ψ implies that the peak response on an Earth meridian occurs at a time $\delta t = \psi/\omega_E$ after that meridian plane containing r. crosses the tide-producing object, where ω_E is the angular rotation rate of the Earth. No departures from a zero phase shift have been detected: the peak response occurs when the meridian plane containing $\mathbf{r}_s$ also includes $\mathbf{R}_p$.

The idal potential at $\mathbf{r}_s$ due to the perturbing source at $\mathbf{R}_p$ is expressed as

$$U_{tidal} = -\frac{Gm_p}{R_p}\left[\left(\frac{r_s}{R_p}\right)^2 P_2(\cos\theta) + \left(\frac{r_s}{R_p}\right)^3 P_3(\cos\theta)\right]$$
$$= U_2 + U_3 \qquad (2.43)$$

where only the quadrupole and octupole terms have been retained. Here, G is the gravitational constant) m_p is the mass of the perturbing source, P_2 and P_3 are Legendre polynomials, and θ is the angle between $\mathbf{r}_s$ and $\mathbf{R}_p$. While the quadrupole displacements arc on the order of 50 cm, the mass and distance ratios of the Earth, Moon, and Sun limit the octupole terms to a few mm. An estimate of the retardation correction (employing the position of the tide-producing mass al, a time earlier than that of the observation by an amount equal to the ligl]t-travel time) snows that this correction is well below 1 mm, and can therefore be neglected.

In a local geocentric VEN coordinate system on a spherical Earth, the tidal displacement vector $\boldsymbol{\delta}$ is

$$\boldsymbol{\delta} = \sum_i [\, g_1^{(i)}, g_2^{(i)}, g_3^{(i)}]^T \qquad (2.44)$$

where the $g_j^{(i)} (i = 2, 3)$ arc the quadrupole and octupole displacements. The components of $\boldsymbol{\delta}$ arc obtained from the tidal potential as

$$g_1^{(i)} = h_i U_i / g \qquad (2.45)$$

$$g_2^{(i)} = l_i \cos\phi_s \left(\frac{\partial U_i}{\partial \lambda_s}\right)/g \qquad (2.46)$$

$$g_3^{(i)} = l_i \left(\frac{\partial U_i}{\partial \phi_s}\right)/g \qquad (2,47)$$

where $h_i (i = 2, 3)$ arc the vertical (quad rupole and octupole) Love numbers, $l_i (i = 2, 3)$ the corresponding horizontal Love numbers, and λ_s and ϕ_s arc the station longitude and latitude, and g the acceleration due to gravity,

$$g = Gm_E / r_s^2 \qquad (2.48)$$

Using the relation between terrestrial and celestial coordinates,

$$\cos\,\mathrm{O} = \sin\phi_s \sin\delta_p + \cos\phi_s \cos\delta_p \cos(\lambda_s + \alpha_G - \alpha_p) \tag{2.49}$$

with α_p, δ_p the right ascension and declination of the perturbing body, and α_G the right ascension of Greenwich, some algebra produces the following expressions for the quadrupole and octupole components of $\boldsymbol{\delta}$ in terms of the coordinates of the station (x_s, y_s, z_s) and the tide-producing bodies (X_p, Y_p, Z_p):

$$g_1^{(2)} \quad . \quad . \quad . \quad (h_2/g)\sum_p \frac{r_s^2}{R_p^5}\frac{(\mathbf{r}_s \cdot \mathbf{R}_p)^2}{2} \quad \frac{r_s^2 R_p^2}{6} \tag{2.50}$$

$$g_2^{(2)} = (l_2/g)\sum_p \frac{3\mu_p r_s^3}{R_p^5}(\mathbf{r}_s \cdot \mathbf{R}_p)(x_s Y_p - y_s X_p)/\sqrt{x_s^2 + y_s^2} \tag{2.51}$$

$$g_3^{(2)} = (l_2/g)\sum_p \frac{3\mu_p r_s^2}{R_p^5}(\mathbf{r}_s \cdot \mathbf{R}_p)\left[\sqrt{x_s^2 + y_s^2}\, Z_p - \frac{z_s}{\sqrt{x_s^2 + y_s^2}}(x_s X_p + y_s Y_p)\right] \tag{2.52}$$

$$g_1^{(3)} = (h_3/g)\sum_p \frac{\mu_p r_s^2}{2R_p^7}(\mathbf{r}_s \cdot \mathbf{R}_p)\left[5(\mathbf{r}_s \cdot \mathbf{R}_p)^2 - 3r_s^2 R_p^2\right] \tag{2.53}$$

$$g_2^{(3)} = (l_3/g)\sum_p \frac{3\mu_p r_s^3}{2R_p^7}\left[5(\mathbf{r}_s \cdot \mathbf{R}_p)^2 - r_s^2 R_p^2\right](x_s Y_p - y_s X_p)/\sqrt{x_s^2 + y_s^2} \tag{2.54}$$

$$g_3^{(3)} = (l_3/g)\sum_p \frac{3\mu_p r_s^2}{2R_p^7}\left[5(\mathbf{r}_s \cdot \mathbf{R}_p)^2 - r_s^2 R_p^2\right]\left[\sqrt{x_s^2 + y_s^2}\, Z_p - \frac{z_s}{\sqrt{x_s^2 + y_s^2}}(x_s X_p + y_s Y_p)\right] \tag{2.55}$$

where μ_p is the ratio of the mass of the disturbing body, p, to the mass of the Earth, and

$$\mathbf{R}_p = [X_p, Y_p, Z_p]^T \tag{2.56}$$

is the vector from the center of the Earth to that body. The summations are over tide-producing bodies, of which only the Sun and the Moon are normally included. Recent work considers 10W-1CVCI planetary contributions (Hartmann and Soffel, 1994; Hartmann and Wenzel, 1994; Williams, 1995), of which that of Venus appears to be the most important. Mathews *et* al. (1995) have recently re-examined the basic definitions underlying the derivation of the tidal potential. They conclude that the most reasonable definition is

one that uses the reference ellipsoid, and thus implies that the Love numbers have a slight latitude dependence.

The above formulation implicitly assumes that the Love numbers h_i and l_i are independent of the frequency of the tide-gcllcratjillg potential. Proper treatment entails a harmonic expansion of Eqs. (2.50)-(2.55) and use of a different set of h_i, l_i for each frequency component. Presently, only the six largest nearly diurnal components are allowed to have Love numbers that differ from the standard values given in Sec V]. Each harmonic term is denoted by its historical (Darwin) name, if one exists, and the Doodson code (IERS, 1992) (*e.g.*, K_1 and Doodson number = 165555). The Doodson notation classifies the tidal components according to increasing speed. The correction to the Love number scaling the solid tidal radial displacement for the kth harmonic term at station s is given by

$$\delta h_2^{sk} = \delta h_2^k H_k(\sqrt{5/24\pi})\ .3\ \sin\phi_s \cos\phi_s \sin(\lambda_s + \theta_k) \tag{2.57}$$

where δh_2^k is the difference between the nominal quadrupole (h_2) Love number (0.609) and the frequency dependent Love number (Wahr, 1979), H_k is the amplitude of the kth harmonic term in the tide generating expansion from Cartwright and Edden (1973), ϕ_s is the geocentric latitude of the the station, λ_s is the East longitude of the station and θ_k is the kth harmonic tide argument. The Love numbers and tidal amplitudes are listed in 'J'able II.

These optional corrections yield (Naudet, 1994) additional purely vertical station displacements (in mm) of:

$$\psi_1\,(1\ 66554) \quad \delta g_1 = \quad 0.37 \sin 2\phi_s \sin(\lambda_s + \alpha_G + l') \tag{2.58}$$

$$(165565) \quad \delta g_1 = -1.84 \sin 2\phi_s \sin(\lambda_s + \alpha_G - \Omega) \tag{2..59}$$

$$K_1\,(1\ 65555) \quad \delta g_1 = -12.68 \sin 2\phi_s \sin(\lambda_s + \alpha_G) \tag{2.60}$$

$$(165545) \quad \delta g_1 = \quad 0.24 \sin 2\phi_s \sin(\lambda_s + \alpha_G + \Omega) \tag{2.61}$$

$$P_1\,(1\ 63555) \quad \delta g_1 = \quad 1.32 \sin 2\phi_s \sin[\lambda_s + \alpha_G - 2(\Omega + l' - D)] \tag{2.62}$$

$$O_1\ (145555) \quad \delta g_1 = \quad 0.62 \sin 2\phi_s \sin[\lambda_s + \alpha_G - 2(\Omega + l')] \tag{2.63}$$

where $\phi_s, \lambda_s, \alpha_G$ are the station latitude and longitude and Greenwich RA, respectively. The astronomical arguments l', F, D, Ω (mean anomaly of the Sun, mean argument of the latitude of the Moon, mean elongation of the Moon from the Sun, and the mean longitude of the ascending lunar node) are defined in Sec. II.E. These displacements are then summed and the total is used as the first order correction to each station's vertical displacement. Horizontal corrections are presently ignored. Note that the largest correction, the K_1 term, is identical to that already recommended in 1985 by the MERIT standards (Melbourne *et al.*, 1983, 1985).

To convert the locally referenced displacement, $\boldsymbol{\delta}$, which is expressed in the local VEN coordinate system, to the Narth-fixed frame, two rotations must be performed. The first, W, rotates by an angle, ϕ_s (station geodetic latitude), about the y axis to an equatorial system. The scc.end, V, rotates about the resultant z axis by angle, $-\lambda_s$ (station longitude), to bring the displacements into the standard geocentric coordinate system. The result is

$$\boldsymbol{\Delta}_{sol} = V W \boldsymbol{\delta} \tag{2.64}$$

where

$$W = \begin{pmatrix} \cos\phi_s & 0 & -\sin\phi_s \\ 0 & 1 & 0 \\ \sin\phi_s & 0 & \cos\phi_s \end{pmatrix} \tag{2.65}$$

and

$$V = \begin{vmatrix} \cos\lambda_s & -\sin\lambda_s & 0 \\ \sin\lambda_s & \cos\lambda_s & 0 \\ 0 & 0 & 1 \end{vmatrix} \tag{2.66}$$

The product of these two matrices

$$VW = \begin{pmatrix} \cos\lambda_s\cos\phi_s & \sin\lambda_s & -\cos\lambda_s\sin\phi_s \\ \sin\lambda_s\cos\phi_s & \cos\lambda_s & -\sin\lambda_s\sin\phi_s \\ \sin\phi_s & 0 & \cos\phi_s \end{pmatrix} \tag{2.67}$$

uses the geodetic latitudes

$$\phi_s = \tan^{-1}\left\{z_s/[r_{sp_s}(1-1/f)^2]\right\} \tag{2.68}$$

where f is the geoid flattening factor and $r_{sp_s} = (x_s^2 + x_s^2)^{1/2}$ is the station radius from the Earth's spin axis. The difference between geodetic and geocentric latitude can affect this model on the order of (tidal effect)/(flattening factor) $\approx$ 1 mm.

b. Pole tide

One of the significant secondary tidal effects is the displacement of a station by the elastic response of the Earth's crust to shifts in the spin axis orientation. The spin axis is known to describe a circular path of $\approx$ 20-m diameter at the north pole with an irregular period somewhat in excess of one year. Depending on where the spin axis pierces the crust at the instant of a VLBI measurement, the "pole tide" displacement will vary from time to time. This effect must be included if centimeter accuracy is desired.

---- Yoder (1984) and Wahr (1985) derived an expression for the displacement of a point at geodetic latitude ϕ_s, longitude λ_s due to the pole tide:

$$\begin{aligned}\boldsymbol{\delta} = -\frac{\omega_E^2 R}{g}[&\sin\phi_s\cos\phi_s(p_x\cos\lambda_s + p_y\sin\lambda_s)\ h\ \hat{\mathbf{r}} \\ &+ \cos 2\phi_s(p_x\cos\lambda_s + p_y\sin\lambda_s)\ l\ \hat{\boldsymbol{\phi}} \\ &+ \sin\phi_s(-p_x\sin\lambda_s + p_y\cos\lambda_s)\ l\ \hat{\boldsymbol{\lambda}}]\end{aligned} \tag{2.69}$$

Here ω_E is the rotation rate of the Earth, R the radius of the (spherical) Earth, g the acceleration clue to gravity at the Earth's surface, and h and l the customary Love numbers. Displacements of the instantaneous spin axis from the long-term average spin axis along the x and y axes are given by p_x and p_y. Eq.(2.69) shows how these map into station displacements along the unit vectors in the radial ($\hat{\mathbf{r}}$), latitude ($\boldsymbol{\phi}$), and longitude ($\boldsymbol{\lambda}$) directions. With the standard values ω_E = 7.292 x 10^{-5} rad/sec, R = 6378 km, and g = 980.665 cm/sec^2, the factor $\omega_E^2 R/g$ = 3.459 x 10^{-3}. Since the maximum values of p_x and p_y are on the order of 10 meters, and $h \approx$ 0.6, $l \approx$ 0.08, the maximum displacement due to the pole tide is 1 to 2 cm, depending on the location of the station (ϕ_s, λ_s).

'] 'he locally referenced displacement $\boldsymbol{\delta}$ is transformed via the suitably modified transformation [Eq. (2.67)] to give the displacement $\boldsymbol{\Delta}_{pol}$ in the standard geocentric coordinate system.

c. *Ocean loading*

This section is concerned with another of the secondary tidal effects, namely the elastic response of the Earth's crust to ocean tides, which moves the observing stations to the extent of a few cm. Such effects are commonly called "ocean loading." The currently standard model of ocean loading is general enough to accommodate externally derived parameters describing the tide phases and amplitudes at a number of frequencies. The locally referenced three-dimensional displacement $\boldsymbol{\delta}$ (components δ_j) clue to ocean loading is related to the frequencies (ω_i), amplitudes (ξ_i^j), and phases (δ_i^j). In a local Cartesian coordinate system (usually with unit vectors in the vertical, East, and North directions) at time t,

$$\delta_j = \sum_{i=1}^{N} \xi_i^j \cos(\omega_i t + V_i - \delta_i^j) \qquad (2.70)$$

The quantities ω_i (frequency of tidal constituent i) and V_i (astronomical argument of constituent i) depend only on the ephemeris in formation (positions of the Sun and Moon). The algorithm of Goad (IERS, 1989) is usually used to calculate these two quantities. On the other hand the amplitude ξ_i^j and Greenwich phase lag δ_i^j of component j are determined by the particular model assumed for the deformation of the Earth. The local displacement vector is transformed via Eqs. (2.67) and (2.64) to the displacement $\boldsymbol{\Delta}_{ocn}$ in the standard geocentric frame.

In present models, the local displacements and their phases, ξ_i^j and δ_i^j, are calculated from an oc.call tidal loading model of choice at as many as 11 frequencies. The eleven components arc denoted, in standard notation: K_2, S_2, M_2, and N_2 (all with approximately 12-110111 periods), K_1, P_1, O_1, Q_1 (24 h), M_f (14 day), M_m (monthly), and S_{sa} (semiannual).

Three choices of ocean loading models have been used over the years. They differ in the displacements that are calculated and the number of components that are considered,

as well as in the numerical values that they yield for the ξ_i^js and δ_i^js. Scherneck's results (1 983, 1 991) are the most complete in the sense of considering both vertical and horizontal displacements and all eleven tidal components. They have now been adopted for the IERS standards (1 992), and compose the default ocean loading model. Goad's model (1983) was adopted in the MERIT and early IERS standards (1989), but only considers vertical displacements. Pagiatakis' (1 982, 1 990) model, based on Pagiatakis, Langley, and Vanicek (1982), considers only six tidal components (S_2, M_2, N_2, K_1, P_1, and O_1).

An extension of the 1991 Scherneck model (Scherneck, 1993) accounts for modulation of the eleven tidal frequencies by multiples of N', the lunar nodal period (1 8.6 years). On the assumption that these additional terms yield ocean loading amplitudes which are in the same ratio to each main loading term as the companion tides are to the main tides, the additional station displacements can be written as

$$\delta_j' = \sum_{i=1}^{N} \sum_{k} r_{ki} \xi_i^j \cos[(\omega_i + n_{ki}\omega_{N'})t + V_i + n_{ki}N' - \delta_i^j)] \qquad (2.71)$$

where the k summation extends over all integer multiples n_{ki} Of the lunar node N', and r_{ki} is the ratio of the tidal amplitude of each companion k to the tidal amplitude of the parent i. Of 26 such components listed by Cartwright and Edden (1973), 20 are estimated to be significant in contributing to the largest ocean loading displacements at the 0.01 mm level. Table 111 snows the multiples n_{ki} and amplitude ratios r_{ki} for these *20* components.

In pushing the limits of Earth modeling to below 1cm accuracy in the mid- 1990s, ocean loading station displacements are one aspect of the models that are undergoing close scrutiny. Initial trials indicate that ocean loading amplitudes can be derived from VLBI experiments at an approximate accuracy level of 1-2 mm (Severs, 1994). When estimating parameters, great care must be used in order to avoid singularities due to the identity of components of station displacements (''confounding of parameters"). Since some components of ocean loading, solid Earth tides, and ocean tidally induced UTPM variations have the same frequencies, certain linear combinations of the station displacements that they cause are identical (see Sections II.C.2.a and II.E.1.c).

3. Non-tidal station motion

Many other processes take place in the Earth's atmosphere and in its crust that affect the location of an observing station on time scales ranging from seconds to years, and distance scales ranging from local to global. Present knowledge of such processes is sketchy, but both theoretical and experimental research are starting to provide useful results. Local processes include the effects of ground water and snow cover redistribution, and magma chamber activity in volcanically active areas. Effects that have more widespread repercussions are atmospheric loading and post-glacial rebound. In contrast to the tidal effects, whose time dependence is fixed by the precisely known motions of the bodies of the Solar system, the non-tidal processes do not have well-known, periodic time dependencies. The two "global" effects, atmospheric loading and post-glacial rebound, are discussed briefly in the next two sections.

a. Atmospheric loading

By analogy with the ocean tides that were considered in the previous section, a time-varying atmospheric pressure distribution can also induce crustal deformation. Rabbel and Schuh (1986) first estimated the effects of atmospheric loading on VLBI baseline determinations, and concluded that they may amount to many millimeters of seasonal variation]]. In contrast to ocean tidal effects, analysis of the situation in the atmospheric case does not benefit from the presence of a well-understood periodic driving force.. Otherwise, estimation of atmospheric loading via Green's function techniques is analogous to methods used to calculate ocean loading effects. Rabbel and Schuh recommend a simplified form of the dependence of the vertical crust displacement on pressure distribution. It involves only the instantaneous pressure at the site in question, and an average pressure over a circular region C of radius $R = 2000$ km surrounding the site. The expression for the vertical displacement (mm) is:

$$\Delta r = -0.35 p_0 - 0.55 \bar{p} \tag{2.72}$$

where p_0 is the local pressure anomaly (relative to the standard pressure of 1013.25 mbar), and $\bar{p}$ is the pressure anomaly within the 2000-km circular region mentioned above (both quantities are in mbar). Note that the reference point for this displacement is the site location at standard (sea level) pressure. The locally referenced Δr is transformed to the standard geocentric coordinate system via the transformation of Eq. (2.67).

Such a rudimentary model is recently being used as an optional part of the VLBI model. A mechanism for characterizing the pressure anomaly expresses the two-dimensional surface pressure distribution (relative to 1013.25 mbar) surrounding a site as a quadratic polynomial

$$p(x,y) = p_0 + A_1 x + A_2 y + A_3 x^2 + A_4 xy + A_5 y^2 \qquad (2.73)$$

where x and y are the local East and North distances of the point in question from the VLBI site. The pressure anomaly $\bar{p}$ may then be evaluated by the simple integration

$$\bar{p} = \iint_C dx\, dy\, p(x,y) \Big/ \int_C dx\, dy \qquad (2.74)$$

giving

$$\bar{p} = p_0 + (A_3 + A_5) R^2/4 \qquad (2.75)$$

It remains the task of the data analyst to perform a quadratic fit to any available area weather data to determine the coefficients A_{1-5}. Future advances in understanding the atmosphere-crust elastic interaction can probably be accommodated by adjusting the coefficients in Eq. (2.72). As an initial step along these lines, a station-dependent factor f is introduced to scale the second coefficient in Eq. (2.72):

$$\Delta r = -0.35 p_0 - 0.55(1+f)\bar{p} \qquad (2.76)$$

This may account for differing geographical features surrounding different sites. In particular, f may depend on the fraction of ocean within the 2000 km radius. Some recent analyses have produced empirical estimates of atmosphere loading coefficients for a number of sites (Manabe *et al.*, 1991; van Dam and Herring, 1994; MacMillan and Gipson, 1994; van Dam *et* al., 1994). It is not yet clear whether the site variation of these coefficients is free from other systematic errors.

b. Post-glacial rebound

Thick glacial ice sheets covering Scandinavia, Greenland, and Canada melted ≈10,000 years ago. The removal of their considerable weight pressing on the Earth's crust is believed to result in relaxation ("rebound") that continues at present (Tushingham and Peltier, 1991). The magnitude of this motion is estimated to be as large as several mm/yr, predominantly in the vertical direction, at sites in and near the locations of ancient glaciers. Current theory of deglaciation effects is not yet sufficiently developed to produce unambiguous results. The parameters describing deglaciation history, as well as the rheological properties of the Earth's mantle, are not accurately known. Nevertheless, it appears that reasonable parameter choices yield some agreement with empirical measurements of baselines in the affected areas (Mitrovica *et al.*, 1993; Peltier, 1995).

In summary, models have been presented that describe the four major time-dependent station motions (solid, pole, and ocean tides, and atmospheric loading). Each of the locally referenced displacement vectors is then transformed to the. standard geocentric coordinate system via rotations like Eq. (2.64). After this transformation, the final station location is

$$\mathbf{r}_t = \mathbf{r}_0 + \boldsymbol{\Delta}_{sol} + \boldsymbol{\Delta}_{pol} + \boldsymbol{\Delta}_{ocn} + \boldsymbol{\Delta}_{atm} \qquad (2.77)$$

D. Source structure

By analogy with the time dependence of station coordinates caused by tectonic and tidal motion, possible non-stationarity of radio source coordinates must also be considered. To a large extent, sue}] effects can be eliminated by judicious choice of objects in planning VLBI experiments. With the exception of special purpose experiments [such as those of Lestrade *et al.* (1995) on radio stars], the sources are well outside our Galaxy, ensuring minimal proper motion. Numerous astrophysical studies during the past two decades have shown that compact extragalactic radio sources exhibit structure on a milliarcsecond scale (e.g., Kellermann and Pauliny-Toth, 1981). Sue]] studies are important for developing models of

the origin of radio emission of these objects. Many radio source structures are found to be quite variable with frequency and time (Zensus and Pearson, 1 987; Taylor *et* al., 1994a, 1994b; Polatidis *et al.*, 1995; Thakkar *et al.*, 1995). Survey maps of 187 radio sources in the Taylor *et al.* 1994a reference showed that only 8 sources had structure on a scale not exceeding 1 mas at an observing frequency of 5 GHz. If extragalactic sources are to serve as reference points in a reference frame that is stable at a level of 1 mas or below, it is important to correct for the effects of their structures in astrometric VLBI observations.

Corrections for the effects of source internal structures arc based on work by Thomas (1980), Ulvestad (1988), and Charlot (1989, 1990a). A varying non-point-like distribution of the intensity of a source yields time dependent corrections to the group delay and delay rate observables, $\Delta\tau_s$ ancl $\Delta\dot{\tau}_s$, that may be written in terms of the intensity distribution $I(\mathrm{s},\omega,t)$ as

$$\Delta\tau_s = \partial\phi_s/\partial\omega, \qquad \Delta\dot{\tau}_s = \partial\phi_s/\partial t \tag{2.78}$$

with

$$\phi_s = \arctan(-Z_s/Z_c) \tag{2.79}$$

and

$$Z_{\{\substack{s\\c}\}} = \int\int d\Omega\ I(\mathrm{s},\omega,t)\left\{\begin{matrix}\sin\\ \cos\end{matrix}\right\}(2\pi\mathbf{B}\cdot\mathrm{s}/\lambda) \tag{2.80}$$

Here ϕ_s is the correction to the phase of the incoming signal, s is a vector from the adopted reference point to a point within the source intensity distribution in the plane of the sky, ω and λ are the observing frequency and wavelength, $\mathbf{B}$ the baseline vector, and the integration is over solid angles Ω. Source intensity dist ribution maps are most conveniently parametrized in terms of one of two models: superpositions of delta functions or Gaussians. At a given frequency, the corresponding intensity distributions arc written as

$$I(\mathrm{s}) = \sum_k S_k\delta(x - x_k,\ y - y_k) \tag{2.81}$$

or

$$I(\mathrm{s}) = \sum_k \frac{S_k}{2\pi a_k b_k} \exp\Big[-[(x - x_k)\cos\theta_k + (y - y_k)\sin\theta_k]^2/2{a_k}^2 - [-(x - x_k)\sin\theta_k + (y - y_k)\cos\theta_k]^2/2{b_k}^2\Big] \quad (2.82)$$

where S_k is the flux of component k, and $\mathbf{s_k}$ (with components x_k, y_k in the plane Of the sky) is its position relative to the reference point. For Gaussian distributions, θ_k is the angle between the major axis of component k and the u axis (to be defined below), and (a_k, b_k) are the full widths at half maximum of the (major, minor) axes of component k normalized by $2\sqrt{2\log 2}$. The quantities $Z_{\{{}^{s}_{c}\}}$ entering the structure phase ϕ_s [Eq. *(2.79)]* are

$$Z_{\{{}^{s}_{c}\}} = \sum_k S_k \left\{ {\sin \atop \cos} \right\} (2\pi \mathbf{B} \cdot \mathbf{s_k}/\lambda) \quad (2.8.3)$$

for delta functions, and

$$Z_{\{{}^{s}_{c}\}} = \sum_k S_k \exp[-2\pi^2(a_k^2 U_k^2 + b_k^2 V_k^2)] \left\{ {\sin \atop \cos} \right\} (2\pi \mathbf{B} \cdot \mathbf{s}_k/\lambda) \quad (2.84)$$

for Gaussians. Here

$$U_k = u\cos\theta_k + v\sin\theta_k \quad (2.85)$$

$$V_k = -u\sin\theta_k + v\cos\theta_k \quad (2.86)$$

with u, v being the projections of the baseline vector $\mathbf{B}$ 011 the plane of the sky in the it-W, N-S directions, respectively.

Maps may be specified in terms of an arbitrary number of either Gaussian or delta function components. At most, six parameters must be specified for each component: its polar coordinates and flux, and, for a Gaussian, its major and minor axes and the position angle of the major axis. The structural correction for phase is computed via Eqs. *(2.79)*, *(2.83)*, and (2.84). For the bandwidth synthesis (BWS) delay observable, the structure correction is the slope of a straight line fitted to the individual structure phases calculated for each frequency channel used during t he observation. For example, for Mark III data there

arc typically 8 channels spanning ≈8.2 to 8.6 GHz at X band, and 6 channels spanning ≈2.2 to 2.3 GHz at S band. Delay rate structure corrections are calculated by differencing the structure phases at the two times used to form the theoretical rate observable (see Section V). In the case of dual-band (S-X) experiments, a linear combination of the structure corrections calculated independently for each band is applied to the dual-band observables.

The practical question to be resolved is whether such structural corrections based on maps yield significant and detectable corrections to the observable at the present levels of experimental and modeling uncertainty. Maps are available for only a fraction of the many hundreds of sources currently observed by VLBI. Some of the extended sources show time variability on a scale of months; since the corrections $\Delta\tau_s$ and $\Delta\dot{\tau}_s$ are quite sensitive to fine details of the strut.turc, in such cases new maps may be required on short time scales. Depending on the relative orientation of the source and VLBI baseline, the delay correction can be as large as ≈1 ns, which is equivalent to tens of cm. Nevertheless, the prognosis appears to be good. Charlot (1990b) found that data from a multiple baseline geodynamics experiment are adequate to map source structures with high angular resolution. More recently Charlot (1994) has also shown that use of maps for the structure of the source 3C 273 improves the fit in analyses of geodetic experiments.

Empirical evaluation of the effects of unknown source strut.turcon VLBI measurements could be made via the time rates of change of the source right ascension α and declination δ, based on a linear model of the motion of source coordinates

$$\alpha = \alpha_0 + \dot{\alpha}(t - t_0) \tag{2.87}$$

$$\delta = \delta_0 + \dot{\delta}(t - t_0) \tag{2.88}$$

Non-zero estimates of the rate parameters $\dot{\alpha}$ and $\dot{\delta}$ could arise either from genuine proper motion or from motion of the effective source centroid sampled by VLBI lllcasLlrelll('[its. Unambiguous interpretation of such results is problematic, but Hon-zero rates can be used as a. crude diagnostic for the presence of structure effects. Apparent source position rates

have been reported by Ma and Shaffer (1991) and Jacobs *et al.* (1993). Significant rates are not believed to represent true proper motion, but rather to be the consequence of a change in the interference pattern caused by ejection of components from the central object.

The JPL VLBI code also provides the option of modeling source structure as a superposition of two δ functions centered at points $P_1(x_1, y_1)$ and $P_2(x_2, y_2)$ respectively, as in Eq. (2.81) above. The parameters describing the two components are: 1) flux ratio $K = S_2/S_1$, where S_k is the flux of the kth component, 2) component separation $s = |\mathbf{s}| = |\overrightarrow{P_1P_2}|$, and 3) position angle O. The position angle is O = 0° when $\overrightarrow{P_1P_2}$ is in the direction of increasing declination δ, and O = 90° when $\overrightarrow{P_1P_2}$ is in the direction of increasing right ascension $\hat{\alpha}$. From Charlot (1990}~), the group delay has the following dependence on the structural parameters:

$$T = \frac{2\pi K\ (1\ -\ K)}{\omega\ (1\ +\ K)}\ \text{“}\ \frac{R[1\ -\ \cos(2\pi R)]}{[K^2\ +\ 2K\ \cos(2\pi R)\ +1]} \tag{2.89}$$

where

$$R = \mathbf{B} \cdot \mathbf{s}/\lambda \tag{2.90}$$

For evaluating partial derivatives of τ that are needed for parameter estimation, the component separation s and baseline **B** are most conveniently written in terms of their components in the celestial system, as

$$\mathbf{s} = \hat{\alpha}\ s\ \sin\theta\ +\ \hat{\delta}\ s\ \cos\theta \tag{2.91}$$

$$\mathbf{B} = \hat{\alpha}\ u\ \lambda\ \ \ +\ \hat{\delta}\ v\ \lambda \tag{2.92}$$

Then R becomes

$$R = s\ (u\ \sin\theta\ +\ v\ \cos\theta)\ /\ \lambda \tag{2.93}$$

E. Transformation from terrestrial to celestial coordinate systems

The Earth is approximately an oblate spheroid, spinning in the presence of two massive moving objects (the Sun and the Moon) which are positioned such that their time-varying

gravitational effects not only produce tides on the Earth, but also subject it to torques. In addition, the Earth is covered by a complicated fluid layer, and is not perfectly rigid internally. As a result, the orientation of the Earth is a very complicated function of time, which to first order can be represented as the composite of a time-varying rotation rate<, a wobble, a nutation, and a precession. The exchange of angular momentum between the solid Earth and the fluids on its surface, as well as between its crust and deeper layers, is not readily predictable, and thus must be continually determined experimentally (Le Mouël *et al*, 1993). Nutation and precession are fairly well modeled theoretically. At the accuracy with which VLBI Call determine baseline vectors, however, even these models are not completely adequate.

Currently, the rotational transformation, Q, of coordinates from the terrestrial frame to the celestial geocentric. frame is composed of 6 separate rotations (actually 12, since the nutation, precession, and "perturbation" transformations, N, P, and Ω, consist of 3 transformations each) applied to a vector in the terrestrial system:

$$\mathrm{Q} = \Omega P N U X Y \tag{2.94}$$

In order of appearance in Eq. (2.94), the transformations arc: the perturbation rotation, precession, nutation, U'J'], and the x and y components of polar motion. All arc discussed in detail in the following four sections. With this definition of Q, if $\mathbf{r}_t$ is a station location expressed in t he terrestrial system, *e.g.*, he result of Eq. *(2.77),* then that location, $\mathbf{r}_c$, expressed in the celestial system is

$$\mathbf{r}_c = Q\mathbf{r}_t \tag{2.95}$$

This particular formulation is analogous to the historical path of astrometry, and is couched in that language. While esthetically unsatisfactory with modern measurement techniques, such a formulation is currently practical for intercomparison of techniques and for effecting a smooth inclusion of the interferometer data into the long historical record of astrometric data. Much more pleasing esthetically would be the separation of Q into two rotation matrices:

$$Q = Q_1 Q_2 \tag{2.96}$$

where Q_2 are those rotations to which the Earth would be subjected if all external torques were removed (approximately UXY above), and where Q_1 are those rotations arising from external torques (approximately ΩPN above). Even then, the tidal response of the Earth prevents such a separation from being perfectly realized. Eventually, the entire problem of obtaining the matrix Q, and the tidal effects on station locations may be solved numerically. Note that the matrices appearing in the transformation of Eq. (2.94) are not the same as those historically used in astrometry. Since we rotate the Earth rather than the celestial sphere, Ω, P, and N are transposes of the conventional transformations from the celestial system of J2000 to coordinates of elate,

1. UT1 and polar motion

The first transformation, Y, is a right-handed rotation about the x axis of the terrestrial frame by an angle Θ_2. Currently, the terrestrial frame is the $_{1_9}03.0$ CIO frame, except that the positive y axis is at 90 degrees east (Siberia). The x axis is coincident with the 1903.0 meridian of Greenwich, and the z axis is the 1903.0 standard pole.

$$Y = \begin{pmatrix} 1 & 0 & 0 \\ 0 & \cos\Theta_2 & \sin\Theta_2 \\ 0 & -\sin\Theta_2 & \cos\Theta_2 \end{pmatrix} \tag{2.97}$$

where Θ_2 is the y pole position published by IERS.

The next rotation in sequence is the right-handed rotation (through an angle Θ_1 about the y axis) obtained after the previous rotation has been applied:

$$X = \begin{pmatrix} \cos\Theta_1 & 0 & -\sin\Theta_1 \\ 0 & 1 & 0 \\ \sin\Theta_1 & 0 & \cos\Theta_1 \end{pmatrix} \tag{2.98}$$

In this rotation, Θ_1 is the IERS x pole position. Note that we have incorporated in the matrix definitions the transformation from the left-handed system used by IERS to the

right-handed system we use. Note also that instead of IERS data used as a pole definition, we could instead use any other source of polar motion data provided it was represented in a left-llalldcd system. The only effect would be a change in the definition of the terrestrial reference system.

The application of "XY" to a vector in the terrestrial system of coordinates expresses that vector as it would be observed in a coordinat e frame whose z axis was along the Earth's ephemeris pole. The third rotation, U, is about the resultant z axis obtained by applying "X}". It is a rotation through the angle, - H, where H is the hour angle of the true equinox of date (i. e., the dihedral angle measured westward between the xz plane defined above and the meridian plane containing the true equinox of date). The equinox of date is the point defined on the celestial equator by the intersection of the mean ecliptic with that equator. It is that intersection where the mean ecliptic rises from below the equator to above it (ascending node).

$$U = \begin{pmatrix} \cos H & -\sin H & 0 \\ \sin H & \cos H & 0 \\ 0 & 0 & 1 \end{pmatrix} \tag{2.99}$$

This angle H is composed of two parts:

$$H = h_\gamma + \alpha_E \tag{2.100}$$

where h_γ is the hour angle of the mean equinox of date, and α_E (equation of equinoxes) is the difference in hour angle of the true equinox of date and the mean equinox of date, a difference which is due to the nutation of the Earth. This set of definitions is cumbersome and couples nuta tion effects with Earth rotation. However, in order to provide a direct estimate of conventional UT1 (universal time) it is convenient to endure this historical approach, at least for the near future.

$UT1$ is defined to be such that the hour angle of the mean equinox of date is given by the following expression (Aoki *et al.*, 1982; Kaplan, 1981):

$$h_\gamma = UT1 + 6^h\ 41'''\ 50^s.54841 + 8640184^s.812866\ T_u$$

$$+ 0^{s}.093101\ T_u^2 - 6'.2\ x\ 10\text{-}^{6} T_u^3$$

where the dimensionless quantity

$$T_u = (\text{Julian } UT1 \text{ date} - 2451545\ .())/36525$$

The actual equivalent expression which is coded is:

$$h_\gamma = 2\pi(UT1 \text{ Julian day fraction}) + 67310\ ^{s},54841$$
$$-i\ 8640184\ ^{s}.8]2866\ T_u - 1\ 0^{s}.093104\ T_u^2 - 6^{s}.2\ \text{X}\ 10^{-6}7: \qquad (2.103)$$

This expression produces a time, $UT1$, which tracks the Greenwich hour angle of the real Sun to within 16^{m}. However, it really is sidereal time, modified to fit our intuitive desire to have the Sun directly overhead at noon on the Greenwich meridian. Historically, differences of $UT1$ from a uniform measure of time, such as atomic time, have been used in specifying the orientation of the Earth.

By the very definition of "mean of date" and '(true of date'), nutation causes a difference In the hour angles of the mean equinox of date and the true equinox of elate. This difference, called the "equation of equinoxes", is denoted by α_E and is obtained as follows:

$$\alpha_E = \tan^{-1}\left(\frac{y_{\gamma'}}{x_{\gamma'}}\right) = \tan^{-1}\left(\frac{N_{21}^{-1}}{N_{11}^{-1}}\right) \quad \text{“ a ’ ’ - ’ (\%)} \qquad (2.104)$$

where the vector

$$\begin{pmatrix} x'_\gamma \\ y'_\gamma \\ z'_\gamma \end{pmatrix} = N^{-1} \begin{pmatrix} 1 \\ 0 \\ 0 \end{pmatrix} \qquad (2.105)$$

is the unit vector, in true equatorial coordinates of date, toward the mean equinox of date. in mean equatorial coordinates of date, this same! unit vector is just (1, 0,0)7'. The matrix N^{-1} is the inverse (or equally, the transpose) of the transformation matrix N, which will be defined below in Eq. (2.1 1 5), to effect t he transformation from true equatorial coordinates of elate to mean equatorial coordinates of date.'

It is convenient to apply "UXY" as a group. To parts in 10^{12}, $XY = YX$. However, with the same accuracy $UXY \neq XYU$. Neglecting terms of $\mathcal{O}(\Theta^2)$ (which produce station location errors of approximately 0.006 mm):

$$UXY = \begin{pmatrix} \cos \Pi & - & \sin \Pi & \sin\Theta_1 \cos \Pi - \sin \Theta_2 \sin \Pi \\ \sin \Pi & & \cos 11 & - \sin \Theta_1 \sin \Pi + \sin \Theta_2 \cos \Pi \\ \sin \Theta_1 & - & \sin \Theta_2 & 1 \end{pmatrix} \tag{2.106}$$

over relatively short time spans, Earth rotation might be modeled as a time-linear function, by analogy with tectonic motion of the stations over longer periods. If PM and UT1 are symbolized by Θ_{1-3}, and the reference time is t_0, then this model is

$$\Theta_i = \dot{\Theta}_i^0 + \dot{\Theta}_i(t - t_0) \tag{2.107}$$

where Θ_i^0 are the values of UTPM at the reference epoch.

a. *Tidal UTPM* variations

Tidally induced shifts of mass in the solid Earth, oceans, and atmosphere produce angular momenta which must be redistributed in a manner that conserves the total angular momentum. The consequences are variations in the orientation and rotation rate of the Earth: modification of polar motion and UT1. Such small effects emerged above the detection threshold in space geodesy in the early 1990s. Modeling them is important if cc~]ltilllcicr-level accuracy is to be attained in interpretation of VLBI measurements.

Just as various tidal forces affect the station locations (Sees. II.C.2.a - II.C.2.c), they also affect polar motion and UT1 (Θ_{1-3}). Equations similar to (2.41) may be written for each of the threw components of Earth orientation:

$$\Theta_i = \Theta_{i0} + \Delta\Theta_{isol} + \Delta\Theta_{iocn} + \Delta\Theta_{iatm} \tag{2.108}$$

where Θ_i (i=1 ,3) symbolizes each Of the three components of UTPM, Θ_{i0} is its value in the absence of tidal effects, and the three A terms arc the respective contributions of solid Earth, ocean, and atmospheric tides. The next two sections describe the current models of solid

and ocean tide contributions that are implemented in current VLBI modeling software. At present, not enough is known about atmospheric tidal effects to quantify their contribution.

b. Solid Earth tide UTPM variations

The pioneering work in tidal effects on Earth orientation was that of Yoder *et al.* (1 981). It was limited to UT1, but included some ocean effects. 'J'heir calculated $\Delta UT1$ can be represented as

$$\Delta UT1 = \sum_{i=1}^{N} \left[A_i \sin \left[\sum_{j=1}^{5} k_{ij} \alpha_j \right] \right] \qquad (2.109)$$

where N (=41) is chosen to include all terms with periods from 5 to 35 days. There are no lower-frequcnc,y contributions until a period of 90 days is reached. However, these long-period terms arc already included in the results reported by the current Earth-orientation measurement services. The values for k_{ij} and A_i, along with the periods involved, are given in Table 4.37.1 of the Explanatory Supplement (Seidelmann *et* al., 1992.) The α_i for i = 1, 5 arc just the five fundamental arguments defined in Eqs. (2.118 - 2.1 22) as l, l', F, D, and Ω, respectively.

c. *Ocean tide UTPM* variations

Redistribution of the angular momentum produced by ocean tides affects the Earth's rotation pole position and velocity. This effect was first quantified by Brosche *et al.* (1 *989,* 1991). The dominant effects on polar motion and UT1 are at diurnal, semidiurnal, fortnightly, mor ıthly, and semiannual frequencies. Assuming that the frequencies slower than fortnightly arc adequately accounted for either in modeling combined solid and ocean tidal effects (not strictly true with the Yoder model), or are already present in the *a priori* UTPM series, only the diurnal and semidiurnal frequencies need to be modeled, Further limiting the model to tidal components with apparent amplitudes larger than 1 μs gives eight components.

For unified notation, define Θ_{1-3} = x, y polar motion and $UT1$, respectively. Then the ocean tidal effects $\Delta\Theta$ can be written as

$$\Delta\Theta_l = \sum_{i=1}^{N}\left[A_{il}\cos\left[\sum_{j=1}^{5} k_{ij}\alpha_j + n_i(h_\gamma + \pi)\right] + B_{il}\sin\left[\sum_{j=1}^{5} k_{ij}\alpha_j + n_i(h_\gamma + \pi)\right]\right] \qquad (2.110)$$

A_{il} and B_{il} are the cosine and sine amplitudes that may be calculated from theoretical tidal models (as in the work of Brosche) or empirically determined from data (Herring and Dong, 1994; Sovers, Jacobs and Gross, 1993; Watkins and Eanes, 1994). Theoretical calculations of polar motion ocean effects have only very recently appeared: Gross (1 993) used Seiler's (1989-1991) ocean model to estimate $A_{i,1-2}$ and $B_{i,1-2}$ (i = 2 to 7). 'I'able IV lists the eight terms currently included in the model. These numerical coefficients are taken from the empirical results of Sovers *et al.* (1993); this is known in our VLBI code as the JPL92 fast UTPM model.

The ocean tidal UTPM effects are also modulated by the 18.6-year lunar node variation (A"). As in the case of ocean loading station displacements (Sec. II.C.2.c), the contributions $\Delta\Theta_l'$ of the companion tides to $\Delta\Theta_l$ can be written as

$$\Delta\Theta_l' = \sum_{i=1}^{N}\sum_{k} r_{ki}\left[A_{il}\cos\left[\sum_{j=1}^{5} k_{ij}\alpha_j + n_i(h_\gamma + \pi) + n_{ki}\omega_{N'})t + n_{ki}N'\right] + B_{il}\sin\left[\sum_{j=1}^{5} k_{ij}\alpha_j + n_i(h_\gamma + \pi) + n_{ki}\omega_{N'})t + n_{ki}N'\right]\right] \qquad (2.111)$$

where the strengths of the companion tides r_{ki} are found in Table III.

Since a rotational frequency of 1 (0) cycles per sidereal day (cpsd) in the celestial frame (S) is identical to a frequency of O (- 1) cpsd in the Earth-fixed frame (B), nutations with sl)acc-fixed frequencies ω_S coincide with polar motions with bocly-fixed frequencies $\omega_B = -1 + \omega_S$. The retrograde parts of the polar motion terms with coefficients $A_{i1,2}$ and $B_{i1,2}$ corresponding to the diurnal tidal components listed in 'J'able IV (i = 5 to 8) are thus equivalent to components of the nutation model, and due care must be taken when both classes of parameters are estimated.

2. Nutation

With the completion of the $UT1$ and polar motion transformations, we are left with a station location vector, $\mathbf{r}_{date}$. This is the station location relative to true equatorial celestial coordinates of date. The last set of transformations are nutation, N, precession, P, and the perturbation rotation, Ω, applied in that order. These transformations give the station location, $\mathbf{r}_c$, in celestial equatorial coordinates:

$$\mathbf{r}_c = \Omega P N \mathbf{r}_{date} \tag{2.112}$$

The transformation matrix N is a composite of three separate rotations (Melbourne *et al.*, 1968):

1. $A(\varepsilon)$: true equatorial coordinates of date to ecliptic coordinates of date,

$$A(\varepsilon) = \begin{vmatrix} 1 & 0 & 0 \\ 0 & \cos\varepsilon & \sin\varepsilon \\ 0 & -\sin\varepsilon & \cos\varepsilon \end{vmatrix} \tag{2.113}$$

2. $C^T(\Delta\psi)$: nutation in longitude from ecliptic coordinates of date to mean ecliptic coordinates of date,

$$C^T(\Delta\psi) = \begin{vmatrix} \cos\Delta\psi & \sin\Delta\psi & 0 \\ -\sin\Delta\psi & \cos\Delta\psi & 0 \\ 0 & 0 & 1 \end{vmatrix} \tag{2.114}$$

where $\Delta\psi$ is the nutation in ecliptic longitude, and

3. $A^T(\bar{\varepsilon})$: ecliptic coordinates of date to mean equatorial coordinates.

in ecliptic coordinates of date, the mean equinox is at an angle $\Delta\psi = \tan^{-1}(y_{\bar{\gamma}}/x_{\bar{\gamma}})$. The angle $\Delta\varepsilon = \varepsilon - \bar{\varepsilon}$ is the nutation in obliquity, and $\bar{\varepsilon}$ is the mean obliquity (the dihedral angle between the plane of the ecliptic and the mean plane of the equator). "Mean" as used in this section implies that the short-period ($T \leq 18.6$ years) effects of nutation have been

removed. Actually, the separation between nutation and precession is rather arbitrary, but historical. The composite rotation is:

$$N = A^T(\bar{\varepsilon})C^T(\Delta\psi)A(\varepsilon) \tag{2.115}$$

$$\begin{vmatrix} \cos\Delta\psi & \cos\varepsilon\sin\Delta\psi & \sin\varepsilon\sin\Delta\psi \\ -\cos\bar{\varepsilon}\sin\Delta\psi & \cos\bar{\varepsilon}\cos\varepsilon\cos\Delta\psi + \sin\bar{\varepsilon}\sin\varepsilon & \cos\bar{\varepsilon}\sin\varepsilon\cos\Delta\psi - \sin\bar{\varepsilon}\cos\varepsilon \\ -\sin\bar{\varepsilon}\sin\Delta\psi & \sin\bar{\varepsilon}\cos\varepsilon\cos\Delta\psi - \cos\bar{\varepsilon}\sin\varepsilon & \sin\bar{\varepsilon}\sin\varepsilon\cos\Delta\psi + \cos\bar{\varepsilon}\cos\varepsilon \end{vmatrix}$$

It should again be pointed out that this is the reverse of the customary astronomical nutation.

The 1980 IAU nutation model (Seidelmann, 1982; Kaplan, 1981) is used to obtain the values of $\Delta\psi$ and $\varepsilon - \bar{\varepsilon}$. The mean obliquity is obtained from Lieske *et* al. (1977) or from Kaplan (1981):

$$\bar{\varepsilon} = 23^\circ\ 26'21.''448 - 46.''8150\ T - 5.''9 \times 10^{-4}T^2 + 1.''813 \times 10^{-3}T^3 \tag{2.116}$$

$$T = (\text{Julian } UT1 \text{ date} - 2451545.0)/36525 \tag{2.117}$$

This nutation in longitude ($\Delta\psi$) and in obliquity ($\Delta\varepsilon = \varepsilon - \bar{\varepsilon}$) can be represented by a series expansion of the sine.s and cosines of linear combinations of five fundamental arguments. These are (Kaplan, 1981; Cannon, 1981):

1. the mean anomaly of the Moon:

$$\alpha_1 = l = 2.35554839 + 8328.691422887 + 1.5180 \times 10^{-4}T^2 + 3.1 \times 10^{-7}T^3 \tag{2.118}$$

2. the mean anomaly of the Sun:

$$\alpha_2 = l' = 6.240035944\ 628.301956027 - 2.80 \times 10^{-6}T^2 - 5.8 \times 10^{-8}T^3 \tag{2.119}$$

3. the mean argument of latitude of the Moon:

$$\alpha_3 = F = 1.627901931\ 8433.466158327 - 6.4272 \times 10^{-5}T^2 + 5.3 \times 10^{-8}T^3 \tag{2.120}$$

4. the mean elongation of the Moon from the Sun:

$$\alpha_4 = D = 5.19846951 + 7771.37714617T - 3.341 \times 10^{-5}T^2 + 9.2 \times 10^{-8}T^3 \quad (2.121)$$

5. the mean longitude of the ascending lunar node:

$$\alpha_5 = -\Omega = 2.18243862 - 33.757045937T + 3.614 \times 10^{-5}T^2 + 3.9 \times 10^{-8}T^3 \quad (2.122)$$

With these fundamental arguments, the nutation quantities can then be represented by

$$\Delta\psi = \sum_{j=1}^{N}\left[(A_{0j} + A_{1j}T) \sin \left[\sum_{i=1}^{5} k_{ji}\alpha_i(T)\right] \right] \quad (2.123)$$

and

$$\Delta\varepsilon = \sum_{j=1}^{N}\left[(B_{0j} + B_{1j}T) \cos \left[\sum_{i=1}^{5} k_{ji}\alpha_i(T)\right] \right] \quad (2.124)$$

where the various values of α_i, k_{ji}, A_j, and B_j are tabulated in Table 3.222.1 of the Explanatory Supplement.

a. *Corrections to the 1980 IAU model*

Additional terms can be optionally added to the nutations $\Delta\psi$ and $\Delta\varepsilon$ in Eqs. (2.123) and (2.124). These include the out-of-phase nutations, the free-core nutations (Yoder, 1983) with period ω_f (nominally 430 days), and the "nutation tweaks" $\delta\psi$ and $\delta\varepsilon$, which are arbitrary constant increments of the nutation angles $\Delta\psi$ and $\Delta\varepsilon$. Unlike the usual nutation expressions, the tweaks have no time dependence. The out-of-phase nutations $\Delta\psi^o$ and $\Delta\varepsilon^o$, which are not included in the IAU1980 nutation series, are identical to Eqs. (2.123) and (2.124), with the replacements sin $\leftrightarrow$ cos:

$$\Delta\psi^o = \sum_{j=1}^{N}\left[(A_{2j} + A_{3j}T) \cos\left[\sum_{i=1}^{5} k_{ji}\alpha_i(T)\right]\right] \quad (2.125)$$

and

$$\Delta\varepsilon^{o} = \sum_{j=1}^{N}\left[(B_{2j} + B_{3j}T)\sin\left[\sum_{i=1}^{5} k_{ji}\alpha_i(T)\right]\right] \tag{2.126}$$

Expressions similar to these are adopted for the free-core nutations:

$$\Delta\psi^{f} = (A_{00} + A_{10}T)\sin(\omega_f T) + (A_{20} + A_{30}T)\cos(\omega_f T) \tag{2.127}$$

and

$$\Delta\varepsilon^{f} = (B_{00} + B_{10}T)\cos(\omega_f T) + (B_{20} + B_{30}T)\sin(\omega_f T) \tag{2.128}$$

If the free-core nutation is to be retrograde, as expected on theoretical grounds, ω_f should be negative. The nutation model thus contains a total of 856 parameters: A_{ij} (i= 0,3; j=1,106) and B_{ij} (i=0,3; j=1 ,106) plus the free-)lutation amplitudes A_{io} (i=0,3), B_{i0} (i=0,3). The only nonzero a *priori* amplitudes arc the A_{0j}, A_{1j}, B_{0j}, B_{1j} (j=1,106).

The nutation tweaks are just constant additive factors to the angles $\Delta\psi$ and $\Delta\varepsilon$:

$$\Delta\psi \rightarrow \Delta\psi + \delta\psi \tag{2.129}$$

and

$$\Delta\varepsilon \rightarrow \Delta\varepsilon + \delta\varepsilon \tag{2.130}$$

Deficiencies in the IAU nutation model became clearly evident in the 1980s (Herring *et al.*, 1 986.) Several methods of correcting them are in current use. The first possibility is to use empirically determined values of $\delta\psi$, $\delta\varepsilon$ that are available from the IERS. If this option is selected, the user is relying on nutation angles that arc determined from other VLBI experiments near the date of interest, and performing interpolation. An alternative is to estimate $\delta\psi$ and $\delta\varepsilon$ from the data during analysis.

Other options arc to select one of the recently published replacements of the 1980 IAU series. Zhu *et al.* (1 989, 1990) have refined the 1980 IAU theory of nutation both by re-examining the underlying Earth model and by incorporating recent experimental results. Herring (1 991) has extended the work of Zhu *et* al. and used geophysical parameters from

Mathews *et al.* (1991) to generate the ZMOA 1990-2 (Zhu, Mathews, Oceans, Anelasticity) nutation series. Kinoshita and Souchay (1 990) have re-examined the rigid-Earth nutation theory, and included all terms larger than 0.005 mas, in particular planetary terms not present in any previous theories. The 263 lunisolar terms have been corrected for the Earth's non-rigidity (Souchay, 1 993).

It should be noted that the paper of Kinoshita and Souchay gives expressions for the lunisolar tidal arguments that arc slightly at variance with the IAU formulas presented above in Eqs. (2.1 1 8-2.1 22). These differences may be of significance in high-accuracy modeling studies. '1'heir expressions for the five usual arguments l, 1', F, D, and Ω, as well as five additional planetary arguments l_V, l_E, l_M, l_J, and 1s are given below (all in units of radians):

1. the mean anomaly of the Moon:

$$\alpha_1 = l = 2.35555590 + 8328.691427\ T \tag{2.131}$$

2. the mean anomaly of the Sun:

$$\alpha_2 = l' = 6.24006013 + 628.301955\ T \tag{2.132}$$

3. the mean argument of latitude of the Moon:

$$\alpha_3 = F = 1.62790523 - 1\ 8433.466158\ T \tag{2.133}$$

4. the mean elongation of the Moon from the Sun:

$$\alpha_4 = D = 5.19846674 - 1\ 7771.377147\ T \tag{2.134}$$

5. the mean longitude of the ascending lunar node:

$$\alpha_5 = \Omega = 2.18243920 - 33.757045\ T \tag{2,135}$$

The Kinoshita-Souchay planetary contributions to $\Delta\psi$ and $\Delta\varepsilon$ are

$$\Delta\psi = \sum_{j=1}^{N}\left[S_{\psi j} \sin\left[\sum_{i=1}^{10} k_{ji}\beta_i(T)\right] + C_{\psi j} \cos\left[\sum_{i=1}^{10} k_{ji}\beta_i(T)\right] \right] \tag{2.136}$$

and

$$\Delta\varepsilon = \sum_{j=1}^{N}\left[S_{\epsilon j} \sin\left[\sum_{i=1}^{10} k_{ji}\beta_i(T)\right] + C_{\epsilon j} \cos\left[\sum_{i=1}^{10} k_{ji}\beta_i(T)\right] \right] \tag{2.137}$$

where the astronomical arguments are symbolized by β_i; the last four β_i are identical with the α_i defined above ($\beta_7 = D = \alpha_4$, $\beta_8 = F = \alpha_3$, $\beta_9 = l = \alpha_1$, $\beta_{10} = \Omega = \alpha_5$), while the first six are

1. the mean anomaly of Venus:

$$\beta_1 = l_V = 3.176146697 + 1021.32855467' \tag{2.138}$$

2. the mean anomaly of Earth:

$$\beta_2 = l_E = 1.753470314 + 628.30758492\ T' \tag{2.139}$$

3. the mean anomaly of Mars:

$$\beta_3 = l_M = 6.203480913 + 334.061243157' \tag{2.140}$$

4. the mean anomaly of Jupiter:

$$\beta_4 = l_J = 0.599546497 + 52.96909651\ T' \tag{2.141}$$

5. the mean anomaly of Saturn:

$$\beta_5 = l_S = 0.874016757 + 21.32990954\ T' \tag{2.142}$$

6. the accumulated general precession:

$$\beta_6 = p_a = 0.024381751' + 5{,}38691 \times 10^{-6}\ T'^2 \tag{2.143}$$

Since the present standard model of nutation is known to be in error by amounts that are large in comparison to present measurement capabilities, the International Astronomical Union (IAU) considers it important to formulate and adopt an improved nutation model by 1997. A working group is presently considering variants of the ZMOA and Kinoshita-Souchay models in this connection.

3. Precession

The next transformation in going from the terrestrial frame to the celestial frame is the rotation P. This is the precession transformation from mean equatorial coordinates of date to the equatorial coordinates of the reference epoch (e.g., J2000). As was the nutation matrix of Eq. (2.1 1 5), this is a rotation whose sense is opposite to that of the conventional astrometric precession. It is a composite of three rotations discussed in detail by Melbourne *et al.* (1968) and Lieske *et al.* (]977):

$$R(-Z) = \begin{pmatrix} \cos Z & \sin Z & 0 \\ -\sin Z & \cos Z & 0 \\ 0 & 0 & 1 \end{pmatrix} \tag{2.144}$$

$$Q(\Theta) = \begin{pmatrix} \cos\Theta & 0 & \sin\Theta \\ 0 & 1 & 0 \\ \sin\Theta & 0 & \cos\Theta \end{pmatrix} \tag{2.145}$$

$$R(-\zeta) = \begin{pmatrix} \cos\zeta & \sin\zeta & 0 \\ -\sin\zeta & \cos\zeta & 0 \\ 0 & 0 & 1 \end{pmatrix} \tag{2.146}$$

$$P = R(-\zeta)Q(\Theta)R(-Z) \tag{2.147}$$

$$= \begin{vmatrix} \cos\zeta\cos\Theta\cos Z & \sin\zeta\sin Z & \cos\zeta\cos\Theta\sin Z + \sin\zeta\cos Z & \cos\zeta\sin\Theta \\ -\sin\zeta\cos\Theta\cos Z & \cos\zeta\sin Z & -\sin\zeta\cos\Theta\sin Z + \cos\zeta\cos Z & -\sin\zeta\sin\Theta \\ -\sin\Theta\cos Z & & -\sin\Theta\sin Z & \cos\Theta \end{vmatrix}$$

The auxiliary angles ζ, Θ, Z depend on precession constants, obliquity, and time as

$$\zeta = 0''.5?71?' + 0''.3018s\ T'^2 + 0''.017998\ T'^3 \quad (2.148)$$

$$Z = 0''.5mT' + 1''.09468\ T'^2 - \} \ 0''.01\ 8203\ T'^3 \quad (2.149)$$

$$\Theta = nT' - 0''.42665\ T'^2 \cdot 0''.0\ 41833\ T'^3 \quad (2.150)$$

where the speeds of precession in right ascension and declination arc, respectively,

$$z_{71} = p_{LS} \cos\bar{\varepsilon}_0 - p_{PL} \quad (2.151)$$

$$z_1 = p_{LS} \sin\bar{\varepsilon}_0 \quad (2.152)$$

and p_{LS} = the luni-solar precession constant, p_{PL} = planetary precession constant, $\bar{\varepsilon}_0$ = the obliquity at J2000, and T' [Eq. (2.1 17)] is the time in centuries past J2000. Nominal values at J2000 are $p_{LS} = 5038''.7784$/cy, $p_{PL} = 10''.5526$/cy; these yield the expressions given by Lieske *et al.* (1977) and Kaplan (1981):

$$\zeta = 2306''.2181T' + 0''.30188\ T'^2 + 0'',017998\ T'^3 \quad (2.153)$$

$$\Theta = 2004''.31097' - 0''.42665\ T'^2 - 0''.041S33\ T'^3 \quad (2.154)$$

$$Z = 2306''.2181\ T' + 1''.09468T'^2 + 0''.018203\ T'^3 \quad (2.155)$$

1 Direct estimates of precession corrections can be obtained from observations. The most recent such result (Charlot *et al.*, 1995) indicates that the current IAU nominal value of p_{LS} is in error by 3.0 milliarcseconds per year. The precession matrix completes the standard model for the orientation of the Earth.

4. Perturbation rotation

The standard model for the rotation of the Earth as a whole may need a small incremental rotation about any one of the resulting axes. Define this perturbation rotation matrix as

$$\Omega = \Delta_x \Delta_y \Delta_z \quad (2.156)$$

where

$$\Delta_x = \begin{pmatrix} 1 & 0 & 0 \\ 0 & 1 & \delta\Theta_x \\ 0 & -\delta\delta\Theta_x & 1 \end{pmatrix} \tag{2,157}$$

with $\delta\Theta_x$ being a small angle rotation about the x axis, in the sense of carrying y into z;

$$\Delta_y = \begin{pmatrix} 1 & 0 & -\delta\Theta_y \\ 0 & 1 & 0 \\ \delta\Theta_y & 0 & 1 \end{pmatrix} \tag{2.158}$$

with $\delta\Theta_y$ being a small angle rotation about the y axis, in the sense of carrying z into x; and

$$\Delta_z = \begin{pmatrix} 1 & \delta\Theta_z & 0 \\ -\delta\Theta_z & 1 & 0 \\ 0 & 0 & 1 \end{pmatrix} \tag{2.159}$$

with $\delta\Theta_z$ being a small angle rotation about the z axis, in the sense of carrying x into y. For angles on the order of 1 arc second we can neglect terms 011 the order $\delta\Theta^2 R_E$ as they give effects 011 the order of 0.15 mm. '1'bus, in that approximation

$$\Omega = \begin{pmatrix} 1 & \delta\Theta_z & -\delta\Theta_y \\ -\delta\Theta_z & 1 & \delta\Theta_x \\ \delta\Theta_y & -\delta\Theta_x & 1 \end{pmatrix} \tag{2.160}$$

In general,

$$\delta\Theta_i = \delta\Theta_i(t) = \delta\Theta_{i0} + \delta\dot{\Theta}_i T + f_i(T) \tag{2.161}$$

which is the sum of an offset, a time-linear rate, and some higher order or oscillatory terms. Currently, only the offset and linear rate are implemented. In Particular, a non-zero value of $\delta\dot{\Theta}_y$ is equivalent to a change in the precession constand, $\delta\Theta_x$ is equivalent to the time rate of change of the obliquity ε. Setting

$$\delta\Theta_x = \delta\Theta_y = \delta\Theta_z = 0 \tag{2.162}$$

gives the effect of applying only the standard rotation matrices.

Starting with the llarth-fixed vector, r_o, we have in Sections II.C through II.E above shown how we obtain the same vector, $\mathbf{r}_c$, expressed in the celestial frame:

$$\mathbf{r}_c = \Omega PNUXY(\mathbf{r}_0 + \boldsymbol{\Delta}) \tag{2.163}$$

F. Earth orbital motion

We now wish to transform these stat ion locations from a geocentric reference frame moving with the Earth to a celestial reference frame which is at rest relative to the center of in.ass of the Solar System. In this Solar System barycentric (SSB) frame we will usc these station locations to calculate the geometric delay (see Section 11 .A). We will then transform the resulting time interval back to the frame in which the time delay is actually measured by the interferometer – the frame moving with the Earth.

Let Σ' be a geocentric frame moving with vector velocity $= \boldsymbol{\beta}c$ relative to a frame, Σ, at rest relative to the Solar System center of mass. Further, let $\mathbf{r}(t)$ be the position of a point (*e.g.*, station location) in space as a function of time, t, as measured in the Σ(SSB) frame. In the Σ' (geocentric) frame, there is a corresponding position $\mathbf{r}'(t')$ as a function of time, t'. We normally observe and model $\mathbf{r}'(t')$ as shown in Sections II.C through II.E. However, in order to calculate the geometric delay in the SSB frame (Σ), we will need the transformations of r(t) ant] $\mathbf{r}'(t')$, as well as of t and t', as we shift frames of reference. Measuring positions in units of light travel time, we have from Jackson (1 975) the Lorentz transformation:

$$\mathbf{r}'(t') = \mathbf{r}(t) + (\gamma - 1)\mathbf{r}(t) \cdot \frac{\boldsymbol{\beta}\boldsymbol{\beta}}{\boldsymbol{\beta}^2} - \gamma\boldsymbol{\beta}t \tag{2.164}$$

$$t' = \gamma[t - \mathbf{r}(t) \cdot \boldsymbol{\beta}] \tag{2.165}$$

and the inverse transformation:

$$\mathrm{r(t)} = \mathbf{r}'(t') - \mathrm{i}\ (\gamma - 1)\mathbf{r}'(t') \cdot \frac{\boldsymbol{\beta}\boldsymbol{\beta}}{\boldsymbol{\beta}^2} - \mathrm{i}\ \gamma\boldsymbol{\beta}t' \tag{2.166}$$

$$t = \gamma[t' + \mathbf{r}'(t') \cdot \boldsymbol{\beta}] \tag{2.167}$$

where

$$\gamma = (1 - \beta^2)^{-1/2} \tag{2.168}$$

Let t_1 represent the time measured in the SSB frame (Σ), at which a wave front crosses antenna 1 at position $\mathbf{r}_1(t_1)$. Let $\mathbf{r}_2(t_1)$ be the position of antenna 2 at this same time, as measured in the SSB frame. Also, let t_2^* be the time measured in this frame at which that same wave front intersects station 2. This occurs at the position $\mathbf{r}_2(t_2^*)$. Following Section II.A, Eq. (2.2) we can calculate the geometric delay $t_2^* - t_1$. Transforming this time interval back to the geocentric (Σ') frame, we obtain

$$t_2^{*\prime} - t_1' = \gamma(t_2^* - t_1) - \gamma[\mathbf{r}_2(t_2^*) - \mathbf{r}_1(t_1)] \cdot \boldsymbol{\beta} \tag{2.169}$$

Assume further that the motion of station 2 (with barycentric velocity $\boldsymbol{\beta}_2$) is rectilinear over this time interval. This assumption is not strictly true but, as discussed below, the resulting error is much less than 1 mm in calculated delay. 'J'bus,

$$\mathbf{r}_2(t_2^*) = \mathbf{r}_2(t_1) + \boldsymbol{\beta}_2(t_2^* - t_1) \tag{2170}$$

which gives:

$$\mathbf{r}_2(t_2^*) - \mathbf{r}_1(t_1) = \mathbf{r}_2(t_1) - \mathbf{r}_1(t_1) + \boldsymbol{\beta}_2(t_2^* - t_1) \tag{2.1'71}$$

and

$$\begin{aligned} t_2^{*\prime} - t_1' &= \gamma(t_2^* - t_1) - \gamma[\mathbf{r}_2(t_1) - \mathbf{r}_1(t_1)] \cdot \boldsymbol{\beta} - \gamma\boldsymbol{\beta}_2 \cdot \boldsymbol{\beta}[t_2^* - t_1] \\ &= \gamma(1 - \boldsymbol{\beta}_2 \cdot \boldsymbol{\beta})(t_2^* - t_1) - \gamma[\mathbf{r}_2(t_1) - \mathbf{r}_1(t_1)] \cdot \boldsymbol{\beta} \end{aligned} \tag{2.172}$$

This is the expression for the geometric delay that would be observed in the geocentric (X') frame in terms of the geometric delay and station positions measured in the SSB system

Since our calculation starts with station locations given in the geocentric frame, it is convenient to obtain an expression for $[\mathbf{r}_2(t_1) - \mathbf{r}_1(t_1)]$ in terms of quantities expressed in the geocentric frame. '1'0 obtain such an expression consider two events $[\mathbf{r}'_1(t'_1), \mathbf{r}'_2(t'_1)]$ that are geometrically separate, but simultaneous, in the geocentric frame, and occurring at time t'_1. These two events appear in the SSB frame as:

$$\mathbf{r}_1(t_1) = \mathbf{r}'_1(t'_1) + (\gamma - 1)\mathbf{r}'_1(t'_1) \cdot \frac{\boldsymbol{\beta}\boldsymbol{\beta}}{\beta^2} + \gamma\boldsymbol{\beta}t'_1 \tag{2,173}$$

and as:

$$\mathbf{r}_2(t_2) = \mathbf{r}'_2(t'_1) + (\gamma - 1)\mathbf{r}'_2(t'_1) \cdot \frac{\boldsymbol{\beta}\boldsymbol{\beta}}{\beta^2} + \gamma\boldsymbol{\beta}t'_1 \tag{2.174}$$

where

$$t_2 - t_1 = \gamma[\mathbf{r}'_2(t'_1) - \mathbf{r}'_1(t'_1)] \cdot \boldsymbol{\beta} \tag{2.175}$$

With these three equations and the expression

$$\mathbf{r}_2(t_2) = \mathbf{r}_2(t_1) + \boldsymbol{\beta}_2[t_2 - t_1] \tag{2.176}$$

we may obtain the vector $\mathbf{r}_2(t_1)$:

$$\mathbf{r}_2(t_1) = \mathbf{r}'_2(t'_1) + (\gamma - 1)\mathbf{r}'_2(t'_1) \cdot \frac{\boldsymbol{\beta}\boldsymbol{\beta}}{\beta^2} - \gamma\boldsymbol{\beta}t'_1 - \gamma\boldsymbol{\beta}_2[\mathbf{r}'_2(t'_1) - \mathbf{r}'_1(t'_1)] \cdot \boldsymbol{\beta} \tag{2.177}$$

This is the position of station 2 at the time $_1$ as observed in Σ. From this we obtain:

$$\mathbf{r}_2(t_1) - \mathbf{r}_1(t_1) = \mathbf{r}'_2(t'_1) - \mathbf{r}'_1(t'_1) - 1\ (\gamma - 1)[\mathbf{r}'_2(t'_1) - \mathbf{r}'_1(t'_1)] \cdot \frac{\boldsymbol{\beta}\boldsymbol{\beta}}{\beta^2} - \gamma\boldsymbol{\beta}_2[\mathbf{r}'_2(t'_1) - \mathbf{r}'_1(t'_1)] \cdot \boldsymbol{\beta} \tag{2.178}$$

As shown in Section II.A, the vectors $[\mathbf{r}_2(t_1) - \mathbf{r}_1(t_1)]$ and $\boldsymbol{\beta}_2$ are all that is needed to obtain $t_2^* - t_1$ for the case of plane waves. For curved wavefronts we will need to know the individual station locations in the barycentric frame as well. These we obtain from Eqs. (2.1 73) and (2.177) with t'_1 set equal to zero. Setting $t'_1 = 0$ is justified since the origin of time is arbitrary when we are trying to obtain time differences.

In coding these transformations, the relationship for the transformation of velocities is also needed. Taking differentials of Eqs. (2,166) and (2.1 67) we have:

$$d\mathbf{r} = d\mathbf{r}' + (\gamma - 1)d\mathbf{r}' \cdot \frac{\boldsymbol{\beta}\boldsymbol{\beta}}{\boldsymbol{\beta}^2} + \gamma\boldsymbol{\beta}dt' \tag{2.179}$$

$$dt = \gamma(dt' + \mathrm{dr}' \cdot \boldsymbol{\beta}) \tag{2.180}$$

Dividing to obtain $d\mathbf{r}/dt$ we obtain for station 2 in the SSB (Σ) frame:

$$\boldsymbol{\beta}_2 = \left[\boldsymbol{\beta}_2' + (\gamma - 1)\boldsymbol{\beta}_2' \cdot \frac{\boldsymbol{\beta}\boldsymbol{\beta}}{\boldsymbol{\beta}^2} + \gamma\boldsymbol{\beta}\right] / \left[\gamma(1 + \boldsymbol{\beta}_2' \cdot \boldsymbol{\beta})\right] \tag{2.181}$$

For station 2 relative to the geocentric. origin, we have from Eqs. (2,94) and (2.95):

$$\boldsymbol{\beta}_2' \approx \Omega PN \frac{dU}{dH} XY\mathbf{r}_2'\omega_E \tag{2.182}$$

where

$$\omega_E = 7.2921151467 \times 10^{-5}\,\mathrm{rad/s} \tag{2.183}$$

is the inertial rotation rate of the Earth as specified in Seidelmann *et al.* (1 992), p.51. This is not a critical number since it is used only for station velocities, or to extrapolate Earth rotation forward for very small fractions of a day (i. e., typically less than 0.01 day $\approx$ 1000 seconds). Actually, this expression is a better approximation than it might seem from the form since the errors in the approximation, $\frac{dH}{dt} = \omega_E$, are very nearly offset by the effect of ignoring the time dependence of PN.

The assumption of rectilinear motion can be shown to result in negligible errors. Using the plane wave front approximation of Eq. (2.2), we can estimate the error $\delta\tau$ in the calculated delay due to an error $\Delta\boldsymbol{\beta}_2$ in the above value of $\boldsymbol{\beta}_2$:

$$67 = \hat{\mathbf{k}} \cdot [\mathbf{r}_2(t_1) - \mathbf{r}_1 \text{ (ii)} \left[\frac{}{1 - \hat{\mathbf{k}} \cdot (\boldsymbol{\beta}_2 + \Delta\boldsymbol{\beta}_2)} - \frac{1}{1 - \mathbf{k} \cdot \boldsymbol{\beta}_2}\right] \approx \tau\Delta\boldsymbol{\beta}_2 \tag{2.184}$$

Further, from Eq. (2.181) above,

$$\Delta\boldsymbol{\beta}_2 \approx \Delta\boldsymbol{\beta}_2' \tag{2.1s<5}$$

since

$$\gamma \approx \mathrm{I} + \mathrm{IO}\text{-}* \tag{2.186}$$

For the vector $\boldsymbol{\beta}_2'$ in a frame rotating with angular velocity ω, the error $\Delta\boldsymbol{\beta}_2'$ that accumulates in the time interval τ due to neglecting the rotation of that frame is

$$\Delta\boldsymbol{\beta}_2' \approx \boldsymbol{\beta}_2'\omega\tau \tag{2.187}$$

Thus for typical]~art}1-fixed baselines, where $\tau \leq 0.02$ s, neglect of the curvilinear motion of station 2 due to the rotation of the Earth causes an error of $< 4 \times 10^{-14}$ s, or 0.012 mm, in the talc.ulatiol~ of τ. Similarly, neglect of the orbital character of the Earth's motion causes a maximum error on the order of 0.0024 mm.

The position, $\mathbf{R}_E$, and velocity, $\boldsymbol{\beta}_E$, of the Earth's center about the center of mass of the Solar System are:

$$\mathbf{R}_E = -\sum m_i \mathbf{R}_i / \sum m_i \tag{2.188}$$

$$\boldsymbol{\beta}_E = -\sum m_i \boldsymbol{\beta}_i / \sum m_i \tag{2.189}$$

where the index 2 indicates the Sun, Moon, and all nine Solar System planets. m_i is the mass of the body indexed by i, while $\mathbf{R}_i$ and $\boldsymbol{\beta}_i$ are that body's center-of-mass position and velocity relative to the center of the Earth in the barycentric frame. In a strict sense, the summation should be over all objects in the Solar System. Except for the Earth-Moon system, each planet mass represents not only that planet's mass, but also that of all its satellites. The $\mathbf{R}_i$ and $\boldsymbol{\beta}_i$ are obtained from the planetary ephemeris in the J2000 frame (Standish, 1982, Standish and Newhall, 1995).

Working in a frame at rest with respect to the center of mass of the Solar System causes relativistic effects due to the motion of the Solar System in a '{fixed frame" to be included in the mean position of the sources and in their proper motion. '1'here are two effects: geometric and aberrational. The geometric effects of galactic rotation can be easily estimated. In the

vicinity of the Suu, the period for galactic rotation is approximately 2.2×10^8 years. Thus our angular velocity about the galactic center is $\approx 2\pi/2.2 \times 10^8 = 3 \times 10^{-8}$ radialls/year. For sources within the Galaxy, at distances approximately equal to our distance from the galactic center, therefore, the apparent positions could change by ≈ 30 nrad/yr. An intercontinental baseline (10,000 km) could thus be in error by as much as 30 cm/yr (1 nrad $\approx$ 1 cm) if measurements were based on sources within the Galaxy. Since our distance from the galactic center is $\approx 2.7 \times 104$ light years, and most extragalactic radio sources are believed to be $\approx 10^9$ light years distant, the potential baseline error is scaled by the ratio of these two distances, $\approx 3 \times 10^{-5}$, and becomes $\approx$ 0.01 lllln/year. Even with the present 15-year history of VLBI data, the purely geometric systematic error due to galactic rotation is probably negligible, aud only exceeds the millimeter level for sources closer than 100 million light years.

A second contribution comes from galactic aberration, which is treated as a special relativistic effect for an observer on a moving platform. Both the galactic latitudes aud longitudes of the sources vary sinusoidally with the galactic rotation period $T_g = 2.2 \times 10^8$ years, amplitudes ranging over $\pm v/c$ (1 'rench, 1968), and the latitude variation is also proportional to the sine of the latitude. The amplitude range is 7.5×10^{-4} radians; thus over half the rotational period at zero galactic latitude, the longitude varies by

$$\mathrm{AO} = (2v/c)/(0.5T_g) = 1.4 \times 10^{-11}\ \mathrm{rad/yr} \qquad (2.190)$$

Over the present 15-year span of VLBI data, the systematic errors induced by aberration arc thus 0.2 nrad (4o pas) in angular measurements, and 2 mm in distance measurements for a 10,000 km baseline. Both are in the range that is currently starting to be detectable, and galactic rotation must be included in the VLBI model in the near future.

G. Antenna geometry

The development in Secs. 11. A to II.F indicates how the time delay model would be calculated for two points fixed with respect to the Earth's crust. Just as the sources are

not point-like (Sec. 11.1)), the antenna system likewise does not necessarily behave as an Earth-fixed point. Not only are there instrumental delays in the system, but portions of the antenna move relative to the Earth. To the extent that instrumental delays are independent of the antenna orientation, they are indistinguishable to the interferometer from clock offsets and secular changes in these offsets. If necessary, these instrumental delays can be separated from clock properties by a careful calibration of each antenna system. That is a separate problem, treated as a calibration correction (e.g., Thomas, 1981), and will not be addressed here.

However, the motions of the antennas relative to the Earth's surface must be considered since they are part of the geometric model. A fairly general antenna pointing system is shown schematically in Fig. 6, which applies to all antennas that are steerable along two coordinates. The unit vector, $\hat{\mathbf{s}}$, to the apparent source position is shown. Usually, a symmetry axis AD will point parallel to $\hat{\mathbf{s}}$. The point A on the figure also represents the end view of an axis which allows rotation in the plane perpendicular to that axis. This axis is offset by some distance L from a second rotation axis BE. All points on this second rotation axis are fixed relative to the Earth. Consequently, any point along that axis is a candidate for the fiducial point which terminates this end of the baseline. The point we actually use is the point P. A plane containing the rotation axis A and perpendicular to BE intersects BE at the point P. This is somewhat an arbitrary choice, one of conceptual convenience.

Consider the plane Q which is perpendicular to the antenna symmetry axis, AD, and contains the antenna rotation axis A. For plane wave fronts it is an isophase plane (it coincides with the wave front). For curved wave fronts it deviates from an isophase surface by $\approx L^2/(2R)$, where R is the distance to the source, and L is taken as a typical antenna offset AP. For $L \approx 10$ meters, $R = R_{moon} = 60R_E \approx 3.6 \times 10^8$ m, and the curvature correction $L^2/(2R) \approx 1.4 \times 10^{-7}$ m is totally negligible. R has to be 5 ktn, or $10^{-3}R_E$, before this deviation approaches a 1 cm contribution to the delay. Consequently, for all anticipated applications of radio interferometry using high-gain radio antennas, the curvature of the wave front may be neglected in obtaining the effect of the antenna orientation on the time

delay.

Provided the instrumental delay of the antenna system is independent of the antenna orientation, the recorded signal is at a constant phase delay, independent of antenna orientation, at any point on the Q plane. Since this delay is indistinguishable from a clock Offset, it will be totally absorbed by that portion of our model.

1. Axis offset

The advantage of choosing the Q plane rather than some other plane parallel to it is that axis A is contained in this plane, and axis A is fixed relative to the BE axis by the antenna structure. If 1 is the length of a line from P perpendicular to the Q plain, the wave front will reach the }tartl)-fixed point P at a time $\Delta t = l/c$ after the wave front passes through axis A. If τ_0 is the model delay for a wave front to pass from P on antenna 1 to a similarly defined point on antenna 2, then the model for the observed delay should be amended as:

$$\tau = \tau_0 - (\Delta t_2 - \Delta t_1) = \tau_0 + (l_1 - l_2)/c \tag{2.191}$$

where the subscripts refer to antennas 1 and 2.

For the inclusion of this effect in the model, we follow a treatment given by Wade (1 970). Define a unit vector $\hat{\mathbf{I}}$ along BE, in the sense of positive away from the Earth. Further, define a vector, $\mathbf{L}$, from P to A ($|\mathbf{L}| = L$). Without much loss of generality in this antenna system, we assume that $\hat{\mathbf{s}}$, L, and I are coplanar. Then:

$$\mathrm{L} = \pm L \frac{\hat{\mathbf{I}} \times (\hat{\mathbf{s}} \times \hat{\mathbf{I}})}{|\hat{\mathbf{I}} \times (\hat{\mathbf{s}} \times \hat{\mathbf{I}})|} \tag{2.192,}$$

where the plus or minus sign is chosen to give $\mathbf{L}$ the direction from P to A. When $\hat{\mathbf{s}}$ and L are parallel or antiparallel, if the antenna comes closer to the source as L increases, the plus sign is used. Since

$$\hat{\mathbf{I}} \times (\hat{\mathbf{s}} \times \hat{\mathbf{I}}) = \hat{\mathbf{s}} - \hat{\mathbf{I}} (\hat{\mathbf{I}} \cdot \hat{\mathbf{s}}) \tag{2.193}$$

$$l = \hat{\mathbf{s}} \cdot \mathbf{L} = \pm L \sqrt{1 - (\hat{\mathbf{s}} \cdot \hat{\mathbf{I}})^2} \tag{2.194}$$

where the sign choice above is carried through.

Curvature is always a negligible effect in the determination of $\hat{\mathbf{s}} \cdot \mathbf{I}$,. Likewise, gravitational effects are sufficiently constant over a dimension H so as to enable one to obtain a single Cartesian frame over these dimensions, to a very good approximation. Consequently, it is somewhat easier to calculate a proper time $\Delta t = \mathrm{l/c}$ in the antenna frame and to include it in the model by adding it to τ_0, taking into account the time dilation in going from the antenna frame to the frame in which τ_0 is obtained.

2. Refraction

If $\hat{\mathbf{s}}_0$ is the unit vector to the source from the antenna in a frame at rest with respect to the Solar System center of mass, a Lorentz transformation yields $\hat{\mathbf{s}}$, the (aberrated) apparent source unit vector in the Itarth-fixed celestial frame. Actually, the antenna does not "look" at the apparent source position $\hat{\mathbf{s}}$, but rather at the position of the source after the ray path has been refracted by an angle ΔE in the Earth's atmosphere. This effect is already included in the tropospheric delay correction (Section IV.B); however since the antenna model uses the antenna elevation angle E_0, the correction must be made here as well. For the worst case (elevation angle of 6°) at average DSN station altitudes ($\approx$1km), the deflection can be as large as 2 x 10--3 radians. '1'bus, $\delta l \approx L \Delta E \approx$ 2 cm for L = 10 meters. A model option permits modification of $\hat{\mathbf{s}}$ to take atmospheric refraction into account. The large-elevation-angle approximation is the inverse tangent law:

$$\Delta E = 3.13 \times 10^{-4} / \tan E_0 \qquad (2.195)$$

where E is the elevation angle, and ΔE the change from the apparent elevation E_0 induced by refraction. This model was implemented only for software comparison purposes, since it gives incorrect results at low elevation angles. In the notation of Section IV.B, a single homogeneous spherical layer approximation yields the bending correction in terms of the zenith troposphere delays ρ_Z, first moment of the wet troposphere refractivity M_{wet}, dry troposphere scale height A, and Earth radius R:

$$\Delta E = \cos^{-1}[\cos(E_0 + (\mathrm{Fe}))/(1 + \chi_0)] - \alpha_0 \tag{2.196}$$

where

$$\chi_0 = (\rho Z_{dry} + \rho Z_{wet}/M_{wet})/\Delta \tag{2,197}$$

$$\alpha_0 = \cos^{-1}[(1 + \sigma')/(1+\sigma)] \tag{2.198}$$

$$\sigma = \Delta/R \tag{2.199}$$

$$\sigma' = \left[(1+ \sigma(\sigma + 2)/\sin^2 E_0\right)^{1/2} - 1\Big]\sin^2 E_0 \tag{2.200}$$

This formula agrees with ray-tracing results to within 1% at 6° and ≈15% at 1° elevation, while the corresponding comparisons for Eq. (2.1 95) give ≈25% at 6° and a factor of 3 at 1°.

Since we are given $\hat{\mathbf{I}}$ in terrestrial coordinates, we first perform the coordinate transformation given by Q in Section II.E:

$$\hat{\mathbf{I}} = Q\hat{\mathbf{I}}_{terrestrial} \tag{2.201}$$

With this done, obtain $\Delta t = l/c$ from Eq. (2.194). Note that for "nearby" sources we also must include parallax (i. e., geographically separate antennas are not pointing in the same direction). If R. is the position of the source as seen from the center of the Earth, and r is the position of a station in the same frame, then the position of the source relative to that station is

$$\mathrm{R} = \mathbf{R}_0 - \mathrm{r} \tag{2.202}$$

and in Eq. (2.194) we make the substitution

$$(\hat{\mathbf{s}} \cdot \hat{\mathbf{I}})^2 = \left[\frac{(\mathbf{R}_0 - \mathbf{r}) \cdot \hat{\mathbf{I}}}{|\mathbf{R}_0 - \mathbf{r}|}\right]^2 \tag{2.203}$$

3. Unique antennas

One of the antennas employed by the IRIS project of NOAA was extensively used in VLBI experiments did not fall into any standard category. It was unique because it was an equatorial mount designed for the latitude of Washington, D.C., but was deployed at Richmond, Florida until it was destroyed in the hurricane of August 1992. The considerable latitude difference, and the axis offset of several meters, make it imperative that the antenna geometry be properly modeled. In the local VEN coordinate frame, the vector $\hat{\mathbf{I}}$ is

$$\begin{pmatrix} \sin\phi_W \\ -\cos\phi_W \sin\epsilon \\ \cos\phi_W \cos\epsilon \end{pmatrix}_1 \tag{2.204}$$

Upon transformation to the Narth-fixed frame via the matrix VW [Eq. (2.67)], it becomes

$$\begin{pmatrix} \cos\lambda(\sin\phi_W \cos\phi - \cos\phi_W \sin\phi \cos\epsilon) + \sin\lambda \cos\phi_W \sin\epsilon \\ \sin\lambda(\sin\phi_W \cos\phi - \cos\phi_W \sin\phi \cos\epsilon) - \cos\lambda \cos\phi_W \sin\epsilon \\ \sin\phi_W \sin\phi + \cos\phi_W \cos\phi \cos\epsilon \end{pmatrix} \tag{2.205}$$

Here (A,+) are the Richmond longitude and latitude, ϕ_W is the latitude of Washington (39.060), and $\epsilon = 0.12°$ W of N is the azimuth misalignment.

Two other one-of-a-kind antennas, in Arecibo, Puerto Rico and Nancay, France, arc seldom used in astromet ric and geodetic VLBI work. The Arecibo antenna has hardware features which make it equivalent to an azi]nutl]-elevation mount. The Nancay array has been treated by Ortega- Molina (1 985).

4. Site vectors

Modeling software must provide the facility to add a time-invariant offset vector in local geodetic coordinates (geodetic vertical, East, and North) from the antenna reference point to a point elsewhere, such as a benchmark on the ground. This is particularly useful in work involving transportable antennas which may be placed in slightly different places relative to an Earth-fixed benchmark each time a site is reoccupied. In modeling that offset vector,

we make the assumption of a plane tangent to the geoid at the reference benchmark and assume that the local geodetic vertical for the antenna is parallel to that for the benchmark. With these assumptions there is an identity in the adjustments of antenna location with changes derived for the benchmark location. The error introduced by these assumptions in a baseline adjustment is approximately ΔB x (d/R_E), where ΔB is the baseline adjustment from its a *priori* value, d is the! separation of the antenna from the benchmark, and R_E is the radius of the Earth. To keep this error smaller than 0.1 mm for baseline adjustments on the order of 1 meter, $d < 600$ meters is required.

More troublesome is that an angular error $\delta\Theta$ in obtaining the local vertical, when using an antenna whose intersection of axes is a distance, H, above the ground, can cause an error of $H\sin\delta\Theta \approx H\delta\Theta$ in measuring the baseline to the benchmark (Allen, 1982). Unless this error is already absorbed into the actual measurement of the offset vector, care must be taken in setting up the antenna so as to make $\delta\Theta$ minimal. For a baseline error < 1 mm, and an antenna height of 10 meters, $\delta\Theta$ < 20 arcseconds is required. Often plumb bobs are used to locate the antenna position relative to a mark on the ground. This mark is, in turn, surveyed to the benchmark. Even the difference in geodetic vertical from the vertical defined by the plumb bob may be as large as 1 arc minute, thus potentially causing an error of 3 mm for antennas of height 10 meters. Consequently, great care must be taken in these measurements, particularly if the site is to be repeatedly occupied by portable antennas of different sizes.

5. Feed rotation

Another physical effect related to antenna structures is the differential feed rotation for circularly polarized receivers. This is caused by the changing orientation of the electromagnetic field relative to a fixed direction on the celestial sphere. Liewer (1985) has calculated the phase shift O for various antenna types. It is zero for equatorially mounted antennas. For altazimuth mounts,

$$\tan O = \cos\phi \sin h/(\sin\phi \cos\delta - \cos\phi \sin\delta \cos h) \quad (2.206)$$

with ϕ = station latitude, h = hour angle, and δ = declination of the source. For X-Y mounts, two cases are distinguished: orientation $N - S$ or E-W. The respective rotation angles are

$$\tan(-\theta) = \sin\phi \sin h/(\cos\phi \cos\delta + \sin\phi \sin\delta \cos h) \quad (N - S) \quad (2.207)$$

$$\tan(-\theta) = -\cos h/(\sin\delta \sin h) \quad (E - W) \quad (2.20s)$$

The effect cancels for group delay data, but can be significant for phase delay and delay rate data (up to 100 fs/s for the latter). The effect on phase delay is

$$T = (\theta_2 - \theta_1)/f \quad (2.209)$$

where f is the observing frequency and θ_i the phase rotation at station i.

Finally, another small correction which accounts for the effect of orientation of hour angle-declination (HA-Dec) and X-Y antennas on the tropospheric path delay was considered by Jacobs (19S8). Details are given in tile troposphere Section, IV.B.

6. Thermal expansion

By analogy with the model for atmospheric loading in Section II.C.3.a, variations of the temperature cause vertical displacements of the antenna reference point. These can amount to several mm for ordinary diurnal or seasonal temperature variations for large antennas. If VLBI data acquired under diverse weather conditions are to be processed simultaneously, it may be important to account for the vertical motion of the reference point.

A rudimentary model of this effect assumes that the vertical displacement Δr of the antenna reference point, a distance h above the ground, is

$$\Delta r = \alpha(T - T_{ref})h \quad (2.210)$$

where α is the coefficient of thermal expansion and T_{ref} is the reference temperature. The reference temperature is taken to be equal to the global average temperature at each station.

or *the* universal average *292 K* (used in tropospheric mapping in Sec. IV. }].]) if the former is not available. A linear expansion coefficient of 12 ppm is appropriate for both steel and concrete. The vertical motion is thus ≈ 0.42 mm/K for a 70-m antenna. Refinements of the simple model would have to consider details of the antenna structure, and allow for thermal lag relative to the ambient temperature (e g., McGinnis, 1977, Nothnagel, Pilhatsch and Haas, 1995).

7. Antenna subreflector focusing

Gravity loading changes an antenna's focal length. Because the component of the gravity load along the antenna's primary axis of symmetry is proportional to $\sin E$ (E = elevation angle), the changes in focal length also have sinusoidal elevation dependence. In Cassegrainian antennas the subreflector may be moved ("autofocused") to compensate for gravity deformations and thereby maintain focus. However, this procedure does not maintain a constant signal path length through the antenna optics and thus introduces systematic errors in the antenna position derived from the measurements. This than.gc in path must be modeled for such experiments, notably the Time and Earth Motion Precision observation (TEMPO) project (Steppe *et al.*, 1994). For example, the Deep Space Network antennas used in TEMPO measurements arc designed to be in focus with no subreflector compensation at E = 45°. For the DSN 70-111 and 34-m high efficiency antennas these additional delays are empirically determined to be, in mm (Jacobs and Rius, 1989, 1990):

$$\tau_{sr}(\text{70-m}) = \quad 77 \sin E \; - \; 54 \tag{2.2]1}$$

$$\tau_{sr}(\text{34-m}) = 13.5 \sin E \; - 9.8 \tag{2,212}$$

where the coefficients, known to within approximately 5%. This functional form clearly exhibits the relationship between subreflector motion and other model parameters. The elevation-dependent term biases the station vertical coordinate, while the constant term is equivalent to the clock offset.

III. CLOCK MODEL

The frequency standards ('(clocks") at each of the two antennas arc normally independent of each other, At tempts are made to synchronize them before an experiment by conventional synchronization techniques, but these techniques are accurate! to only a few' μs ill epoch and $\approx$ 10-]2 in rate, More importantly, clocks often exhibit "jumps" and instabilities at a level that would greatly degrade interferometer accuracy if not modeled. To account for these clock effects, an additional "delay" τ_c is included in the model delay, a delay that models the behavior of a station clock as a piecewise quadratic function of time throughout an observing session. Usually, however, only the linear portion of this model is needed. For each station this clock model is given by:

$$\tau_c = \tau_{c1} + \tau_{c2}(t - t_{ref}) + \tau_{c3}(t - t_{ref})^2/2 \qquad (3.1)$$

The reference time, t_{ref}, may be set by the user, or by default it is taken as the midpoint of the interval over which the *a priori* clock parameters, τ_{c1}, T_{c2}, τ_{c3}, appl y.

In addition to the effects of the lack of synchronization of clocks between stations, three are other differential instrumental effects which may contribute to the observed delay. In general, it is adequate to model these effects as if they were '(clock-like". Note that the instrumental effects on delays measured using the multifrequency bandwidth synthesis tech - nique (Thomas, 1981) may be different from the instrumental effects on delays obtained from phase measurements at a single frequency. This is because the bandwidth synthesis process obtains group delay from the slope of phase versus frequency ($\tau = \frac{\partial\phi}{\partial\nu}$) across multiple frequency segments spanning the receiver passband. '1'bus, any frequency-independent instrumental contribution to the measured interferometer phase has no effect on the delay determined by the bandwidth synthesis technique. However, if tile delay is obtained directly from the phase measurement, ϕ, at a given frequency, ν, then the phase delay $\tau_{pd} = \frac{\phi}{\nu}$) does have that instrumental contribution.

Because of this difference, it is necessary to augment the '(clock" model for phase delay measurements:

$$\tau_{c_{pd}} = \tau_c - \{ \tau_{c4}(t - t_{ref}) + \tau_{c5}(t - t_{ref})^2/2 \tag{3.2}$$

where τ_c is the clock model for bandwidth synthesis observations and is defined in Eq. *(2.67)*. Since the present system measures both bandwidth synthesis delay and phase delay rate, all of the clock parameters described above must be used. However, in a '(perfectly" calibrated interferometer, $\tau_{c4} = \tau_{c5} = 0$. This particular model implementation allows simultaneous use of delay rate data derived from phase delay, with group delay data derived by means of the bandwidth synthesis technique.

An options] refinement of the clock model is also available. For dual-frequency (S/X) delays, an additional clock offset may be estimated. It originates from the differential instrumental delay and fringe fitting delays for S- ant] X-band data, which may be sizeable. For dual-frequency observables, the clock model depends on this differential instrumental delay and on the frequencies ω_S, ω_X in the individual bands as

$$\tau_{c6}\ \omega_X^2/(\omega_X^2 - \omega_S^2) \tag{3.3}$$

The differential instrumental delay τ_{c6} is normally highly correlated with the usual clock offset τ_{c1}, but under some circumstances may convey additional information.

To model the interferometer delay on a given baseline, a difference of station clock terms is formed:

$$\tau_c = \tau_{c_{station\ 2}} - \tau_{c_{station\ 1}} \tag{3.4}$$

Specification of a reference clock is unnecessary until the parameter adjustment step, and need not concern us in the description of the model.

IV. ATMOSPHERIC DELAY

Prior to its arrival at each antenna in Earth-based experiments, the radio wave front must pass through the atmosphere. This section is concerned with modeling the additional delay due to the atmosphere, It is conveniently divided into two parts: contributions from

charged particles in the upper atmosphere (ionosphere), and neutral molecules in the lower atmosphere (troposphere).

A. Ionosphere

The uppermost component of the Earth's atmosphere, the ionosphere, is a layer of plasma at about 350 km altitude, created primarily by the ultraviolet portion of the sunlight and the solar wind. in the quasi-longitudinal approximation (Spitzer, 1 962) the refractive index of this medium is

$$n = \left[1 - \left(\frac{\nu_p}{\nu}\right)^2 \left(1 \pm \frac{\nu_g}{\nu}\cos\Theta\right)^{-1}\right]^{1/2} \tag{4.1}$$

where the plasma frequency, ν_p, is

$$\nu_p = \left(\rho c^2 r_0/\pi\right)^{1/2} \approx 8.97 \times 10^3 \rho^{1/2} \tag{4.2}$$

the electron gyrofrequency, ν_g, is

$$\nu_g = \frac{eB}{2\pi mc} \tag{4.3}$$

and Θ is the angle between the magnetic field B and the direction of propagation of the wave front. Here ρ is the number density of the electrons, e and m are the electron charge and mass, r_0 is the classical electron radius, and c is the speed of light.

Tables V and VI give the plasma frequency, ν_p, and gyrofrequency, ν_g, for the three regimes of a radio signal's ray path: Earth, interplanetary, and interstellar space. Given the S-band (ν_S = 2.3 GHz) and X-band (ν_X = 8.4 GHz) frequencies typically used for geodetic and astrometric V],]]], the importance of correcting for plasma and gyrofrequency can be parameterized by the ratios of ν_p and ν_g to ν_S and to ν_X respectively.

Relative to vacuum as a reference, the phase delay of a monochromatic signal traversing this medium of refractive index n is

$$\tau_{pd} = \frac{1}{c}\int (n - 1)dl \approx -\frac{1}{2c}\int \left(\frac{\nu_p'}{\nu}\right)^2 \left[1 + \frac{1}{4}\left(\frac{\nu_p'}{\nu}\right)^2 + \frac{1}{8}\left(\frac{\nu_p'}{\nu}\right)^3 + \ldots\right]dl \tag{4.4}$$

Whew

$$\frac{\nu'_p}{\nu} = \left(\frac{\nu_p}{\nu}\right)\left[1 \pm \left(\frac{\nu_g}{\nu}\right) \text{cd})\right]\text{-}]" \tag{4.5}$$

For 8.4 GHz, we may approximate this effect to parts in 10^6 - 10^7 by:

$$\Delta_{pd} \approx \frac{-q}{\nu^2}\left[1 \pm \left(\frac{\nu_g}{\nu}\right)\cos\Theta\right]^{-1} \approx \frac{-q}{\nu^2}\left[1 - \left(\frac{\pm\nu_g}{\nu}\right)\cos\Theta\right] \tag{4.6}$$

where

$$_{\text{q}} = \frac{cr_0}{2\pi}\int \rho dl = \frac{cr_0 I_e}{2\pi} \tag{4.7}$$

and where I_e is the total number of electrons per unit area along the integrated line of sight. The bar symbolizes a geometrical average. If we also neglect the term $\overline{(\nu_g \cos\Theta)}/\nu$, then the expression for Δ_{pd} becomes simple and independent of the geometry of the traversal of the wave front through the ionosphere:

$$\Delta_{pd} = -q/\nu^2 \tag{4.8}$$

This delay is negative. '1'bus, a phase advance actually occurs for a monochromatic signal. Since phase delay is obtained at a single frequency, observables derived from phase delay (*e.g.*, phase delay rates) experience an increment which is negative (the observable with the medium present is smaller than it would be without the medium). In contrast, group delays measured by a technique such as bandwidth synthesis ($\tau_{gd} = \frac{\partial\phi}{\partial\nu}$) experience an additive delay which can be derived from Eq. (4.8) by differentiating $\phi = \nu\Delta_{pd}$ with respect to frequency:

$$\Delta_{gd} = q/\nu^2 \tag{4.9}$$

Notice that the sign is now positive, though the group delay is of the same magnitude as the phase delay advance. For group delay measurements, the measured delay is larger with the medium present than without the medium.

For a typical ionosphere, $\tau \approx 0.1$ to 2 ns at local zenith for v = 8.4 GHz. This effect has a maximum at approximately 1400 hours local time and a broad minimum during local

night. For long baselines, the effects at each station are quite different. Thus, the differential effect may be of the same order as the maximum.

For the interplanetary medium and at an observing frequency of 8.4 GHz, a single ray path experiences a delay of approximately $6 \times$ 10-7 s in traversing the Solar System. However, the differential delay between the ray paths to the two stations on the Earth is considerably smaller, since the gradient between the two ray paths should also be inversely proportional to the dimensions of the plasma region (i. e., one astronomical unit as opposed to a few thousand kilometers). The ray path from a source at a distance of 1 megaparsec (3 x 10^7 kin) experiences an integrated plasma delay of approximately 5000 seconds for a frequency of 8.4 GHz. In this case, however, the typical dimension is also that much greater, and so the differential effect on two ray paths separated by one Earth radius is still not as great as the differential delays caused by the Earth's ionosphere.

1. Dual-frequency calibration

These plasma effects can best be removed by the technique of observing the sources at two frequencies, ν_1 and ν_2, where $\nu_{1,2} >> \nu_p$ and where $|\nu_2 - \nu_1|/(\nu_2 + \nu_1) \approx 1$. Then at the two frequencies ν_1 and ν_2 we obtain

$$\tau_{\nu 1} = T + q/\nu_1^2 \tag{4.10}$$

and

$$\tau_{\nu 2} = \tau + q/\nu_2^2 \tag{4.11}$$

Multiplying each expression by the square of the frequency involved and subtracting, we obtain

$$\tau = a\, \tau_{\nu 2} + b\, \tau_{\nu 1} \tag{4.12}$$

where

$$a = \nu_2^2/(\nu_2^2 - \nu_1^2) \tag{4.13}$$

and

$$b = -\nu_1^2/(\nu_2^2 - \nu_1^2) \tag{4.14}$$

This linear combination of the observables at two frequencies thus removes the charged particle contribution to the delay.

For uncorrelated errors in the frequency windows, the overall error in the derived delay can be modeled as

$$\sigma_\tau^2 = a^2\sigma_{\tau_{\nu 2}}^2 + b^2\sigma_{\tau_{\nu 1}}^2 \tag{4.15}$$

Modeling of other error types is more difficult and will not be treated here. Since the values of a and b are independent of q, these same coefficients apply both to group delay and to phase delay.

If we had not neglected the effect of the electron gyrofrequency in the ionosphere, then instead of Eq. (4.1 2) above, we would have obtained

$$\tau = a\tau_{\nu 2} + b\tau_{\nu 1} + q\,\overline{\nu_g \cos\Theta}/[\nu_2\nu_1(\nu_2 - \nu_1)] \tag{4.16}$$

where a and b are defined as in Eqs. (4.1 3) and (4.1 4), respectively.

If we express the third term on the right-hand side in units of the contribution of the ionosphere at frequency ν_2, we obtain

$$\tau = a\tau_{\nu 2} + b\tau_{\nu 1} + \Delta_{pd}\nu_2\,\nu_g \cos\Theta/[\nu_1(\nu_2 + \nu_1)] \tag{4.1'7}$$

For X band $\Delta_{pd} \approx 0.1$ to 2 ns at the zenith. When using S baud as the other frequency in the pair, this third term is $\approx 2 \times 10^{-4}\Delta_{pd}\cos\Theta \approx 0.2$ to 4 ps at zenith. in the worst case of high ionospheric electron content, and at low elevation angles, this effect could reach 1 mm of total error in determining the total delay using the simple formula of Eq. (4.1 2) above. Notice that the effect becomes much more significant, at lower frequencies.

2. Total electron content

In the absence of the dual-frequency observation capability described above, one can improve the model of the interferometer by modeling the ionosphere, using whatever measurements of the total electron content are available. The model we have chosen to implement is very simple. Its formalism is similar to that of the troposphere model, except that, the ionosphere is modeled as a spherical shell for which the bottom is at the height h_1 above the geodetic surface of the Earth, and the top of the shell is at the height h_2 above that same surface (see Fig. 7). For each station the ionospheric delay is modeled as

$$\tau_i = kgI_e S(E)/\nu^2 \tag{4.18}$$

where

$$k = \frac{0.1cr_0}{2\pi} \tag{4.19}$$

I_e is the total electron content at zenith (in electrons per meter squared x 10-17), and $g = 1$ (−1) for group (phase) delay. E is the apparent geodetic elevation angle of the source, $S(E)$ is a slant range factor discussed below, and v is the observing frequency in gigahertz.

The slant range factor (see Fig. 7) is

$$S(E) = \frac{\sqrt{R^2 \sin^2 E + 2Rh_2 + h_2^2} - \sqrt{R^2 \sin^2 E + 2Rh_1 + h_1^2}}{h_2 - h_1} \tag{4.20}$$

This expression is strictly correct for a spherical Earth of radius R, and a source at apparent elevation angle E. The model employed uses this expression, with the local radius of curvature of the geoid surface at the receiving station R taken to be equal to the distance from the station to the center of the Earth. The model also assumes this same value of R can be used at the ionospheric penetration points, *e.g.*:

$$R_i = R + h_i \tag{4.21}$$

This is not strictly true, but is a very close approximation, particularly compared to the crude nature of the total electron content determinations on which the model also depends.

The total ionospheric contribution 011 a given baseline is

$$\tau_I = \tau_{i_{station\ 2}} - \tau_{i_{station\ 1}} \qquad (4.2'2)$$

W c assume that the ionospheric total electron content, I_e, is the sum of two parts, one obtained by sonic external set of measurements such as Faraday rotation or GPS techniques, and the other by some specified additive constant:

$$I_e = I_{e\ meas} + I_{e\ add} \qquad (4.23)$$

These external measurements, in general, are not along directions in the ionosphere coincident with the ray paths to the interferometer. '1'bus, for each antenna, it is necessary to map a measurement made along one ray path to the ray paths used by the interferometer. Many different techniques to do this mapping have been suggested and tried; all of them are of dubious accuracy. In the light of these problems, and in the anticipation that dual-frequency observations will be employed for the most accurate interferometric work, we have implemented only a simple hour-angle mapping of the time history of the measurements of I_e at a given latitude and longitude to the point of interest. in this model we allow the user to adjust the "height", h, of the ionosphere, but require

$$h_1 = 11 - 35\,\text{km}$$
$$h_2 = h + 70\ \text{km} \qquad (4.24)$$

Nominally, this "height" is taken to be 350 km. Setting this height to zero causes tile algorithm to ignore the ionosphere model, as is required if dual-frequency observations have already been used to remove the plasma effects. As in the troposphere model, these corrections can also be incorporated as calibrations into the input data stream. Then the user is free to accept the passed correction, and use this model as a small alteration of the previously invoked model, or to remove the passed corrections.

The deficiencies of these ionosphere models for sillgle-frequency observations are compounded by the lens effect of the solar plasma. in effect, the Solar System is a spherical plasma lens which will cause the apparent positions of the radio sources to be shifted from

their actual positions by an amount which depends on the solar weather and on the Sun - l~,artl]-source angle. Since both the solar weather and the Sun-Earth-source angle change throughout the year, very accurate single-frequency observations over the ti me scale of a year are virtually impossible unless simultaneous auxiliary experiments are performed.

B. Troposphere

Permanent and induced dipole moments of the molecular species present in the atmosphere modify its index of refraction and thus delay the passage of radiation at microwave frequencies. The neutral atmosphere is composed of two major constituents, customarily called "dry" and "wet". The dry portion, primarily oxygen and nitrogen, is very nearly in hydrostatic equilibrium, and its effects can be quite accurately estimated simply by measuring the barometric pressure at the surface. Typically, at sea level in the local zenith direction, the additional delay that the incoming signal experiences due to the troposphere is approximately 6 nanoseconds or 2 meters. Except for winds aloft, unusually strong lee wave.s behind mountains (e.g., Owens Valley, California), or very high pressure gradients, an azimuthally symmetric model based 011 measurements of surface barometric pressure is considered adequate. The limits of validity of azimuthal symmetry arc starting to be investigated (MacMillan, 1995). Rough esti mates in the past have indicated that, except in the unusual cases mentioned above, the error in such an assumption causes sub-centimeter errors in the baseline.

Unfortunately, the wet component of the atmosphere (both water vapor and condensed water in the form of clouds) is not so easily modeled. The experimental evidence (Resch, 1984) is that it is "clumpy", and not azimuthally symmetric about the local vertical at a level which can cause many centimeters of error in a baseline measurement. Furthermore, because of incomplete mixing, surface measurements are inadequate in esti mating this contribution which even at zenith can reach 20 or 30 cm. Ideally, thi S portion Of the tropospheric d elay should be determined experimentally at each site at the time of the VLBI measurements.

This is particularly true for short and intermediate (B < 1 000 km) baselines, where the elevation angles of the two antennas are highly correlated during the observations. On longer baselines, both the independence of the elevation angles at the two antennas, and the fact that often the mutual visibility requirements of VLBI constrain the antennas to look only in limited azimuthal sectors, allow the use of the interferometer data themselves to quantify the effect of the water vapor as part of the parameter intimation process. Recent water vapor radiometer (WVR) measurements along the lines of sight of VLBI observations (Teitelbaum *et al.*, 1 995) yield wet troposphere delays that agree with VLBI parameter estimates on the level of a few mm, and give a threefold reduction in residuals. Similar results have been obtained occasionally during the past two decades (Elgered *et al.*, 1991); it is hoped that recent advances in WVR technology will permit routine calibration of VLBI measurements in the near future. Because state-of-the-art WVR measurements arc not presently routinely available, VLBI processing software should at the minimum have the capability to model the neutral atmosphere at each station as a two-component effect, with each component being an azimuthally symmetric function of the local geodetic elevation angle.

At each station the delay experienced by the incoming signal clue to the troposphere can most simply be modeled using a spheri cal-shell troposphere consisting of wet and dry components:

$$\tau_{trop\ station\ i} = \tau_{wet\ trop\ i} + \tau_{dry\ trop\ i} \tag{4.25}$$

The total troposphere delay model for a given baseline is then:

$$\tau_t = \tau_{trop\ station\ 2} - \tau_{trop\ station\ 1} \tag{4.26}$$

If E_i is tile apparent geodetic elevation angle of the observed source at station i, wc have (dropping the subscript i):

$$\tau_{trop} = \rho_{Z_{dry}} R_{dry}(E) + \rho_{Z_{wet}} R_{wet}(E) \tag{4.27}$$

where ρ_Z is the additional delay at local zenith due to the presence of the troposphere, and R is the so-called "mapping function".

For some geodetic experiments, the observed delay can be accurately calibrated for the total tropospheric delays at the two stations, which are in turn calculated on the basis of surface pressure measurements for the dry component, and water-vapor radiometer (WVR) measurements for the wet component. At a fixed location, the dry zenith delay (m) is related to the surface pressure p(mbar) as

$$\rho_{Z_{dry}} = 2.2768 \times \text{lo-3p}/(1 - 0.00266 \cos 2\phi - 0.00028h) \tag{4.28}$$

where the factor in the denominator corrects for a non-spherical Earth (Saastamoinen, 1972), ϕ is the station geodetic latitude [see Eq. (2.68)], and h is the station altitude (km). The wet zenith delay $\rho_{Z_{wet}}$ can be inferred from WVR measurements performed in the vicinity of the VLBI stations at the time of the experiment. These corrections are recorded in the input data stream to the modeling software in such a way that they can be removed and replaced by an alternate model if desired, In the absence of such external calibrations, it was found that modeling the zenith delay as a linear function of time can improve troposphere modeling considerably. The dry and wet zenith parameters are written as

$$\rho_{Z_{d,w}} = \rho^0_{Z_{d,w}} + \dot{\rho}_{Z_{d,w}}(t - t_0) \tag{4.29}$$

where t_0 is a reference time. The time rates of change, $\dot{\rho}_{Z_{d,w}}$, may then be estimated from fitting the data.

Another way of introducing realistic variations of tile troposphere with both time and geometry is through the "(frozen flow" turbulent troposphere model of Treuhaft and Lanyi (1987). This model provides estimates of correlations of the tropospheric delays observed in different parts of the sky at different times. The resulting correlation matrix among the observations can then be included in the least-squares parameter estimation procedure. Additional parameters which characterize the strength, extent, and direction of the turbulent flow are required to implement the Treuhaft-Lanyi model. These are just recently starting to be quantified, for example by Naudet (1 995).

1. Mapping functions

The earliest and simplest mapping function used for VLBI modeling is that obtained by C. C. Chao (1 974) via analytic fits to ray tracing, a function which he claimed to be accurate to the level of 1% at 6° elevation angle and to become much more accurate at higher elevation angles.

$$R_{dry,wet} = \frac{1}{\sin E + \frac{A_{dry,wet}}{\tan E + B_{dry,wet}}} \tag{4.30}$$

where

$$A_{dry,wet} = (0.00143,\ 0.00035) \tag{4.31}$$

$$B_{dry,wet} = (0.0445, 0.017) \tag{4.32}$$

Marini (1 972) introduced a mapping function that takes the form of a continued fraction,

$$R = \frac{1}{\sin E + \frac{a}{\sin E + \frac{b}{\sin E + c}}} \tag{4.33}$$

As more accurate measurements in the 1 %S0s demanded more accurate troposphere modeling, numerous improved mapping functions were developed. Many of these have mathematical forms that are variants of Marini's continued fraction, and contain constants derived from analytic fits to ray-tracing results either for standard atmospheres or for observed atmospheric profiles based on radiosonde measurements. The functions of Davis *et al.* (1985) (CfA), Ifadis (1986), Herring (1992) (MTT), and Niell (1995) (NMF) fall into this category. Some of them contain parameters that are to be determined from surface meteorological measurements. The Ifadis and NMF functions attempt to represent weather variations analytically as a function of time of year and location, and contain no adjustable parameters. Another tropospheric mapping function, due to Lanyi (1984) is unique in that it does not

fully separate tile dry and wet components and thus gives a more faithful representation of the physical effects. It also contains the most complete set of atmospheric parameters, and we will present some details for this representative of such a class of functions. Several reviews have recently evaluated the multitude of tropospheric mapping functions that arc now available: Gallini (1994), Mendes and Langley (1 994), and Estefan and Sovers (1994).

Motivation for and full details of the development of a new tropospheric mapping function Were given by Lanyi (1 984). It is based on an ideal model atmosphere whose temperature is constant from the surface to the top of the inversion layer h_1, then decreases linearly with height at a rate W (lapse rate) from there to the tropopause height h_2, and is constant again above h_2. Here we give only a brief summary of the functional form. The tr opospheric delay is written as:

$$\tau_{trop} = F(E)/\sin E \tag{4.34}$$

where

$$F(E) = \rho_{Z_{dry}} F_{dry}(E) + \rho_{Z_{wet}} F_{wet}(E) + [\rho^2_{Z_{dry}} F_{b1}(E) + 2\rho_{Z_{dry}}\rho_{Z_{wet}} F_{b2}(E) + \rho^2_{Z_{wet}} F_{b3}(E)]/\Delta + \rho^3_{Z_{dry}} F_{b4}(E)/\Delta^2 \tag{4.35}$$

The quantities $\rho_{Z_{dry}}$ and $\rho_{Z_{wet}}$ have the usual meaning: zenith dry and wet tropospheric delays. A is the atmospheric scale height, A = kT_0/mg_c, k = Boltzmann's constant, T_0 = average surface temperature, m = mean molecular mass of dry air, and g_c = gravitational acceleration at the center of gravity of the air column, With the standard values k = 1 .3806(ix10-]6 erg/K, m = 4.8097x10- ^{23}g, g_c = 978.37 cm/s^2, and the average temperature for DSN stations T_0 = 292 K, the scale height A = 8567 m. The dry, wet, and bending contributions to the delay, $F_{dry}(E)$, $F_{wet}(E)$, and $F_{b1,b2,b3,b4}(E)$, are expressed in terms of moments of the refractivity. The latter arc evaluated for the ideal model atmosphere and thus give the dependence of the tropospheric delay on the four model parameters T_0, W, H_1, and h_2. Note that Lanyi's formulation [Eq. (4.35)] differs from the simple model [Eq. (4.27)] in the presence of the "bending" terms F_{b1-4}. These account for the influence of the dry and wet constituents in bending the incoming ray path.

Four meteorological parameters may override the default (global average) values of the Lanyi model. These are: 1) the surface temperature T_0, which determines the atmosphere scale height; 2) the temperature lapse rate W, which determines the dry model parameter α; 3) the inversion altitude h_1, which determines q_1; and 4) the tropopause altitude h_2, which determines q_2. A fifth parameter, the surface pressure p_0, may be used to calibrate the dry zenith delay via Eq. (4.28). Table VII summarizes the four parameters and derived quantities, and their default values. Approximate sensitivities of the tropospheric delay to the meteorological parameters arc given in the last column. These values arc calculated at 6° elevation, which is the approximate limit of validity of the Lanyi model. At this elevation, the ray path traverse.sapproxilnatcly 10 zenith atmospheres,

2. Antenna axis offset altitude correction

Antennas with non-zero axis offsets, whose second rotation axis (A in Fig. 6) moves vertically with changing orientation, have zenith troposphere delays that may vary by 1 to 2 mm over the range of available orientations. Equatorial and X-Y mounts fall in this class. At low elevation angles this zenith variation is magnified by the mapping function to 1-2 cm. These variations must be modeled in experiments whose accuracies arc at the millimeter level (*e.g.*, short-baseline phase delay measurements). Reports by Jacobs (1 988,1991) derive the corrections based on considering only the dry troposphere component, and include all terms necessary to achieve an accuracy of a few millimeters at the lowest elevations. The correction to be added to the zenith dry tropospheric delay is

$$\delta\tau = - \rho z_{d,y}(H/\Delta)\ \psi \tag{4.36}$$

where H is the antenna axis offset, A the dry troposphere scale height ($\approx$8.6 kin), and ψ is an angular factor that varies with the type of mount. For equatorial mounts,

$$\psi = \cos\phi\ \mathrm{Cos}\ h \tag{.1.37}$$

where ϕ is the geodetic latitude and h the local hour angle east of the meridian. The Richmond antenna correction has this form with ϕ replaced by ϕ_W and h by a pseudo-hour angle h_R (see Section II.G.3), where

$$h_R = \arctan\left(\cos E \sin(\theta - c)/[\cos\phi_W \sin E - \sin\phi_W \cos E \cos(\theta + c)]\right) \tag{4.38}$$

For north-south oriented X-Y mounts,

$$\psi = \sin E/(1 - \cos^2 \mathrm{OCOS211})'/2 \tag{4.39}$$

where E is the elevation angle and θ the azimuth (E of N). Finally, for east-west oriented x-Y mounts,

$$\psi = \sin E/(1 - \sin^2\theta \cos^2 E)^{1/2} \tag{4.40}$$

V. PHASE DELAY RATE (FRINGE FREQUENCY)

The interferometer is capable of producing four data types: group delay, phase delay, and their time rates of change. The time rate of change of group delay can not be measured accurately enough to be useful for geodetic or astrometric purposes. All the models discussed above are directly applicable either to group delay or to phase delay. However, the model for the time rate of change of phase delay (fringe frequency) must be either constructed separately, or its equivalent information content obtained by forming the time difference of two phase delay values constructed from the delay-rate measurements as shown below. The latter route is taken in the JPL software, since then only models of delay are needed. The two phase delay values, $\tau_{pd}(t \pm \mathrm{A})$, used to represent the c]clay-rate measurement information content are obtained from the expression

$$\tau_{pd}(t \pm \Delta) = \tau_m(t \pm \Delta) + \tau_r(t) \pm \dot{\tau}_r\Delta \tag{5.1}$$

where $\tau_m(t)$ is the model used in the delay extraction processing step, $\tau_r(t)$ is the residual of the observations from that model, and $\dot{\tau}_r$ is the residual delay rate of the data relative

to that model. This modeling for the delay extraction step is described by Thomas (1 981), and is done in analysis steps prior to and completely separate from the modeling described in the present paper. The output of these preceding steps is such that the details of all processing prior to the modeling described here are transparent to this step. Only total interferometer delays and differenced total interferometer phase delays (these phase delays are divided by the time interval of the difference) serve as input to the final modeling step. One of the requirements of these previous processing steps is that the model delay used be accurate enough to provide a residual phase that is a linear function of time over the observation interval required to obtain the delay information. A linear fit to this residual phase yields the value of $\dot{\tau}_r$, the residual delay rate. Using these two values of τ_{pd}, obtained from Eq. (5.1) above, the phase delay rate $\dot{\tau}_{pd}(t)$ is approximated as a finite difference, R, by the following algorithm:

$$R = [\tau_{pd}(t + \Delta) - \tau_{pd}(t - \Delta)]/(2\Delta) \tag{5.2}$$

This value and the group delay measurement, τ_{gd}, are the two data types that normally serve as the interferometer data input to be explained by the model described in this report. The software, however, also has the option to model phase delay, τ_{pd}, directly. In the limit $\Delta \to 0$, this expression for differenced phase delay approaches the instantaneous time rate of change of phase delay (fringe frequency) at time t. In practice, Δ must be large enough to avoid roundoff errors that arise from taking small differences of large numbers, but should also be small enough to allow R to be a reasonably close approximation to the instantaneous delay rate. A suitable compromise appears to be a Δ in the vicinity of 1 second. Fortunately, the capability to model interferometer performance accurately is relatively insensitive to the choice of Δ over a fairly wide range of values. To be specific, if $\tau_{pd}(t)$ is expanded to third order in Δ, the numerically evaluated rate becomes

$$R = \dot{\tau}_{pd}(t) + \dddot{\tau}_{pd}(t)\,\Delta^2/6 \tag{5.3}$$

Thus the error made in approximating the time derivative as R is proportional to $\dddot{\tau}_{pd}\Delta^2$. This term amounts to a few times 10^{-15} s/s for a 10,000 km baseline and $\Delta = 2$ sec.

VI. PHYSICAL CONSTANTS

Most of the recent implementations of VLBI models in software try to adhere to recommendations of the IERS Standards (1 992), and the associated values of physical constants. Those which affect the results of VLBI modeling implementations are given below:

Symbol	Value	Quantity
c	299792.458	Velocity of light (kin/s)
r_0	2.817938 X 10^{-15}	Classical radius of the electron (meters)
R_E	6378.140	l'equatorial radius of the Earth (km)
ω_E	7.2921151467 x 10^{-5}	Rotation rate of the Earth (rad/s)
f	298.257	Flattening factor of the geoid
h_2	0.609	Vertical quadrupole Love number
l_2	0.0852	Horizontal quadrupole Love number
h_3	0.292	Vertical octupole Love number
l_3	0.01.51	Horizontal octupole Love number
g	980.665	Surface acceleration due to gravity (cm/s^2)
γ_{PPN}	1	Parametrized post-Newtonian gamma factor

Another group of constants is associated with the planetary ephemeris. These constants include all planetary masses; those most important in VLBI modeling are:

AU	1.495978707 x 10^8	Astronomical unit (km)
GM_S	1.32712440 x 10^{11}	Mass of Sun (km^3/s^2)
GM_E	39s600.4356	Mass of Earth (km^3/s^2)
M_E/M_M	81.300585	Earth/Moon mass ratio

where the numerical values arc taken from the most recent JPL Solar System ephemeris, DE403 (Standish and Newhall, 1995).

VII. FUTURE MODEL IMPROVEMENTS

The model of VLBI observable which was developed in Sections II-V has, with some variations, been used by a number of research groups to analyze geodetic and astrometric experiments during the past two decades (Kondo *et al.*, 1992; Ma *et al.*, 1992; NEOS, 1994; Sovers *et al.*, 1 993). Such analyses have presently reached an approximate accuracy level of 1 cm on intercontinental baselines (1 ppb). Data analysis has provided continuous feedback by characterizing previously unknown and unquantified aspects of the model (e.g., nutation, tidal variations, troposphere.) We expect such interplay to continue in the future as both experimental and theoretical techniques are refined. This section gives brief summaries of areas which will require close attention in the future if the current VLBI model is to be improved to achieve and surpass true part-per-billion accuracy. Some of these refinements are already being incorporated in modeling software packages.

A. Relativity

Second-order general relativistic effects have not been carefully investigated, and could potentially contribute at the picosecond level.

Variations of the Earth's gravitational potential must be taken into account in defining proper lengths. This correction is estimated by Thomas (1991) to amount to 2 mm for a 10,000 km baseline. Similarly, variations in the gravitational potential at the station clocks are only approximately accounted for by means of Eq. (2,34).

Hirayama *et al.* (1 987) and Fairhead and Bretagnon (1990) have extended the work of Moyer (1981) on the "time ephemeris". Higher-order special relativistic terms are found to contribute to $TDB - TDT$ at the μs level.

B. Effects of the Galaxy

Galactic effects may soon emerge above the detection threshold. The rotational motion of the structure as a whole affects all observations, and was estimated at 15 prad/yr. It will need to be taken into account for observations spanning more than two decades.

C. Earth tidal models

Direct contributions of the planets to solid Earth tidal displacements can reach the millimeter level, and may need to be included.

In addition to the eight frequencies considered in the model described in Section II.E.1.a, short-period variations of UTPM may have other components significant at the mm level that will emerge as data analyses are refined.

Empirical estimates of ocean loading amplitudes for several IRIS stations (Sovers, 1994) indicate that the best theoretically derived amplitudes might be in error by several mm. Future refinements in data analyses, and improved global ocean models from the recent TOPEX/Poseidon mission (Le Provost *et al.*, 1 995) are expected to improve the accuracy of the ocean loading model to the mm level,

Resonance with the Earth's free core nutation may modify some of the amplitude corrections at nearly diurnal frequencies by ≈1 mm.

Ocean tides cause motion of the center of mass of the solid Earth due to motion of the center of mass of the oceans (Brosche and Wünsch, 1 993). The amplitude of this displacement can be as large as 1 cm at the usual diurnal and semidiurnal tidal frequencies. Its effect on VLBI observations must be assessed.

The retarded tidal potential effect mentioned in Section II.C.2.a can be as large as several tenths of mm. 'Thus, for correct modeling at the mm level, the light travel time should be accounted for,

D. Source structure

Estimates of parameters for simplified structural models might provide improved data analyses via "poor man's mapping".

E. Earth orientation models

There are short-period deficiencies in the present IAU models for the orientation of the Earth in space that may be as large as 1 to 2 milliarcseconds, and longer-term deficiencies on the order of 1 milliarcsecond per year (3 cm at one Earth radius). VLBI measurements made during the past decade indicate the need for revisions of this order of the annual nutation terms and the precession constant [Eubanks *et al.* (1985), Herring *et al.* (1986)]. The 18.6-year components of the IAU nutation series are also in error, and present data spans are just approaching durations long enough to separate them from precession. Options to improve the nutation model were discussed in Section III.E.2.a. Any of these constitute a provisionally improved model, especially for the annual and semiannual nutations, until the IAU series is officially revised.

Future refinements of the equation of equinoxes [Eq. (2.104)] will probably lead to changes on the order of tens of μs in the hour angle.

F. Antenna deformation

Gravity loading may cause variations in the position of the reference point of a large antenna that are as large as 1 cm in the local vertical direction. Liewer (1986) presents evidence that this causes systematic errors and that their dependence on antenna orientation and temperature may be modeled.

G. Antenna alignment

The geometric structure of each antenna, as well as its alignment with respect to local site features, Should be carefully checked against design specifications. For example, hour angle misalignment on the order of 1 arc minute can cause 1 mm delay effects for DSN II A-Dec antennas with 7-m axis offsets.

H. Ionosphere

The limits of validity of the dual-frequency calibration procedure need to be carefully established, in conjunction with consideration of plasma effects for ray paths near the Sun. In addition, corrections for the gyrofrequency effect may reach millimeter order.

1. Troposphere

New techniques for characterizing the atmosphere are expected to allow more realistic modeling of the tropospheric delay than the simple spherical-shell model underlying all the results of Section IV.}]. When comprehensive atmospheric data from a region surrounding each observing site are available, present computer speeds permit estimating the tropospheric delay by means of a complete ray-tracing solution for every observation. Meanwhile, improvements in tropospheric mapping should be sought by modeling variations of the temperature profile as a function of season, latitude, altitude, and diurnal cycle. Efforts are also under way (e.g., MacMillan, 1995) to model azimuthal gradients in the troposphere. Persistent equator-to-pole gradients in pressure, temperature, and tropopause height suggest that *a priori* modeling of north-soul,]] gradients may be beneficial. East-west gradients, which are probably dominated by weather systems passing over a site, are likely to be more difficult to model without extensive weather data.

J. Thermal effects

Thermal expansion of the portion of an antenna above the reference point will induce delay signatures that are ≈9 ps (3 mm) peak-to-peak for a typical 34-m dish. It is thus imperative to model this effect for achievement of the highest accuracy.

K. Phase delay rate

Rather than modeling the delay rates as finite differences of model delays, direct analytic expressions for derivatives of delays could be implemented. This would eliminate questions concerning the choice of the time difference A discussed in Section V. Care must be exercised, however, to ensure consistency between definitions of modeled and observed delay rates.

ACKNOWLEDGMENTS

We would like to express our appreciation to Brooks Thomas and James Williams, who initiated VLBI studies at JPL during the late 1960s and 1970s. The Mastcrfit/Modest computer code is part of their legacy. Brooks and Jim continue to provide theoretical and practical guidance to JPL VLBI studies. Substantial revisions of the VLBI model arose from close cooperation with many colleagues in the Tracking Systems and Applications Section at JPL during the two subsequent decades. Continued clarification of the documentation and additional modeling were required and implemented as the experiments were refined. Most recently, we have benefitted from the help of Gabor Lanyi related to the various atmospheric and antenna effects which are becoming more important as higher measurement accuracy is approached. Patrick Chariot and Jim Ulvestad pioneered the implementation of source structure corrections. Many other colleagues contributed to improvements of JPL VLBI modeling over the years. Among them are Steve Allen, Rachel Dewey, Chad Edwards, Marshall Eubanks, Jean-François Lestrade, Kurt Liewer, Steve Lowe, Chuck Naudet, Larry Romans, Alan Steppe, Bob Treuhaft, and Mike Watkins. Chopo Ma and Dave Gordon

of GSFC participated in a recent comparison between their Calc 8.1 and JPL's Modest software, which was helpful in clarifying many aspects of the model. Critical reviews of this manuscript were kindly done by Jay Lieske and Jim Williams. The work described in this paper was performed at the Jet Propulsion Laboratory, California institute of Technology, under contract with the National Aeronautics and Space Administration,

REFERENCES

Allen, S. L., 1982, "Mobile Station Locations", Jet Propulsion laboratory IOM 335.1-71, Pasadena, CA.

Andersen, 1'. -11., 1995, "High-precision Station Positioning and Satellite Orbit Determination", NDRE *Publication 95/01094*, Kjeller, Norway.

Aoki, S., B. Guinot, G. H. Kaplan, H. Kinoshita, 1). D. McCarthy, and 1'. K. Seidelmann, 1 982, Astron. Astrophys. **105**, 359.

Argus, D. F'., and R. G. Gordon, 1991, Geophys. Res. Lett. **18**, 2039.

hare, C., B. G. Clark, K. 1. Kellermann, H. Cohen, and D. 1,. Jauncey, 1967, Science 157, 189.

Bosworth, J. M., R. J. Coates, and 'J'. 1,. Fischetti, 1993, in *Contributions of Space Geodesy 10 Geodynamics: Technology*, edited by]). E. Smith and 1).],. Turcotte, Geodynamics Series, Vol. 25 (Amer. Geophys. Union, Washington, DC), 1.

Brosche, 1'., U. Seiler, J. Sundermann, and J. Wünsch, 1989, Astron. Astrophys. 220, 318.

Brosche, 1'., J. Wünsch, J. Campbell, and H. Schuh, 1991, Astron. Astrophys. 245, 676.

Brosche, P., and J. Wünsch, 1993, Astron. Nachr. 314, 87.

Broten, N. W., 'I'. H. Legg, J. L. Locke, C. W. McLeish, R. S Richards, R. M. Chisholm, 11. P. Gush, J. I,. Yen, and J. A. Gait, 1967, Nature 215, 38.

Bureau International de l'Heure, 1983, "Annual Report for 1982" (Observatoire de Paris, Paris, France).

Bureau International des Poids et Mesures, 1990, "Circular T30", Sèvres, France.

Burke, B. F., 1991, "Introduction to Orbiting VLBI", in *Advances in Space Research*, **11**, 349.

Campbell, J., 1988, "European VLBI for Geodynamics", in *Proceedings of the 3rd International Conference on the WEGENER/MEDLAS Project*, University of Bologna, Bologna, Italy, p. 361.

Cannon, W. H., 1981, "A Survey of the Theory of the Earth's Rotation", Jet Propulsion Laboratory Publication 82-38, Pasadena, CA.

Carter, W. E., 1983, Revs. of Geophys. Space Phys. 21, 565.

Cartwright, D. E., and A. C. Edden, 1973, Geophys. J. Roy. Astron. Soc. 33, 253.

Chao, C. C., 1974, "The Troposphere Calibration Model for Mariner Mars 1971", Jet Propulsion laboratory Technical Report 32-1587, Pasadena, CA.

Charlot, P., 1989, 'Structure des Sources Radio Extragalactiques dans les Observations VLBI d'Astrométrie et de Géodynamique" (Ph. D. thesis, Observatoire de Paris, Paris, France).

Charlot, P., 1990a, Astron. J. **99**, 1309.

Charlot, P., 1990b, Astron. Astrophys. 229, 51.

Charlot, P., 1994, in *URSI/IAU Symposium on VLBI Technology – Progress and Future Observational Possibilities*, edited by 'J', Sasao, S. Manabe, O. Kawaya, and M. Inoue (Terra Scientific Publishing, Tokyo, Japan), p. 287.

Charlot, P., O. J. Sovers, J. G. Williams, and X X Newhall, 1995, Astron. J. 109, 418.

Clark, T. A., 1979, Revs. of Geophys. Space Phys. 17, 1430.

Davis, J. L., T. A. Herring, I. I. Shapiro, A. E. E. Rogers, and G. Elgered, 1985, Radio Science 20, 1593.

DeMets, C., R. G. Gordon, D. F. Argus, and S. Stein, 1990, Geophys. J. Int. 101, 425.

DeMets, C., R. G. Gordon, D. F. Argus, and S. Stein, 1994, Geophys. Res. Lett. **21**, 2191.

Elgered, G., J. L. Davis, T. A. Herring, and 1.1. Shapiro, 1991, J. Geophys. Res. 96, 6541.

Estefan, J. A., and O. J. Sovers, 1994, *A Comparative Survey of Current and Proposed Tropospheric Refraction-Delay Models for DSN Radio Metric Data Calibration*, Jet Propulsion Laboratory Publication 94-24, Pasadena, CA.

Eubanks, T. M., J. A. Steppe, and O. J. Sovers, 1985, in *Proceedings of the International Conference on Earth Rotation and the Terrestrial Reference Frame*, Ohio State University, Columbus, Ohio, Vol. 1, p. 326.

Fairhead, L., and P. Bretagnon, 1990, Astron. Astrophys. 229, 240.

Fanselow, J. 1,., 1983, *Observation Model and Parameter Partials for the JPL VLBI Parameter Estimation Software "MA STERFIT" -. V1.0*, Jet Propulsion Laboratory Publication 83-39, Pasadena, CA.

Folkner, W. hi., P. Charlot, M. H. Finger, J. G. Williams, O. J. Sovers, (X X) Newhall, and E. M. Standish, 1994, Astron. Astrophys. 287, 279.

French, A. P., 1968, in *Special Relativity*, MIT introductory Physics Series (Norton, New York), pp. 41, 44, 132.

Fukushima, T., M. K. Fujimoto, 11. Kinoshota, and S. Aoki, 1986, Celestial Mechanics 38, 215.

Fukushima, 'J'., 1994, Astron. Astrophys. 291, 320.

Gallini, T. E., 1994, *A Survey of Tropospheric Refraction Models* (Aerospace Corp., El Segundo, CA), Report '1'01{-94(4488)-1 1.

Goad, C. C., 1983, in IAU, IUGG Joint Working Group on the Rotation of the Earth, "Project MERIT Standards", *United States Naval Observatory Circular No. 167* (U.S. Naval Observatory, Washington, DC), p. A7-I.

Gontier, A.-hJ., "Orientation de la Terre par Mesure VLBI", Ph. D. thesis, Observatoire de

Paris, Paris, France, 1992.

Gross, R.S., 1993, Geophys. lies. Lett. 20, 293.

GSFC VLBI Group, 1981, *CALC for the HP 1000: Version 5.0*, Computer Management Branch Report, Goddard Space Flight Center, Greenbelt, MD.

Hartmann, '1'., and M. H. Soffel, 1994, Astron. J. 108, 1115.

Hartmann, T., and H.-G. Wenzel, 1994, Geophys. Res. Lett. 21, 1991.

Hellings, R. W., 1986, Astron. J. 91, 650; erratum *ibid.*, p. 1446.

Herring, 'I'. A., 1991, in *Proceedings of the 127th Colloquium of the 1A U: Reference Systems*, edited by J. A. Hughes, C. A. Smith, and G. H. Kaplan (U. S. Naval observatory, Washington, DC), p. 157.

Herring, T. A., 1992, in *Refraction of Transatmospheric Signals in Geodesy*, edited by J. C. DeMunck and T. A. Th. Spoelstra, Netherlands Geodetic Commission, Publications on Geodesy, No. 36 (Delft, Netherlands), p. 157.

Herring, 'I'. A., C. R. Gwinn, and I. I. Shapiro, 1986, J. Geophys. Res. 91, 4745.

Herring, T. A., and 1). Dong, 1994, J. Geophys. Res. 99, 18051.

Hinteregger, H. F., 1.1. Shapiro, D. S. Robertson, C. A. Knight, R. A. Ergas, A. R. Whitney, A. E. E. Rogers, J. M. Moran, 'I'. A. Clark, ant] B. F. Burke, 1972, Science 178, 396.

Hirayama, Th., H. Kinoshita, M.-K. Fujimoto, and T. Fukushima, 1987, in *Proc. IA G Symposia at IUGG XIX General A ssembly, Vancouver, Canada*, (Bureau Central de l'IAG, Paris, France), Tome 1, p. 91.

Holdridge, 1)., 1967, in *JPL Space Programs Summary 37-48*, Vol. *111: Supporting Research and Advanced Development*, Jet Propulsion laboratory, Pasadena, CA, p. 2.

Ifadis,].,] 986, *The Atmospheric Delay of Radio Waves: Modeling the Elevation Dependence*

on a Global Scale (Chalmers University of Technology, School of Electronic and Computer Engineering, Gothenburg, Sweden), Tech. Report No. 38L.

International Earth Rotation Service, 1989, *IERS Standards (1989), IERS Technical Note* 3, edited by D. D. McCarthy (Observatoire de Paris, Paris, France), p. 37.

International Earth Rotation Service, 1992, *IERS Standards* (1992), *IERS Technical Note* 13, edited by 1). D. McCarthy (Observatoire de Paris, Paris, France).

International Earth Rotation Service, 1995a, "IERS 1994 Annual Report", (Observatoire de Paris, Paris, France).

International Earth Rotation Service, 1995b, *IERS Conventions, IERS Technical Note 21*, edited by 1). D. McCarthy (Observatoire de Paris, Paris, France).

Jackson, J. D., 1975, *Classical Electrodynamics* (Wiley, New York), p. 517.

Jacobs, C. S., 1988, Jet I'repulsion Laboratory IOM 335.3-88-01$ Pasadena, CA.

Jacobs, C. S., and A. Rius, 1989, in *Proceedings of the 7th Working Meeting on European VLBI for Geodesy and Astrometry*, held at Madrid, Spain, October 26-27, p,. 64.

Jacobs, C. S., and A. Rius, 1990, Jet Propulsion Laboratory IOM 335.6-90-034, Pasadena, CA.

Jacobs, C. S., 1991, Jet Propulsion Laboratory IOM 335.6-91-015, Pasadena, CA.

Jacobs, C. S., O. J. Sovers, J. G. Williams, and E. M. Standish, 1993, "The Extragalactic and Solar System Celestial Frames: Accuracy, Stability, and Interconnection", in *Advances in* Space *Research, 13, p.* (1 1)161.

Kaplan, G. H., 1981, in *United States Naval Observatory Circular No. 163*, [1. S. Naval Observatory, Washington), 1)(;.

Kellermann, K.]., ant]]. 1. K. Pauliny-Toth, 1981, Ann. Rev. Astron. Astrophys. *19,* 373.

Kinoshita, H., and J. Souchay, 1990, Cel. Mech. and Dyn. Astron. 48, 187.

Kondo, 'T'., J. Amagai, Y. Koyama, and K. Heki, 1992, "Data Analysis of Geodetic VLBI Organized by the Communications Research laboratory", Kashima Space Center Report, Kashima, Japan.

Ishimori, H., *et* al., 1993, in *Contributions of Space Geodesy to Geodynamics: Technology*, edited by D. E. Smith and D. L. Turcotte, Geodynamics Series, Vol. 25 (Amer. Geophys. Union, Washington, DC), 65.

Lanyi, G. E., 1984, in *Telecommunications and Data Acquisition Prog. Rept. 42-78*, pp. *152-159*, Jet Propulsion laboratory, Pasadena, CA.

Le Mouël, J.-L., D. E. Smylie, and T. Herring, 1993, Eds., *Dynamics of Earth's Deep Interior and Earth Rotation*, Geophysical Monograph 72, IUGG Volume 12 (IUGG/AGU, Washington, DC).

Le Provost, c., A. F. Bennett, and D. E. Cartwright, 1995, Science, 267, 639.

Lestrade, J.-F'., *et al.*, 1995, Astron. Astrophys. (in press).

Lieske, J. H., T. Lederle, W. Fricke, and B. Morando, 1977, Astron. Astrophys. **58**, 1.

Liewer, K. M., 1985, Jet Propulsion Laboratory IOM 335.4-49?', Pasadena, CA.

Liewer, K. M., 1986, private communication.

Lowe, S. 'T'., 1992, Jet Propulsion Laboratory Publication 92-7, Pasadena, CA.

Ma, C., 1978, NASA Technical Memo 79582, Goddard Space Flight Center (Greenbelt, MD).

Ma, C., and D. B. Shaffer, 1991, in *Proceedings of the 127th Colloquium of the IAU: Reference Systems*, edited by J. A. Hughes, C. A. Smith, and G. H. Kaplan (U. S. Naval Observatory, Washington, DC), p. 135.

Ma, C., J. W. Ryan, and D. S. Caprette, 1992, *Crustal Dynamics Project Data Analysis* –

1991: VLBI Geodetic Results 1979-1990, NASA Technical Memo 104552, Goddard Space Flight Center (Greenbelt, MD).

MacMillan, D. S., 1995, Geophys. Res. Lett. 22, 1041

MacMillan, D. S., and J. M. Gipson, 1994, J. Geophys. Res. 99, 18081.

Manabe, S., T. Sate, S. Sakai, and K. Yokoyama, 1991, "Atmospheric Loading Effect on VLBI Observations", in *Proceedings of the A GU Chapma n Conference on Geodetic VLBI: Monitoring Global Change*, NOAA Tech. Report NOS 137 NGS 49, p. 111.

Marini, J. W., 19'72, Radio Science, 7, 223.

Mathews, 1'. hi., B. A. Buffett, T. A. Herring, and 1. I. Shapiro, 1991, J. Geophys. Res. **96B**, 8219.

Mathews, P. M., B. A. Buffett, and 1.1. Shapiro, 1995, Geophys. Res. Lett. 22, 579.

McGinnis, H., 1'977, in *Deep Space Network Prog. Rept. 42-41, pp. 218-225,* Jet Propulsion Laboratory, Pasadena, CA.

Melbourne, W. G., J. D. Mulholland, W. L. Sjogren, and F. M. Sturms, Jr., 1968, Jet Propulsion laboratory Technical Report 32-1306, Pasadena, CA.

Melbourne, W., R. Anderle, M. Feissel, R. King, D. McCarthy, D. Smith, B. Tapley, R. Vicente, 1983, Eds., *Project MERIT Standards*, United States Naval observatory Circular No. 167 (U.S. Naval Observatory, Washington, DC).

Melbourne, W., R. Anderle, M. Feissel, R. King, D. McCarthy, D. Smith, B. Tapley, R. Vicente, 1985, Eds., *Project MERIT Standards*, United States Naval Observatory Circular No. 167, Update #1 (U. S. Naval Observatory, Washington, DC).

Melchior, 1'., 1966, *The Earth Tides* (Pergamon, New York), p. 114.

Mendes, V. B., and R. B. Langley, 1994, *A Comprehensive Analysis of Mapping Functions*

in Modeling Tropospheric Propagation Delay in Space Geodetic Data, paper presented at 1<1S94, International Symposium on Kinematic Systems in Geodesy, Geomatics and Navigation, Banff, Canada, Aug. 30 - Sept. 2.

Minster, J. B., and T. 11. Jordan, 1978, J. Geophys. Res. **83**, 5331.

Misner, C. W., K. S. Thorne, and J. .4. Wheeler, 1973, *Gravitation (W.* H. Freeman, New York).

Mitrovica, J. X., J. 1,. Davis, and 1.1. Shapiro, 1993, Geophys. Res. Lett. 20, 2387

Moran, J. M., 1'.1'. Crowther, B. F. Burke, A. 11. Barrett, A. E. E. Rogers, J. A. Ball, J. C. Carter, and C. C. Bare, 1967, Science **157**, 676.

Moyer, T. D., 1971, Jet Propulsion Laboratory Technical Report 32-1527, Pasadena, CA, p. 12.

Moyer, '1'.])., 1981, Cel. Mech. 23, 33.

Naudet, C. J., 1994, private communication.

Naudet, C. J., 1995, Eos Trans. AGU, 76, S92.

NEOS Annual Report for 1993, 1994, U .S. Naval Observat ory (Washington, D C).

Newhall, (X X), Preston, R. A., and Esposito, P. B., 1 986, in *Astrometric Techniques, Proceedings of IAU Symposium 109*, edited by 11. K. Eichhorn and R. J. Leacock (Reidel, Dordrecht).

Niell, A. E., 1995, J. Geophys. Res. (in press).

Nothnagel, A., M. Pilhatsch, and R. Haas, 1995, in *Proceedings of the 10th Working Meeting on European VLBI for Geodesy and Astrometry*, held at Matera, Italy, May 24-26, 1995.

Ortega-h401iIla, A., 1985, "Détermination du Centre de Phase du Radiotélescope de Nançay pour les Observations V],]]]", Report of Observatoire de Paris-Meudon (Meudon, France).

Pagiatakis, S. D., R. B. Langley, and P. Vanicek, 1982, presented at the 3rd International Symposium on the Use of Artificial Satellites for Geodesy and Geodynamics (National Technical University, Athens, Greece).

Pagiatakis, S. D., 1982, *Ocean Tide Loading, Body Tide and Polar Motion Effects on Very Long Baseline Interferometry*, (Dept. of Surveying Engineering, University of New Brunswick Fredericton, N. B., Canada), Technical Report No. 92.

Pagiatakis, S. D., 1990, Geophys. J. Int. 103, 541.

Peltier, W. R., 1995, Geophys. lies. Lett. 22, 465.

Polatidis, A. G., P. N. Wilkinson, W. Xu, A. C. S. Readhead, '1'. J. Pearson, G. B. Taylor, and R. C. Vermeulen, Astrophys. J. Suppl. Ser. **98**, 1.

Rabbel, W., and 11. Schuh, 1986, J. Geophysics 59, 164

Ray, J. R., 1991, Revs. of Geophys. Suppl. 29, 148.

Ray, J. R., C. Ma, J. W. Ryan, T. E. Clark, R. J. Eanes, M. M. Watkins, B. E. Schutz, and B. 1). Tapley, 1991, Geophys. Res. Lett. 18, 231.

R esch, G. M., 1984, in *Geodetic Refraction: Effects of Electromagnetic Wave Propagation Through the Atmosphere*, edited by 1". K. Brunner (Springer, Berlin), p. 53.

Rius, A., N. Zarraoa, E. Sardon, and C. Ma, 1992, Bull. Geod. *66, 21*

Robertson, D. S., 1975, "Geodetic and Astrometric Measurements with Very Long Baseline Interferometry", Ph.D. Thesis, M.I.T. Also available as NASA GSFC X-document # X-922-77-228 and NOAA reprint, National Geodetic Information Center, Silver Spring, MD, 1985.

Robertson,]). }{., 1991, Rev. Mod. Phys. 63, 899.

Rogers, A. E. E., 1991, in *Proceedings* of *the AG* U *Chapman Conference on Geodetic VLBI:*

Monitoring Global Change, NOAA Tech. Report NOS 137 NGS49, p. 1.

Ryan, J. W., 1989, "CALC-7.0 Release Document", internal memorandum, Goddard Spatc Flight Center, Greenbelt, MD.

Saastamoinen, J., 1972, "Atmospheric Correction for the Troposphere and Stratosphere in Radio Ranging of Satellites", in *The Use of Artificial Satellites for Geodesy*, edited by S. W. Hendrickson, A. Mancini and H.H. Chovitz, Geophys. Monograph 15, Amer. Geophys. Union, Washington, DC.

Scherneck, H. G., 1983, *Crustal Loading Affecting VLBI Sites* (University of Uppsala, Institute of Geophysics, Dept. of Geodesy, Uppsala, Sweden), Report No. 20.

Scherneck, H.G., 1991, Geophys. J. Int. 106, 677.

Scherneck, H.G., 1993, private communication.

Seidelmann, P. K., 1982, Celestial Mechanics 27, 79.

Seidelmann, P. K., B. Guinot, and L. E. Doggett, 1992, in *Explanatory Supplement to the Astronomical Almanac*, edited by P. K. Seidelmann (University Science Books, Mill Valley, CA), p. 39.

Seiler, U., 1989, "An Investigation of the 'Tides of the World Ocean and their Instantaneous Angular Momentum Budget", *Mitteilungen Institut für Meereskunde* (University of Hamburg, Germany).

Seiler, U., 1990, in *Earth's Rotation from Eons to Days*, edited by P. Brosche and J. Sündermann (Springer, New York), p. 81.

Seiler, U., 1991, J. Geophys. Res. **96**, 10287,

Shahid-Saless, B., R. W. Hellings, and N. Ashby, 1991, Geophys. Res. Lett. 18, 1139.

Shapiro, I. I., 1976, in *Astrophysics; Radio Observations*, edited by M. L. Meeks, Vol. 12,

Part C, Methods of Experimental Physics (Academic, NY), 261.

Smith, D. E., and D. L. Turcotte, 1993, Eds., *Contributions of Space Geodesy to Geodynamics: Crustal Dynamics*, Geodynamics Series, Vols. 23-25 (Amer. Geophys. Union, Washington, D(').

Souchay, J., 1993, Private communication

Sovers, O. J., and C. Ma, 1985, in *Telecommunications and Data Acquisition Prog. Rept. 42-83*, pp. *101-112,* Jet Propulsion Laboratory, Pasadena, CA.

Sovers, O. J., C. S. Jacobs, and R. S. Gross, *1993,* J. Geophys. Res. *98,* 19959.

Sovers, O. J., 1 *994,* Geophys. Res. Letters **21**, 357.

Sovers, O. J., and C. S. Jacobs, 1994, *Observation Model and Parameter Partials for the JPL VLBI Parameter Estimation Software "MODEST" - 1994,* Jet Propulsion laboratory Publication 83-39, Rev. 5, Pasadena, CA.

Spitzer, 1,., Jr., 1962, *Physics of Fully Ionized Gases,* (Interscience Publishers, New York).

Standish, E. M., 1982, Astron. Astrophys. 114, 297.

Standish, E. M., and X X Newhall, 1995, in *Dynamics, Ephemerides, and Astrometry of Solar System Bodies,* Proceedings of IAU Symp. 172, Kluwer, Dordrecht.

Steppe, J, A., S. 11. Oliveau, and O. J. Sovers, 1994, "Earth Rotation Parameters from DSN V],}]]: 1994", in *Earth Orientation, Reference Frames and Atmospheric Excitation Functions submitted for the 1993 IERS Annual Report,* edited by P. Charlot (Observatoire de Paris, Paris, France), p. R-19.

Tausner, M. J., 1966, *General Relativity and its Effects on Planetary Orbits and Interplanetary Observations,* (Lincoln laboratory, Massachusetts Institute of Technology, Cambridge, MA), Technical Report No. 425.

Taylor, G. B., R. C. Vermeulen, T. J. Pearson, A. C. S. Readhead, D. R. Henstock, I. W. A. Browne, and P. N. Wilkinson, 1994a, in *Compact Extragalactic Radio Sources*, Proceedings of a workshop at Socorro, NM, Feb. 11-12, 1994, edited by J. A. Zensus and K. I. Kellermann.

Taylor, G. B., R. C. Vermeulen, T. J. Pearson, A. C. S. Readhead, D. R. Henstock, I. W. A. Browne, and P. N. Wilkinson, 1994b, Astrophys. J. Suppl. Ser. 95, 345.

Teitelbaum, L., 1995, submitted to *Telecommunications and Data Acquisition Prog. Rept.*, Jet Propulsion laboratory, Pasadena, CA.

Thakkar, D. D., W. Xu, A. C. S. Readhead, T. J. Pearson, G. B. Taylor, R. C. Vermeulen, A. G. Polatidis, and T. N. Wilkinson, Astrophys. J. Suppl. Ser. 98, 33.

Thomas, J. B., 1980, Jet Propulsion laboratory Publication 80-84, Pasadena, CA.

Thomas, J. B., 1981, Jet Propulsion Laboratory Publication 81-49, Pasadena, CA.

Thomas, J. B., 1987, Jet Propulsion Laboratory Publication 87-29, Pasadena, CA.

Thomas, J. B., 1991, private communication.

Thompson, A. R., J. M. Moran, and G. W. Swenson, Jr., 1986, *Interferometry and Synthesis in Radio Astronomy*, (Wiley, New York).

Treuhaft, R. N., 1991, private communication.

Treuhaft, R. N., and G. E. Lanyi, 1987, Radio Science 22, 251.

Treuhaft, R. N., and S. T. Lowe, 1991, Astron. J. 102, 1879.

Treuhaft, R. N., and J. B. Thomas, 1991, Jet Propulsion laboratory IOM 335.6-91-016, Pasadena, CA.

Tushingham, A. M., and W. R. Peltier, 1991, J. Geophys. Res. 96, 449?

Ulvestad, J. S., 1988, in *The Impact of VLBI on Astrophysics and Geophysics*, Proceedings

of IAU Symp. 129, edited by M. J. Reid and J. M. Moran, Kluwer, Dordrecht, p. 429.

van Dam, T. M., and T. A. Herring, 1994, J. Geophys. Res. 99, 4505.

van Dam, T. M., G. Blewitt, and M. B. Heflin, 1994, J. Geophys. Res. **99**, 23939.

Wade, C. M., 1970, Astrophys. J. 162, 381.

Wahr, J. M., 1979, "The Tidal Motions of a Rotating, Elliptical, Elastic, and Oceanless Earth", (Ph. D. Thesis, University of Colorado, Boulder, CO).

Wahr, J. hi., *1985,* J. Geophys. Res. *90,* 9363.

Watkins, M. M., and R. J. Eanes, 1994, J. Geophys. Res. **99**, 18073.

Whitney, A. R., 1974, "1'recision Geodesy and Astrometry Via Very-Long-Baseline Interferometry", Ph.D. Thesis, M.].'].'.

Williams, J, G., 1970a, in *JPL Space Programs Summary 37-62, Vol. II: The Deep Space Network,* Jet 1'repulsion Laboratory, Pasadena, CA, p. 49.

Williams, J. G., 1970b, Jet 1'repulsion Laboratory IOM 391-1 09, Pasadena, CA.

Williams, J. G., 1995, Astron. J. (in press).

Yatskiv, Ya. S., A. N. Kur'janova, and M. M. Medvedsky, 1991, "Program Complex "Kiev-Gill'' for Reduction of the VLBI Observations", Preprint 1'1'1''-91-371', (Institute for Theoretical Physics, Kiev, Ukraine).

Yoder, C. F., J. G. Williams, and M. E. Parke, 1981, J. Geophys. Res. 86, 881

Yoder, C. F., 1983, private communication.

Yoder, C. h'., 1984, private communication.

Zarraoa, N., A. Rius, E. Sardon, H. Schuh, and J. Vierbuchen, 1989, in *Proceedings of the 7th Working Meeting on European VLBI for Geodesy and Astrometry,* edited by A. Rius,

Madrid, Spain, p. 92.

Zensus, J. A., and T. J. Pearson, 1987, Eds., *Superluminal Radio Sources*, (Cambridge Univ. Press, New York).

Zhu, S. Y., and E. Groten, 1989, Astron. J. **98**, 1104.

Zhu, S. Y., E. Groten, and Ch. Reigber, 1990, Astron. J. 99, 1024.

FIGURES

FIG. 1. Schematic VLBI experiment.

FIG. 2. Geometry for calculating the transit time of a plane wave front.

FIG. 3. Geometry for talc.ulatillg the transit time of a curved wave front.

FIG. 4. Schematic representation of the geodesic connecting two points in the presence of a gravitational mass.

FIG. 5. Schematic representation of the motion of a gravitating object during the transit time of a signal from the point of closest approach to reception by an antenna.

FIG. 6. Generalized schematic representation of the geometry of a steerable antenna..

FIG. 7. Geometry of the spherical ionospheric shell used for ionospheric corrections.

TABLES

TABLE I. Tectonic Plate Rotation Velocities: NNR-Nuvel1A Model

(Units are nanoradians/year).

Plate	ω_x	ω_y	ω_z
Africa	0.891	- 3.099	3.922
Antarctica	- 0.821	- 1.701	3.706
Arabia	6.685	-0.521	6.760
Australia	7.839	5.124	6.282
Caribbean	-0.17'8	--3.385	1.581
cocos	--10.425	-21.605	10.925
Eurasia	- 0.981	-2.395	3.153
India	6.670	0.040	6.790
Juan de Fuca	5.200	8.610	-5.820
Nazca	-1.532	*–8.577*	*9.609*
North America	0.258	. ..3.599	- 0.153
Pacific	-1,510	4.840	-9.970
Philippine	10.090	-7.160	--9.670
Rivera	-9.390	-30.960	12.050
Scotia	-0.410	--2.660	-1.270
South America	–1.038	--1.515	-0.870

TABLE II. Frequency Dependent Solid Earth Tide Parameters.

Component (k)	h_2^k	H_k (mm)
ψ_1 (166<5,54)	().937	3
(165565)	0.514	50
K_1 (165555)	0.520	369
(165545)	0.526	-7
P_1 (163555)	0.581	-122
O_1 (1.45555)	0.603	-262

TABLE III. Lunar Node Companions to Ocean Tides.

i Component	n_{ki} Companion	r_{ki}: Relative Amplitude
K_2 (275555)	-1	0.0128
	+1	4-0.2980
	42	+0.0324
S_2 (273555)	-1	+0.0022
M_2 (255555)	-2	+0.0005
	-1	-0.0373
N_2 (245655)	-1	-0.0373
K, (165555)	-1	--0.0198
	+1	+0.1356
	+2	–0.0029
P_1 (163555)	-1	-0.0112
0, (145555)	--2	-0.0058
	-1	+0.1885
Q_1 (135655)	-2	-40.0057
	-1	+0.1884
M_f (075555)	+1	+0.4143
	+2	-10.0387
M_m (065455)	-1	–0.0657
	+1	--0.0649
S_{sa} (057555)	+1	–0.0247

TABLE IV. Ocean Tidally Induced Periodic Variations in Polar Motion (JPL92 Model).

Index	Tide, period		Argument coefficient						A_{i1}	B_{i1}	A_{i2}	B_{i2}	A_{i3}	B_{i3}
i		(hours)	k_{i1}	k_{i2}	k_{i3}	k_{i4}	k_{i5}	n_j		(μas)			(0.1//.s)	
1	K_2	11.967	o	o	0	0	o	-2	-2	65	44	-57	-9	26
2	S_2	12.000	0	0	2	-2	2	-2	101	166	126	-89	-4	52
3	M_2	12.421	0	0	2	0	2	-2	26	283	247	-2	-104	149
4	N_2	12.658	1	0	2	0	'2	-2	-15	56	19	-11	-23	,20
5	K_1	23.934	0	0	0	0	0	-1	-583	2780	-2950	376	35	151
6	P_1	24.066	0	0	2	-2	2	-1	154	46	42	-17	-32	-64
7	O_1	25.819	0	0	2	0	2	-I	242	-152	2	-30	-135	-166
8	Q_1	26.868	1	0	2	0	2	-1	72	-32	26	i'	-40	-53

TABLE V. Plasma Effects.

Plasma	$\rho(e/m^3)$	ν_p (kHz)	(l/p/l/s)	(ν_p/ν_X)
Earth's ionosphere	10^{12}	8900	4 x 10-"^{3}	10^{-3}
Interplanetary	$10^7 - 10^8$	28-89	4X 10^{-5}	10^{-5}
Interstellar	105	3	1.2X 10^{-6}	3X1 O-7

TABLE VI. Electron Gyrofrequency Effects.

Magnetic field	B (gauss)	ν_g (kHz)	(ν_g/ν_S)	(ν_g/ν_X)
Earth	0.2	600	3x 10^{-4}	7.5x 10^{-5}
Interplanetary	10^{-4}	0.3	1.5×10^{-7}	3.2x 10^{-8}
Interstellar	10^{-6}	0.003	1.5×10^{-9}	3.2 X 10^{-10}

TABLE VII. Surface Meteorological Parameters in the Lanyi Mapping Function.

Parameter	Default	Derived parameter and value	Sensitivity (6°)
T_0	292 }<	$\Delta = kT_0/mg_e = 8.567$ km	--7 mm/K
W	6.8165 K/km	$\alpha = 100\,T_0/W\Delta = 5.0$	20 mm/K/km
h_1	1.25 km	$q_1 = h_1/\Delta = 0.1459$	- 20 mm/km
h_2	12.2 km	$q_2 = h_2/\Delta = 1.424$	5 mm/km

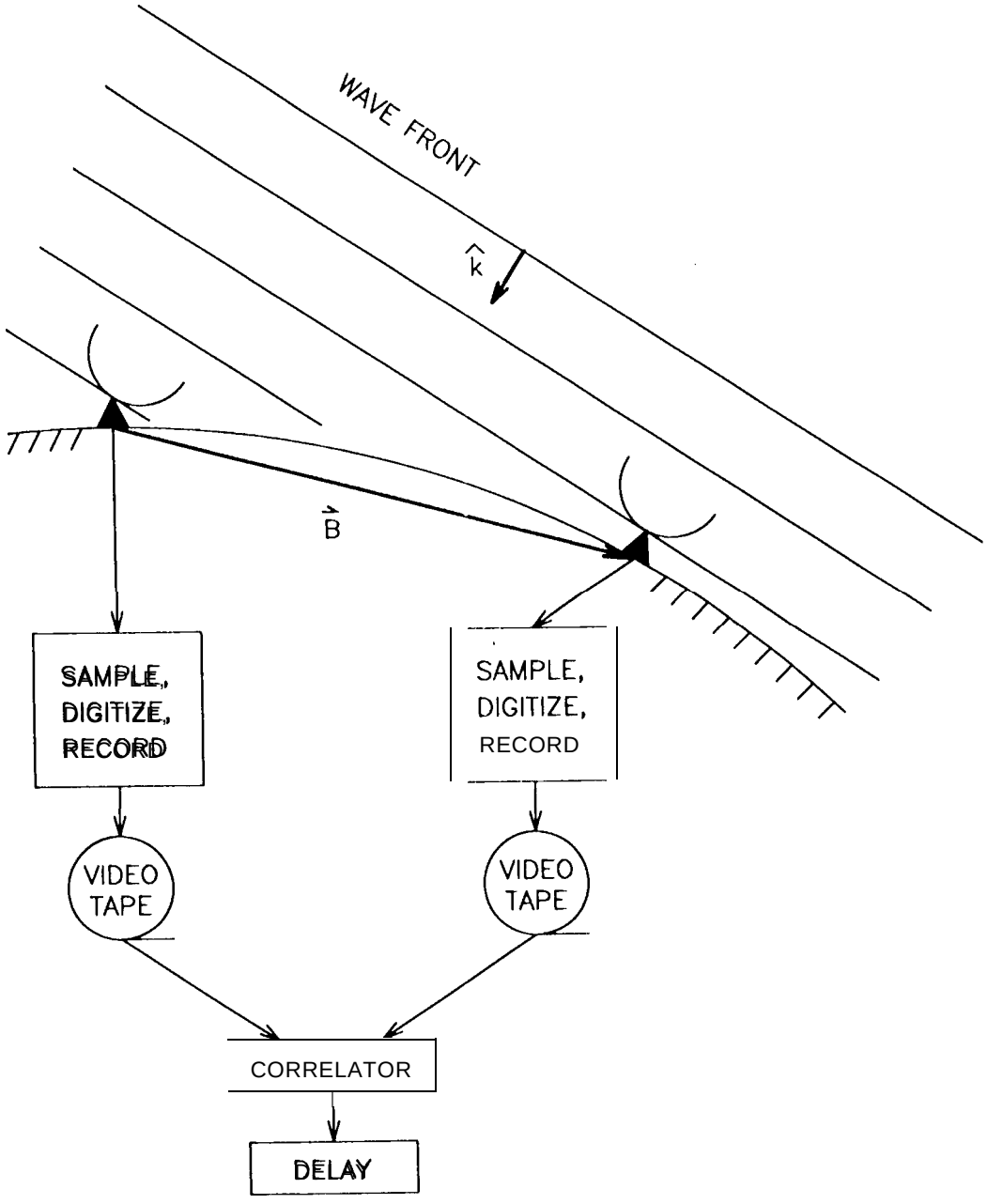
WAVE FRONT
$\hat{k}$
$\vec{B}$
SAMPLE, DIGITIZE, RECORD
SAMPLE, DIGITIZE, RECORD
VIDEO TAPE
VIDEO TAPE
CORRELATOR
DELAY

Fig. 1

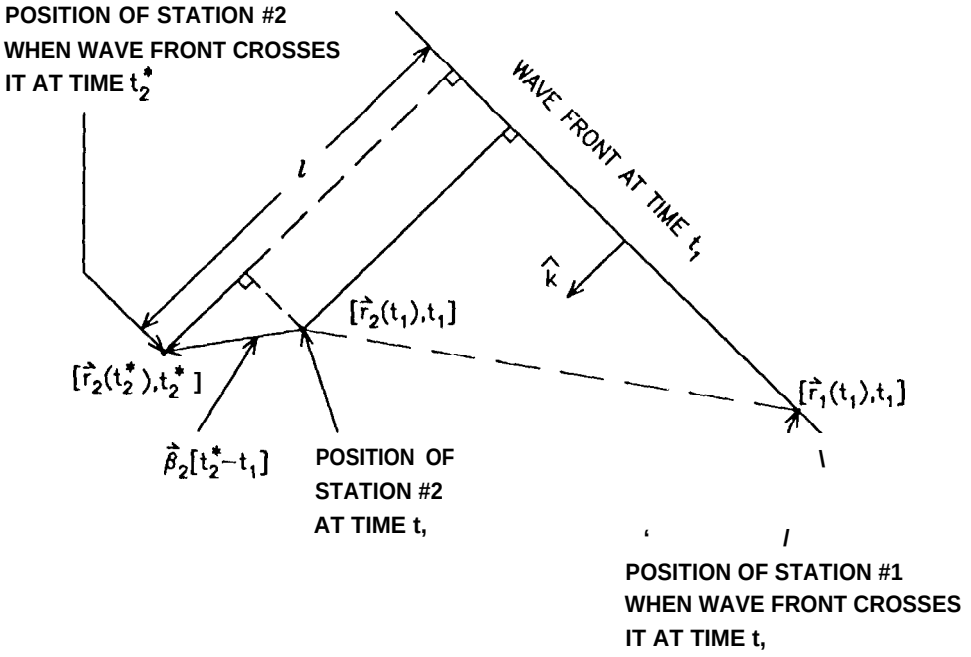
POSITION OF STATION #2
WHEN WAVE FRONT CROSSES
IT AT TIME t_2^*
WAVE FRONT AT TIME t_1
l
$\hat{k}$
$[\vec{r}_2(t_1),t_1]$
$[\vec{r}_2(t_2^*),t_2^*]$
$[\vec{r}_1(t_1),t_1]$
$\vec{\beta}_2[t_2^*-t_1]$
POSITION OF
STATION #2
AT TIME t_1
POSITION OF STATION #1
WHEN WAVE FRONT CROSSES
IT AT TIME t_1

Fig. 2

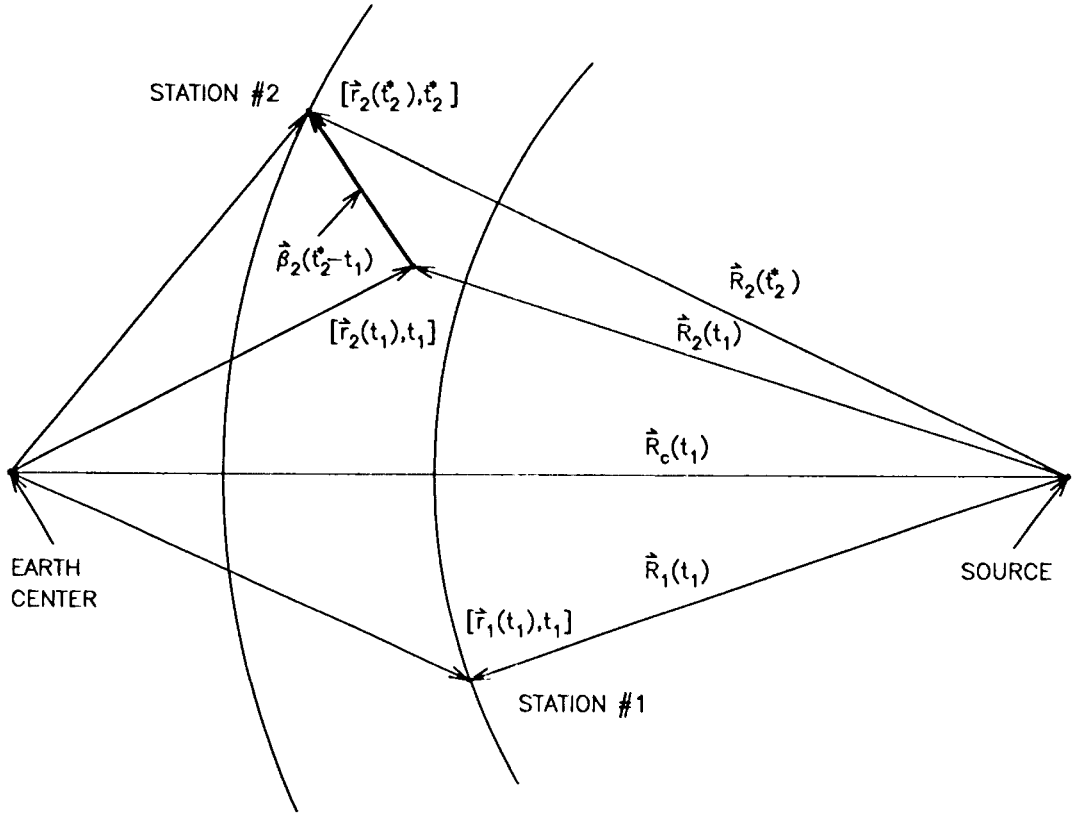
STATION #2
$[\vec{r}_2(t_2^*), t_2^*]$
$\vec{\beta}_2(t_2^* - t_1)$
$[\vec{r}_2(t_1), t_1]$
$\vec{R}_2(t_2^*)$
$\vec{R}_2(t_1)$
$\vec{R}_c(t_1)$
EARTH CENTER
$\vec{R}_1(t_1)$
SOURCE
$[\vec{r}_1(t_1), t_1]$
STATION #1

Fig. 3

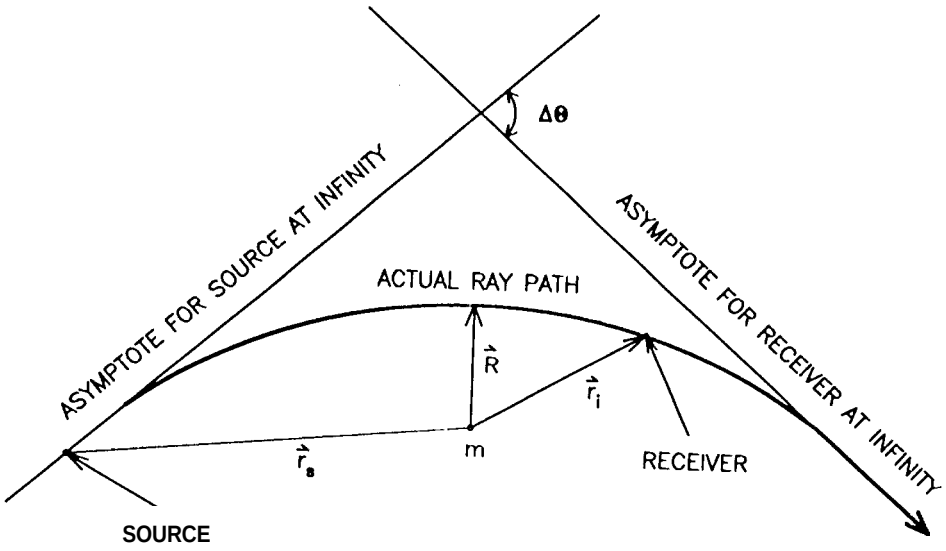
Δθ
ASYMPTOTE FOR SOURCE AT INFINITY
ASYMPTOTE FOR RECEIVER AT INFINITY
ACTUAL RAY PATH
$\vec{R}$
$\vec{r}_i$
$\vec{r}_s$
m
RECEIVER
SOURCE

Fig. 4

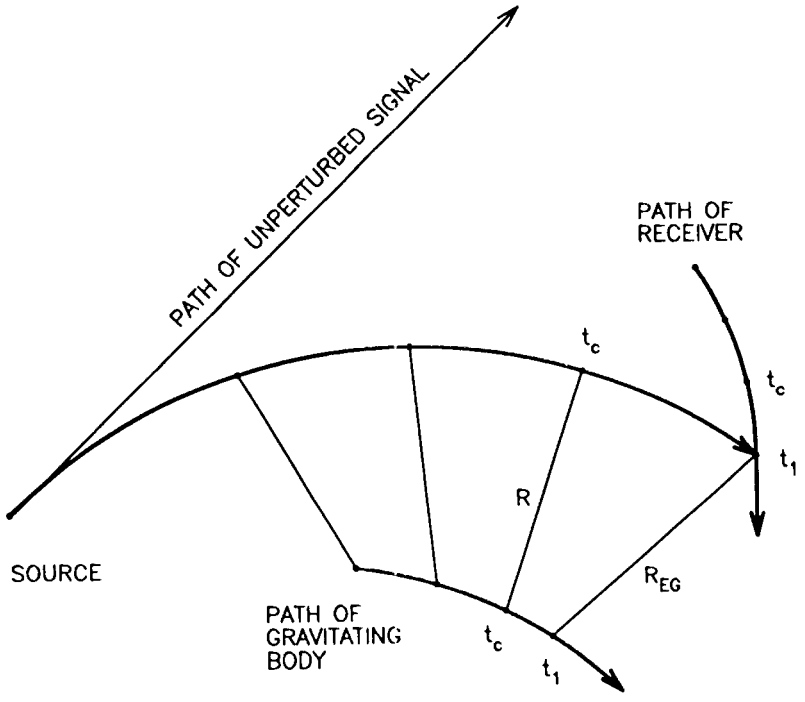
PATH OF UNPERTURBED SIGNAL
PATH OF RECEIVER
t_c
t_c
t_1
R
SOURCE
R_{EG}
PATH OF GRAVITATING BODY
t_c
t_1

Fig. 5

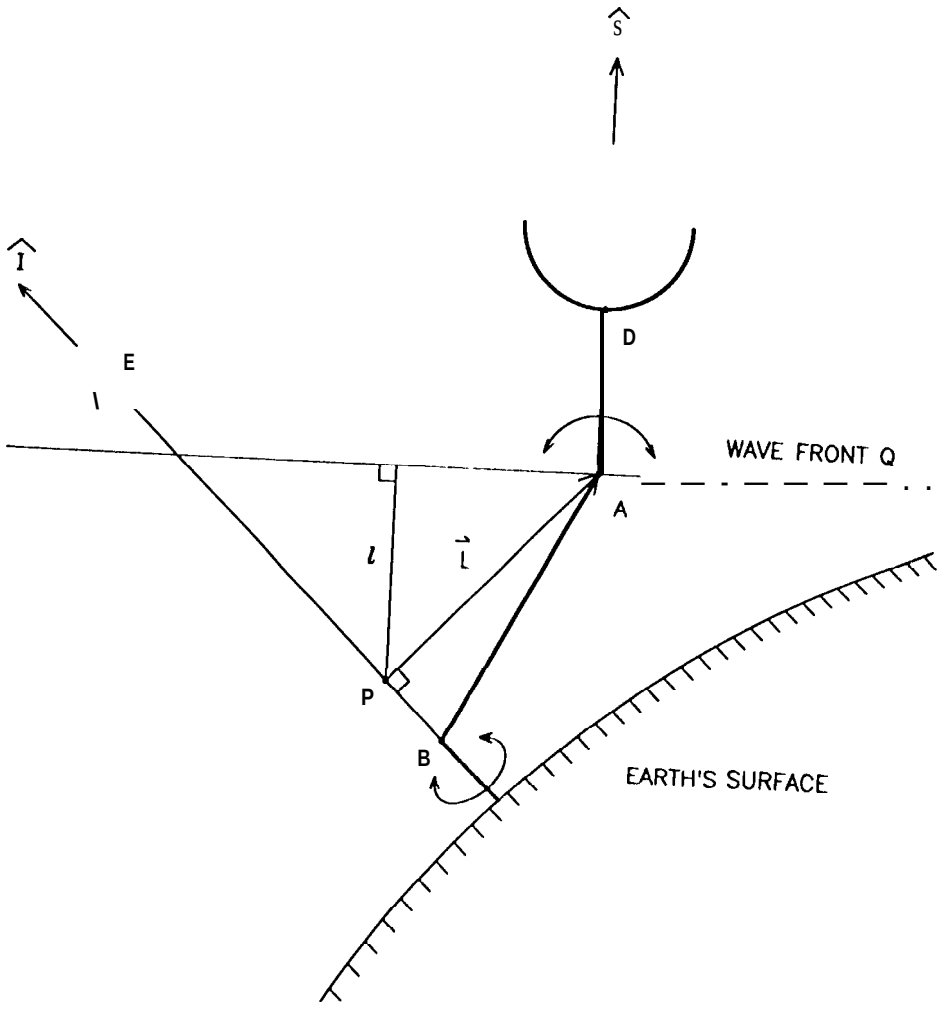

Fig. 6

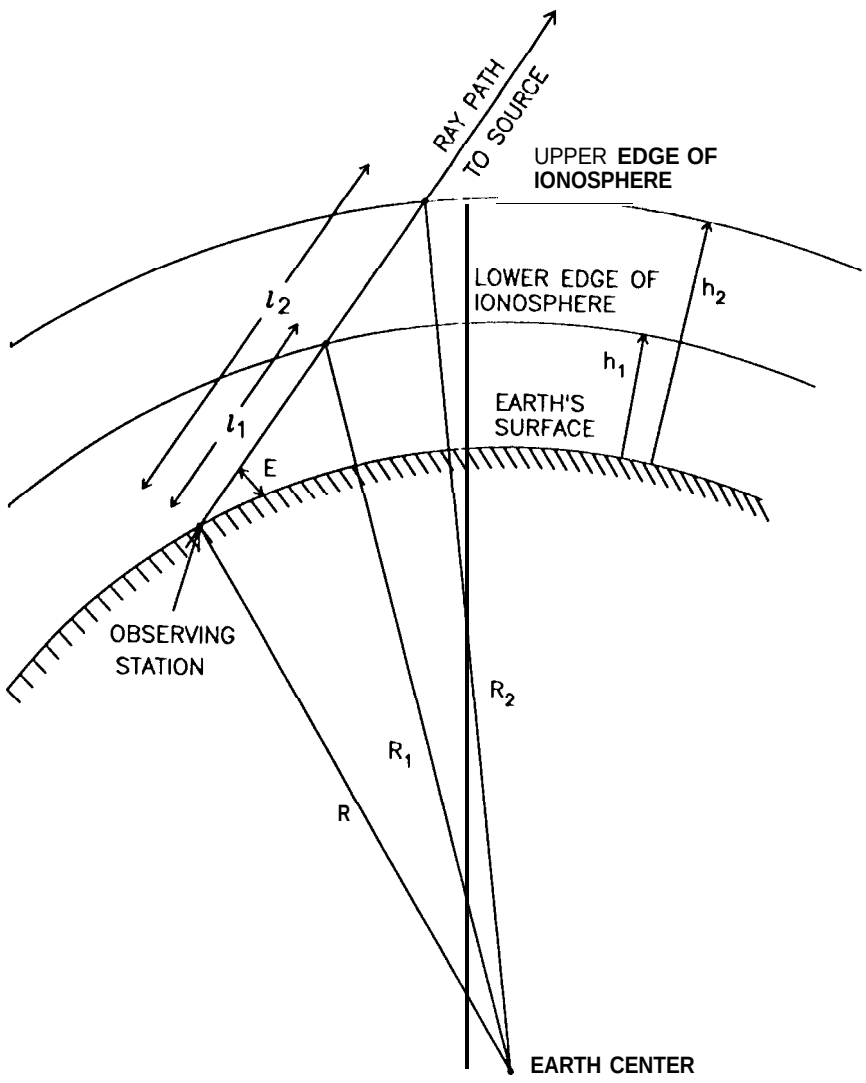
RAY PATH
TO SOURCE
UPPER EDGE OF
IONOSPHERE
LOWER EDGE OF
IONOSPHERE
l_2
h_2
h_1
l_1
EARTH'S
SURFACE
E
OBSERVING
STATION
R_2
R_1
R
EARTH CENTER

Fig. 7